2006-05-01

The Computerised Design of Prestressed Cncrete Slabs

Ronan Hogan
Technological University Dublin, ronan.hogan@tudublin.ie

Dublin Institute of Technology
School of Civil and Building Services Engineering
Faculty of Engineering

The Computerised Design of Prestressed Concrete Slabs

Ronan Hogan, B.Sc. (Eng)

Submitted for MPhil award
May 2006

Vol. 1 of 2

Supervisors: Dr. Tom Dunphy and Mr. Eddie Fallon

I certify that this thesis which I now submit for examination for the award of Master of Philosophy, is entirely my own work and has not been taken from the work of others save and to the extent that such work has been cited and acknowledged within the text of my work.

This thesis was prepared according to the regulations for postgraduate study by research of the Dublin Institute of Technology and has not been submitted in whole or in part for an award in any other Institute or University.

The Institute has permission to keep, to lend or to copy this thesis in whole or in part, on condition that any such use of the material of the thesis be duly acknowledged.

Signature  Date 13/11/06

Acknowledgements

I would like to thank my supervisors Mr Eddie Fallon and Dr. Tom Dunphy for the guidance and support I received. At every stage help was available to deal with obstacles both large and small.

A number of the other lecturing staff are also due thanks for their help, most notably Dr. Barry Duignan, Mr. Ed Mullarkey and Mr. Ross Galbraith. I also greatly appreciate the comments and feedback given by Dr. John O'Donnell who acted as my internal reader for the thesis. Andrew Carroll and Mike Flaherty from the IT department are also due my gratitude for assisting with the numerous requests for software and support.

Thanks is also due to Dr. Steve Jerrams and Research Support Unit in D.I.T. for the financial support that allowed this project to continue unimpeded by such concerns.

Finally, thanks to my friends and family for their support especially Ela Krawczyk and Conal Bradley.

Abstract

This research was aimed at the development of a finite element based software package for the analysis and design of prestressed concrete slabs. Many of the existing packages used in this area carry out a simplified two dimensional analysis of the slab which does not account for the secondary stresses set up by the presence of openings and notches in the slab. In an attempt to overcome this particular weakness, a finite element analysis package was written to help produce a more rigorous analysis of the stresses developed in prestressed concrete.

The aims of the research were the examination of prestressed concrete theory, the identification of a suitable finite element model and the implementation of both theory and model through a purpose written software package. A combination of two finite element models, plate bending and plane stress, were used to simulate the effect of the axial stress imparted to the concrete by the strands and the moment applied to the section due to the eccentricity of the strands. The stresses encountered at transfer and during service conditions were examined in the software. Good programming practices such as minimised storage structures and the development of an efficient matrix solver were integral to the development of an effective software tool. Finally, the results produced by the software were examined and compared with those calculated using an established finite element analysis package. Ansys was chosen for this purpose as it has the flexibility to be applied to this particular application.

The process of writing the software showed that an extensive amount of work was involved in debugging the code. An understanding was developed of the stages of evolution through which software of this type passes before completion. The software produced results that were broadly in line with those predicted by Ansys. However, the arduous task of setting up the model in Ansys showed that software tailored for use in the prestressed concrete field that would produce reasonably accurate results would have a place in industry.

Table of contents

VOLUME 1

Table of Figures

Table of Tables

Nomenclature

$\bar{y}$	Distance to centroid in the y-direction
ω	Applied uniformly distributed load
ϕ	Creep coefficient
φ	Nominal diameter of the strand
ν	Poisson's ratio
α	Prestressing force loss ratio
ε_{∞}	Final creep strain
$\delta_{\omega\text{-creep}}$	Additional deflection occurring after creep has occurred
$\delta_{\omega\text{-serv}}$	UDL deflection as measured after member has gone into service
$\delta_{\omega\text{-tran}}$	UDL deflection as measured soon after transfer
α_1, α_2	Constants used in displacement function
ε_c	Strain in the concrete
σ_{cg}	Stress in concrete at the strand depth due to self-weight
δ_{creep}	Decrease in the upward camber due to creep losses
ε_{cu}	Ultimate concrete strain
σ_{cv}	Total Stress in concrete at the strand depth post transfer
ε_e	Concrete prestrain at the strand level
α_e	Modular ratio
γ_m	Partial safety factor for strength of materials
δ_{max}	Maximum deflection
δ_{min}	Minimum deflection
ε_{pa}	Strain in the strand due to applied load
ε_{pb}	Strain in the strand at the ultimate limit state
ε_{pe}	Strain in the strand due to prestress
ω_{perm}	Permanent UDL (uniformly distributed load)
$\delta_{permanent}$	Deflection due to permanent loads
δ_{Pi}	Deflection due to prestressing before service losses occur
$\delta_{prestress}$	Deflection due to prestressing force
ε_s	Strain in the steel

ω_{semi}	Semi-permanent UDL
$\delta_{semi\text{-}permanent}$	Deflection due to semi-permanent loads
ε_u	Concrete stain at stand level at collapse
θ_x	Rotation about the x-axis
ε_x	Strain in the x-direction
σ_x	Stress in the x-direction
γ_{xy}	Shear strain in the x-y plane
τ_{xy}	Shear stress in the x-y plane
θ_y	Rotation about the y-axis
ε_y	Strain in the y-direction
σ_y	Stress in the y-direction
[ ]	Indicates a matrix
[A]	Coefficient matrix associated with displacements
[B]	Matrix relating element strains to element nodal displacements
[D]	Elasticity matrix
[H]	Stress-displacement matrix
$[H^b]$	Stress-displacement matrix relating to plate bending elements
$[H^e]$	Elemental stress-displacement matrix
$[H^p]$	Stress-displacement matrix relating to plane stress elements
$[K^b_{ij}]$	Sub matrix ij relating to the plate bending stiffness
$[K^e]$	Stiffness matrix
$[K^p_{ij}]$	Sub matrix ij relating to the plane stress stiffness
[L]	Factorised matrix
{ }	Indicates a vector
$\{\delta^{*e}\}$	Arbitrary set of nodal displacements
$\{\delta(x, y)\}$	Displacement at any point in a plate
$\{\sigma\}^b$	Stresses due to plate bending
$\{\sigma\}^p$	Stresses due to plane stress
$\{\delta^e\}$	Displacement matrix
$\{F^e\}$	Nodal forces vector
A	Area of concrete in the cross-section
A_{cc}	Area of concrete in compression

A_{ps}	Area of the prestressing strand
b	Breath of the section
b_v	Effective width of section resisting shear.
d	Depth from the top fibre of concrete to centre of the strand
D	Flexural rigidity
D_1	Coupling rigidity
d_c	Depth from the top fibre of concrete to centre of compression block
D_x	Flexural rigidity in the x-direction
D_{xy}	Torsional rigidity
D_y	Flexural rigidity in the y-direction
e	Eccentricity of the stand
E_c	Final Young's Modulus of mature concrete
E_{ci}	Young's modulus of the concrete at transfer
E_s	Young's Modulus of steel
F_c	Compressive force in the concrete
f_c	Compressive stress
F_{ci}	Strength of the concrete at transfer
f_{cu}	Characteristic strength of concrete
$F_{p,\ 0.1}$	0.1% proof stress
f_{pb}	Stress in the strands
f_{pt}	Stress in the bottom fibre of the concrete due to prestress
f_{pu}	Characteristic strength of the strands
F_t	Force in the prestressing strand
f_t	Principle tensile stress
F_x	Force in the x-direction
F_y	Force in the y-direction
F_z	Force in the z-direction
G	Modulus of elasticity in shear
h	Overall depth of section
I	Second moment of area
I_x	Second moment of area of section about the x-axis
I_y	Second moment of area of section about the y-axis
k_1	Characteristic ratio of stress block

K_t	Coefficient relating to the surface grip provided by the strands
L	Span of the member
l_t	Transmission distance
M	Applied moment
M_0	Moment necessary to produce zero stress in the bottom fibre
M_f	Moment due to prestressing force after losses
m_{ii}	Elements within the [L] matrix
M_p	Moment due to eccentric prestressing force
M_s	Applied moment at service
M_{sw}	Moment due to self-weight
M_u	Ultimate moment capacity of a section
M_{ult}	Bending moment at the ultimate limit state
M_x	Internal bending moment in the x-direction
M_{xy}	Internal twisting moment in the x-y plane
M_y	Internal bending moment in the x-direction
P	Prestressing force
P_0	Prestressing force before transfer
P_f	Prestressing force after losses
P_i	Prestressing force before service losses occur
P_{losses}	Loss in prestressing force
P_x	Prestressing force at a distance x from the end of the member
s_x	Width of element
s_y	Height of element
t	Thickness of the plate
T_x	Moment about the x-axis
T_y	Moment about the y-axis
T_z	Moment about the z-axis
u	Displacement in the x-direction
v	Displacement in the y-direction
v_c	Design concrete shear stress
V_{c0}	Uncracked shear capacity
v_{c0}	Uncracked shear strength
v_{cr}	Cracked shear strength of the section

V_{ult}	Shear force at the ultimate limit state
w	Deflection of the plate in the z-direction
W_{ext}	External work
W_{int}	Internal work
x	Depth of compression block
y	Distance from top or bottom fibre to neutral axis

1. INTRODUCTION

1.1. Introduction

Precast concrete construction is an increasingly attractive method for delivering high quality structures in an environment where tight construction programs are the norm. As is apparent throughout Dublin, very few building sites are green field developments with most building sites having a footprint identical to the building being constructed on it. With these limitations on both time and storage space on construction sites the advantages of precast concrete become clear. The precast member arrives on site on a truck and is placed by crane most likely within a few hours, removing the need for storage on site. The biggest advantages are achieved where precast beams and slabs are utilised. In-situ beam and slab construction requires temporary formwork to be constructed, reinforcement to be placed and checked, and the concrete itself to be placed and compacted. Precast concrete construction on the other hand allows the member to be cast under factory conditions with good quality control being much easier to achieve than on site, the only concern is placing the member by crane.

Prestressing concrete slabs allows even greater efficiency to be achieved with thinner and lighter cross-sections carrying similar loads with excellent deflection performances. This efficiency also allows greater spans to be constructed and heavier loads imposed. Specialist structures such as car parks in which spans of the order of 16.5m are commonplace are often constructed almost entirely from precast concrete with the prestressed slabs providing the flooring.

1.2. Research aims and objectives

The aim of this project was to develope a prototype structural engineering software package to assist in the analysis and design of prestressed concrete slabs. The analysis of prestressed slabs is often complicated by the presence of openings and line loads due to walls at various locations along the span of the slab making the use of analyses based on simple elastic methods impractical.

The use of a finite element method of analysis allows for an accurate evaluation of the stresses and deflections throughout the slab. The analysis tool envisaged would allow slab manufacturers, without a large technical staff with specialised knowledge in finite element analysis, to carry out reasonably detailed analyses of slabs.

The key areas requiring study and investigation before the heart of the project could commence were as follows:

- Prestressed concrete theory
- Finite element theory
- Matrix algebra
- Programming techniques
- The use of Ansys for testing purposes

The final product is intended to present the user with the simplest possible interface, completely tailored towards the prestressed concrete industry, and one of the main goals is to hide the complexity of finite element from the user.

1.3. Background to the research

The genesis of this research stemmed from a query from within the precast concrete industry relating to the establishment of critical stresses on slabs with notches or openings and complicated loading patterns. As noted earlier, elastic analysis provides a crude estimation of the actual stresses encountered in these more complicated situations and therefore a definite gap exists in the designer's arsenal of methods and techniques for checking stresses.

Therefore, the author therefore is focusing this research on uniting two established areas of theory to produce the software – that of prestressed concrete and that of the finite element method. It is not the author's aim to develop new theories but to employ tried and trusted methods within a software package to produce the prototype for a software suite required by industry.

1.4. The outline of the thesis

This thesis details the processes involved in producing the prototype analysis software. Chapters two and three describe the theory of prestressed concrete theory and also that of the finite element method both of which will be employed in the software. The chapter relating to prestressed concrete also deals with the method of manufacture to help the reader understand its implications for the application of the theory. The fourth chapter examines the programming techniques employed to implement the theories that were discussed in the previous chapters. This chapter also shows the logical progression through the software from the initial selection of geometry to the display of results as well as discussing the logic of these processes. Chapter 5 investigates the debugging process used to check the software during the development phase and the testing that was subsequently carried out. The chapter will focus particularly on the use of Ansys to model prestressed slabs. Chapter 6 shows the results of a number of analyses carried out in Ansys according to the procedure established in the previous chapter. These results will then be compared with results of analyses carried out in the software produced. Finally Chapter 7 gives the conclusions of the research and outlines further research that could be carried out on the topic.

2. PRESTRESSED CONCRETE

2.1. Introduction

Prestressed concrete can be defined as '*concrete in which internal stress of such a magnitude and distribution have been introduced that the stresses resulting from the given applied loading are counteracted to a desired degree*' (Kong and Evans 1998:333). In the simplest possible terms the aim of prestressing is to prevent tension from occurring in the member. The internal stresses that are induced in the concrete are developed essentially by stressing a number of steel strands to seventy percent of their breaking stress, pouring concrete into a mould with the strands in place and once the concrete has obtained sufficient strength releasing the strands. As these stands relax and attempt to shorten back to their original length the bond between the strands and concrete transmits the force into the concrete which in turn develops compressive stresses. Figure 2.1 (O'Brien and Dixon 1995:291) shows this process.

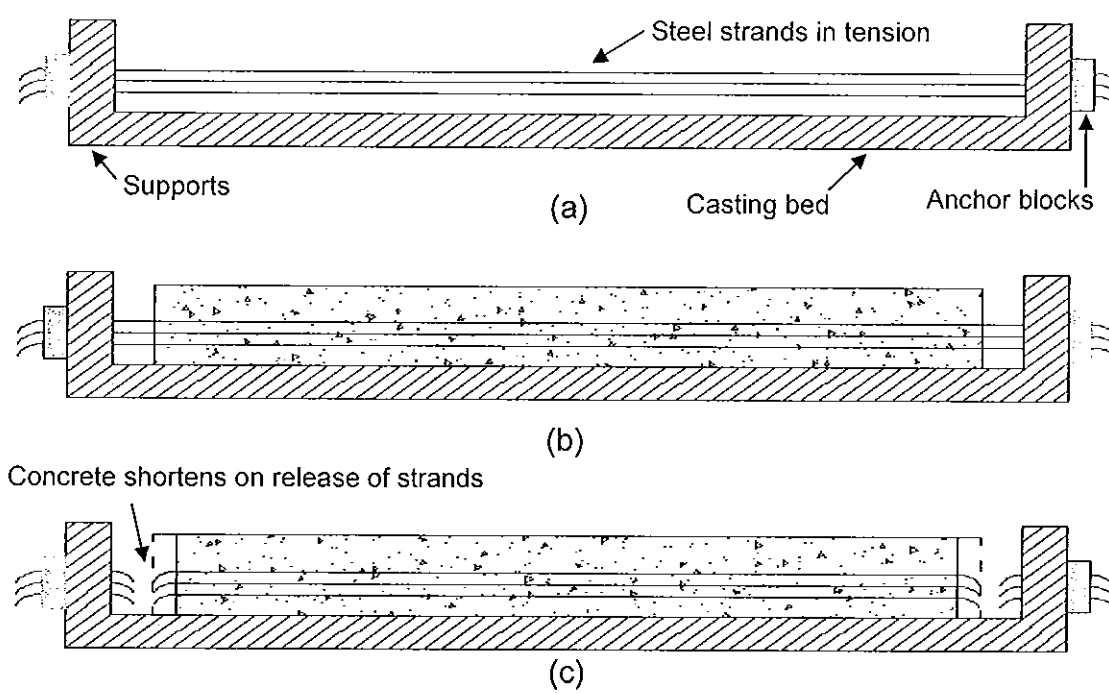

Figure. 2.1 (a) strands are tensioned (b) concrete is cast (c) strands are cut

Concrete has a compressive strength approximately ten times greater than its tensile strength and therefore for some design work this tensile strength is

actually ignored. By inducing a sufficiently large compressive stress in the concrete during the manufacturing of the slab, the tensile stress due to the service bending moment are negated.

2.2. Theory

The design of prestressed concrete elements is similar in many ways to that of post tensioned members. The main design differences between pre-tensioned and post-tensioned members is the eccentricity of the strands and the difference in how stresses are transferred from to steel to the concrete. Post-tensioned members may have varying eccentricity along the length of the member. Due to the manufacturing technique used in producing precast slabs the eccentricity of the strand is constant along the length of the member. With post-tensioning however, the ducting in which the strand is situated may follow almost any pattern and therefore give the designer particular eccentricity values at various locations along the slab. The second difference stems from the nature of the transfer of stresses from the strand to the concrete. The jacking force is applied at the ends of the member after the concrete has achieved the required strength and therefore unlike prestressed concrete slabs a uniform force along the length of the member is achieved.

2.2.1. The basic principles

A typical prestressed beam is show below in Figure 2.2(a) to demonstrate the benefits of prestressing over ordinary reinforced concrete. A beam is taken as the example but slabs are designed using the same method where the slab is treated as a wide and shallow beam. The beam shown has a single strand with a tensile force 'P' acting upon it. This strand is at a distance 'e' from the centroid. In the case of a solid body, such as that shown, the centroid is located at mid-depth. It should be noted however that most slabs are not solid and the centroid must be found for these sometimes complex cases. The force 'P' acting at an eccentricity 'e' results in a moment about the centroid given by 'M_p'. The stresses resulting from 'P' and 'M_p' are given in Figure 2.2(b) and 2.2(c), with the result of these two stresses combined shown in Figure 2.2(d). The

stresses that have been set up thus far in this model do not account for the self weight of the beam or any of the applied loads.

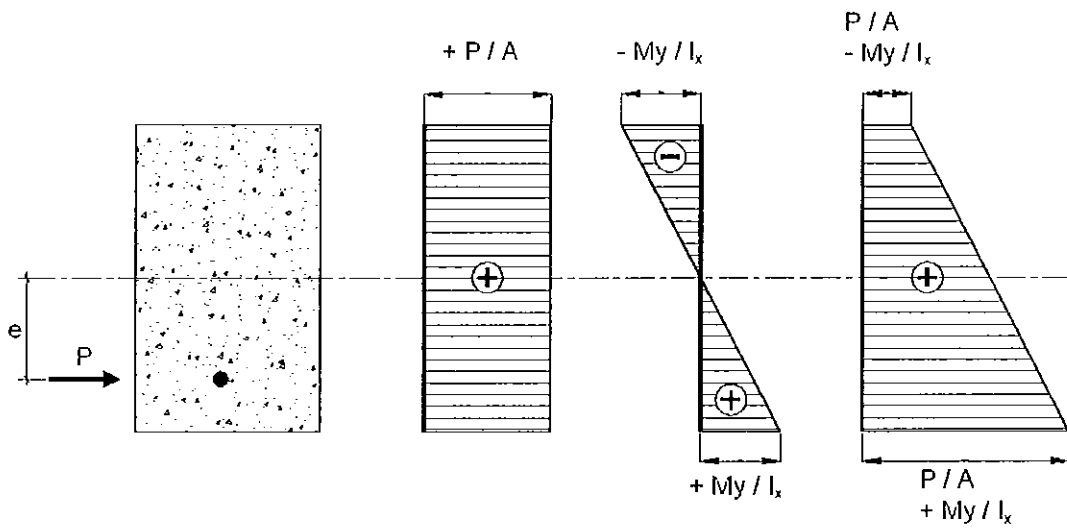

Figure 2.2 stress profile due to prestressing

The importance and effect of the eccentricity of the strand is best demonstrated by comparing an example of an eccentrically and a non-eccentrically prestressed member. Figure 2.3(a) shows the stresses resulting from the prestressing of a beam with an eccentric strand. The moment due to the prestressing force is given by 'M_p'. A gravity load is then applied to the member resulting in a bending moment which gives a stress profile shown in Figure 2.3(b). The combined effect of the prestressing stresses and the stresses due to the applied loads are given by Figure 2.3(c).

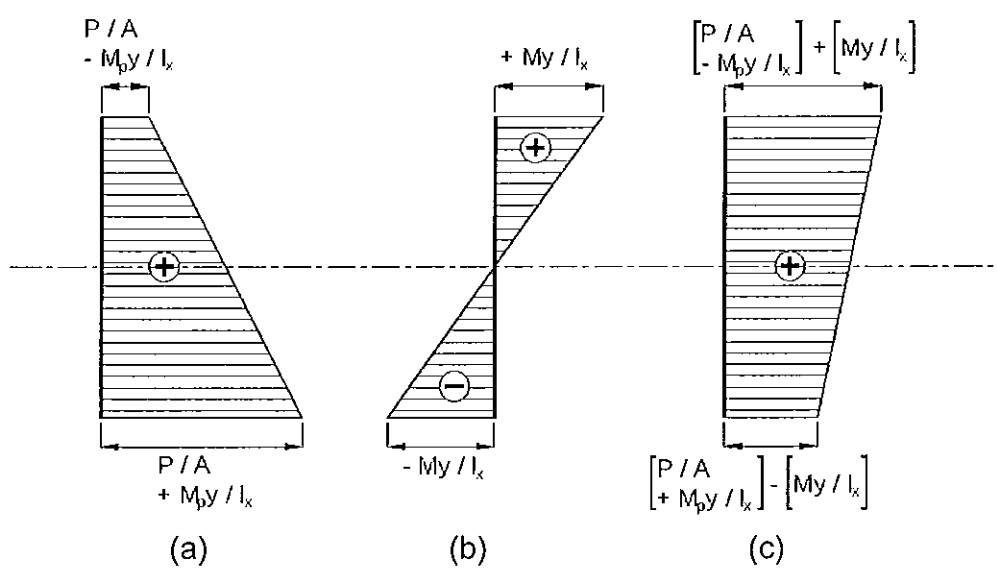

Figure 2.3 benefit of eccentrically applying prestress force

In contrast, if the prestressing strand was located at the centroid of the member, the stress profile shown in Figure 2.4(a) would be the result. The applied loads would again result in the same stress profile as given in Figure 2.3(b) which is repeated for clarity below in Figure 2.4(b). Again the resulting combined stress profile is shown in Figure 2.4(c).

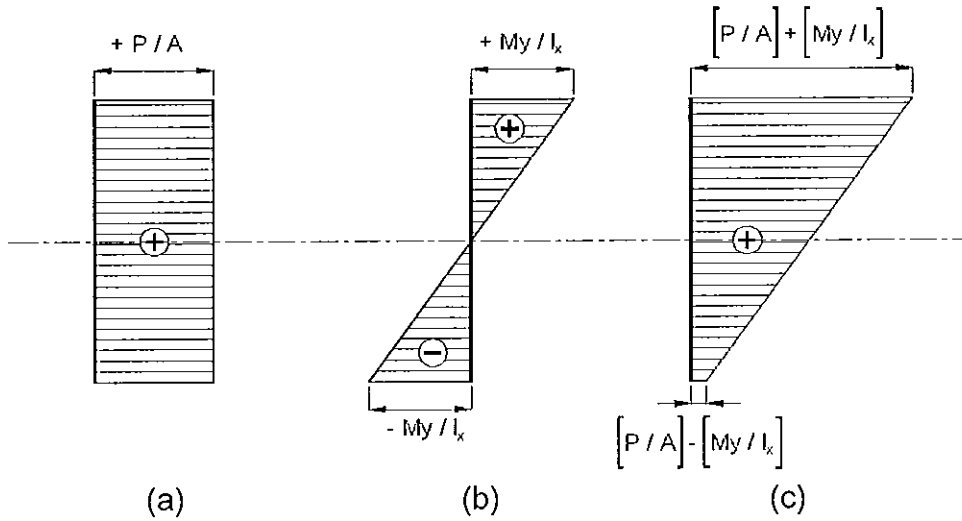

Figure 2.4 effect of applying prestress force centroidally

A comparison of the two combined stress profiles shows that the top stresses in the centroidally prestressed member are significantly higher than those at the same location in the eccentrically prestressed member. Also the compressive stress in the bottom fibre of the centroidally prestressed member is very low and a small increase in the applied moment would reduce these stresses even further to the point where tensile stresses would then occur. As will be explained below, limited tensile stresses are allowed in some prestressed concrete members but generally this can be seen as a limiting factor with regard to a members capacity. The eccentrically prestressed member has a more even distribution of stresses throughout its depth potentially allowing significantly greater applied loads to be carried.

At this point it should be clarified that the British standards set out three different serviceability classifications which relate to the tensile stresses that are allowed in the slab (BS 8110: Part 1: 1997, Clause 4.3.4.3).

Class 1 members are designed allowing no tensile stresses

Class 2 members allow tensile stresses however their magnitude is limited to no greater than the design flexural tensile strength of the concrete. The tensile strength is generally taken as $0.45\sqrt{f_{cu}}$. This class is precluded from showing any visible signs of cracking

Class 3 members also allow tensile stresses and furthermore the member is assumed to have to have cracking on the tension face. The design is carried out based on an uncracked section with a hypothetical tensile stress capacity greater than that outlined for class 2 members. Crack widths are limited however and the British standards recommend limits on the crack widths of 0.2mm for normal conditions and 0.1mm for more severe conditions. In practice this is achieved by limiting the hypothetical design tensile strength, for example, a member cast from 50N/mm^2 concrete under normal conditions has an allowable crack with of 0.2mm. Table 4.2 in BS8110: Part 1: 1997 then allows a hypothetical design tensile stress of 5.8N/mm^2 to be used in the calculations.

Generally slabs are designed as class 2 members as this leads to the most efficient design whist still satisfying other requirements such as deflection and durability.

2.2.2. Stresses

It can be seen from the manufacturing process that the members go though two distinctly different loading patterns from when the members are first cast to the stage when the structure has gone into service. The first stage is encountered when the strands are released allowing the prestressing force in the member to develop in what is most likely young concrete. This case is called 'transfer'. Once the slab has obtained its full design strength and has been brought to site and placed, it will be subject to greater imposed loads. This case is known as 'service'.

2.2.2.1. Transfer

As will be outlined later in Section 2.5, the practicalities of manufacturing slabs dictate that the less time the slabs are left on the casting beds the more slabs can be produced. As the concrete mix used gains most of its strength in the first twenty four hours after casting this allows the slabs to be moved to a suitable storage location to continue gaining strength. The normal duration of the curing and initial strength development period is as little as 10 hours. At this point the strands are cut and, as they attempt to contract, the force is imparted to the concrete through the bond between the strands and the concrete.

Figure 2.5(a) shows an eccentrically prestressed member similar to that in Figure 2.2(a). If it is assumed that the prestressing force is of a similar magnitude in both diagrams but the eccentricity is greater in Figure 2.5(a) then the resulting stresses due to the eccentricity will also be greater, see Figure 2.5(c).

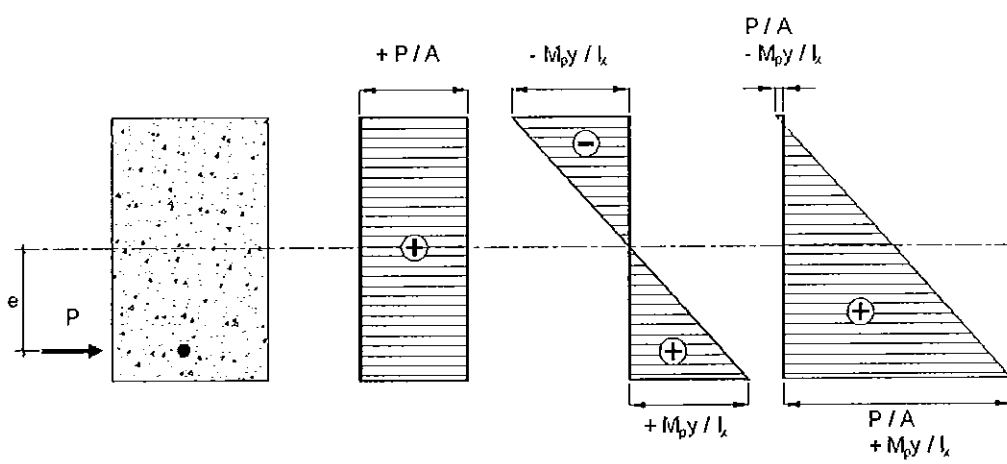

Figure 2.5 stress check at transfer state

The resulting stress profile, given in Figure 2.5(d), shows a larger compressive stress in the bottom of the member and a small tensile stress in the top. As noted earlier tensile stress are often undesirable. However, at the moment when the strands are cut and transfer occurs, the member cambers upwards due to eccentric prestressing force. As this slight upward camber occurs the contact between the casting bed and the under side of the member is broken and its weight is carried by its two ends. The self weight induces a small

bending moment in the member denoted by 'M_{sw}'. Figures 2.6(a), (b) and (c) show how the stress resulting from this small bending moment effects the overall stress.

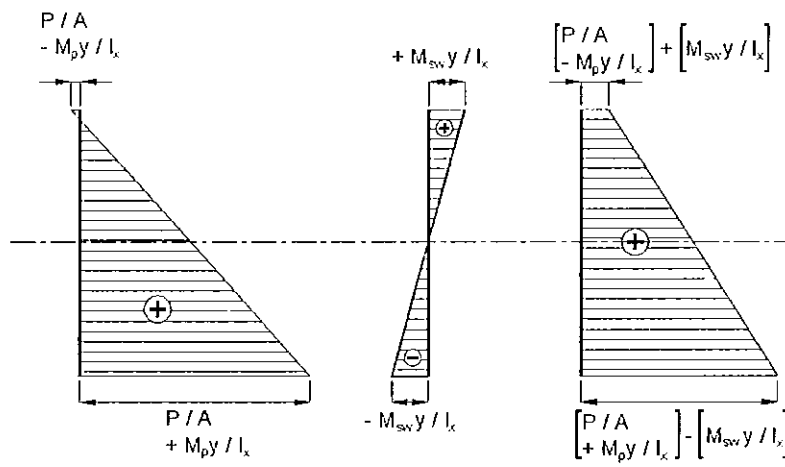

Figure 2.6 contribution of self weight at transfer

The self weight bending stresses, M_{sw}, shown in Figure 2.6(b) when added to the stresses generated by the prestressing process help to reduce the compressive stresses in the fibres and more importantly negate the tensile stresses in the top fibres. If the top fibre stresses are compressive, even if these stresses are very small, then cracking will not occur.

The check for the bottom fibre compressive stress is carried out based on a concrete strength that is achieved normally in less than a day. A number of cube tests would be carried out to verify that this 'transfer strength' has been reached.

2.2.2.2. Service

The other stress condition that must be checked is when the beam is at the service stage. The unfactored applied loads give rise to the moment at service which is given by 'M_s'. The peak service stresses occur when the building has been fully completed and has gone into active use, at which stage the losses in the prestressing force discussed in Section 2.3 will have occurred. The final prestressing force which is typically about eighty percent of the initial prestressing force is given by 'P_f'.

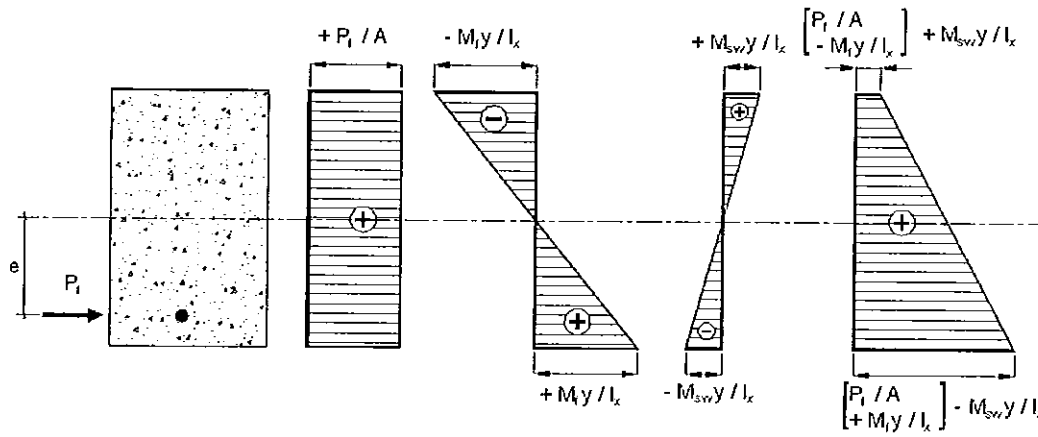

Figure 2.7 stress check at service state before loading

Figure 2.7(c) shows the effective prestressing stresses after losses have been taken into account. Once again the stresses due to moments caused by self weight are show in Figure 2.7(d). This will contribute towards reducing the stresses giving the stress profile show in Figure 2.7(e). This profile is the state of stress in the section before the imposed service loads are applied.

Shown in Figure 2.8(b) is the stress profile due to the applied loads encountered by the slab during service. It can be seen again that the stresses due to the applied service loads reverse the stresses in the member. The resulting profile in Figure 2.8(c) gives the net stresses in the section that must be checked. The bottom fibre is only critical if there are tensile stresses present in the case of a class 1 member or tensile stresses greater than $0.45\sqrt{f_{cu}}$ in the case of class 2 members as any compressive stresses that may occur would be relatively small.

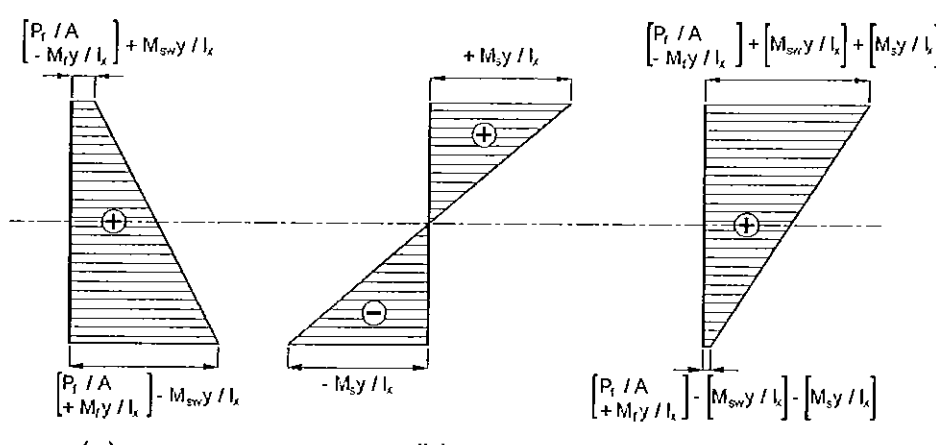

Figure 2.8 stress check at service state after application of loads

The top fibre stress must be checked to ensure that the compressive stress is less than the allowed stress in the concrete. The design strength of the concrete is based on the twenty eight day strength for the service checks as at least this length of time will have passed from casting to introducing the structure to its use.

2.2.3. Ultimate limit state

The design checks discussed above relate to the stress checks carried out for a member under normal working conditions experienced during 'service'. However ultimate limit state design checks require the designs to be checked at the most extreme case. At the ultimate limit state all factors of safety are applied to check the slab for shear and bending. To this end, the imposed dead and live loads and the self-weight are factored up whilst material strengths are reduced to allow for imperfections.

2.2.3.1. Ultimate moment capacity

The ultimate moment capacity checks carried out on prestressed members is similar to that for ordinary reinforced concrete members with a prestrain in the steel. The member would be cracked in tension from the bottom most fibre to the neutral axis as expected in a similar reinforced concrete member. The compression stress block used is shown in Figure 2.9 and has been taken directly from BS 8110: Part 1: 1997, clause 3.4.4.4.

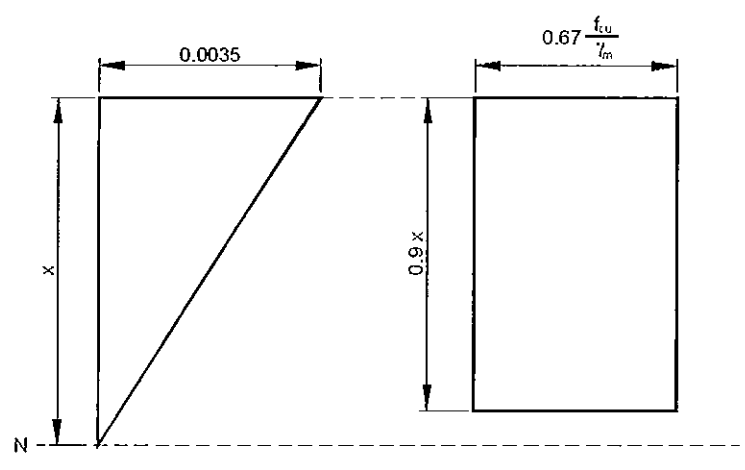

Figure 2.9 simplified compression block

The ultimate moment capacity, M_u, is given by the following formula derived simply by taking the moment of the force acting through the strand about the centre of the compression block. The depth from the top fibre to the neutral axis is denoted by 'x'. Equation 2.1 gives the ultimate moment capacity of a solid slab.

$$M_u = f_{pb} A_{ps} (d - 0.45x) \qquad (2.1)$$

The area of the strands 'A_{ps}' and the effective depth to the centroid of the strands 'd' are found from the table of properties for strands and simple geometry respectively. However the stress in the strands 'f_{pb}' is more difficult to evaluate due to the stress-strain properties of the steel used in the prestressing process and the presence of the prestress force itself. The more general case of a voided slab presents further complications as the compression block would not be rectangular and therefore the depth to the centroid could not be assumed to be at half the depth of the compression block. Figure 2.10(a) shows the compression block for a voided slab. The simplified stress block given in BS 8110 allows for a uniform stress profile to be taken over 0.9 times the depth to the neutral axis rather than the more complicated parabolic stress profile.

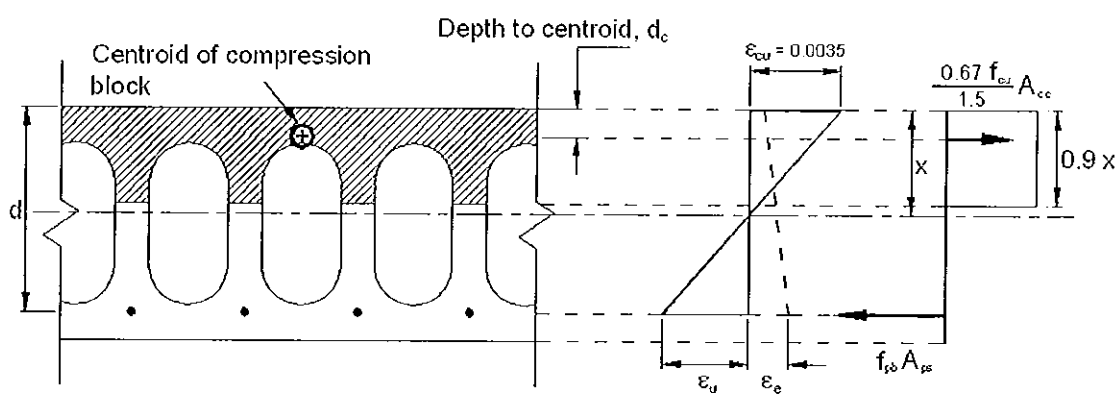

Figure 2.10 compression block for a typical voided slab

The depth to the centroid of the simplified compression block is found by dividing the first moment of area of the compression block about its top fibre by its area. This quantity is denoted by 'd_c'. Once 'd_c' has been established, the lever arm about which the prestressing force is acting may be found. The moment capacity equation given above in Equation 2.2 can be altered to reflect the general case for a voided slab as given in Figure 2.10(c) or solid slab.

$$M_u = f_{pb} A_{ps} (d - d_c) \tag{2.2}$$

The remaining variable, 'f_{pb}', the stress in the strands presents a more challenging calculation. The stain in the strand at the ultimate limit state, ε_{pb}, is given by Equation 2.3.

$$\varepsilon_{pb} = \varepsilon_{pe} + \varepsilon_{pa} \tag{2.3}$$

The two component strains, ε_{pe} and ε_{pa} represent the strain due to the strand prestress and the strain due to the applied load respectively. The force taken for calculating ε_{pe} is the post losses prestressing force which gives Equation 2.4

$$\varepsilon_{pe} = \frac{\left(P_f \Big/ A_{ps} \right)}{E_s} \tag{2.4}$$

The strain resulting from the additional applied loads has two components, the concrete prestrain at the strand level ε_e, and the concrete strain at the strand level at collapse, ε_u. This is given in Equation 2.5

$$\varepsilon_{pa} = \varepsilon_e + \varepsilon_u \tag{2.5}$$

$$\text{Where } \varepsilon_e = \frac{\frac{P}{A} + \frac{Pe^2}{I_x}}{E_c} \tag{2.6}$$

To find the concrete strain at failure refer to Figure 2.10(b) where it can be seen that:

$$\varepsilon_u = \frac{d - x}{x} \varepsilon_{cu} \tag{2.7}$$

These strains can be summed as follows and then an expression for x, the depth to the neutral axis, can be derived.

$$\varepsilon_{pb} = \varepsilon_{pe} + \varepsilon_e + \left(\frac{d - x}{x} \varepsilon_{cu} \right) \tag{2.8}$$

$$x = \frac{\varepsilon_{cu} d}{\varepsilon_{pb} - \left(\varepsilon_{pe} + \varepsilon_e - \varepsilon_{cu} \right)} \tag{2.9}$$

The next step involves equating the internal forces within the slab, i.e. the tensile force in the steel strands and the compressive force in the compression block for the concrete. The force in the steel is given by Equation 2.10.

$$F_t = A_{ps} f_{pb} \tag{2.10}$$

The compressive force is a function of design stress of concrete and the area of concrete in the notional compression block as shown below.

$$F_c = \frac{0.67 f_{cu}}{1.5} A_{cc} \tag{2.11}$$

If the section under examination is a solid rectangular member then $A_{cc} = 0.9bx$, where b is the breadth of the member. By equating the forces and expressing the variables in terms of the stress, f_{pb}, the following equation is found where k_1 is equal to 0.405

$$f_{pb} = \frac{k_1 f_{cu} b}{A_{ps}} x \tag{2.12}$$

Equation 2.9 can be substituted into Equation 2.12 to allow the stress in the strand, f_{pb}, to be related to the strain ε_{pb}

$$f_{pb} = \frac{k_1 f_{cu} b}{A_{ps}} \frac{\varepsilon_{cu} d}{\varepsilon_{pb} - \left(\varepsilon_{pe} + \varepsilon_e - \varepsilon_{cu}\right)} \tag{2.13}$$

As all the other variables in this equation are known, it is now possible to plot the range of strain verses stress values that satisfy this equation. However, only one point will also satisfy the constraints given by the stress-strain diagram for the steel. Shown below is a solution which satisfies both constraints.

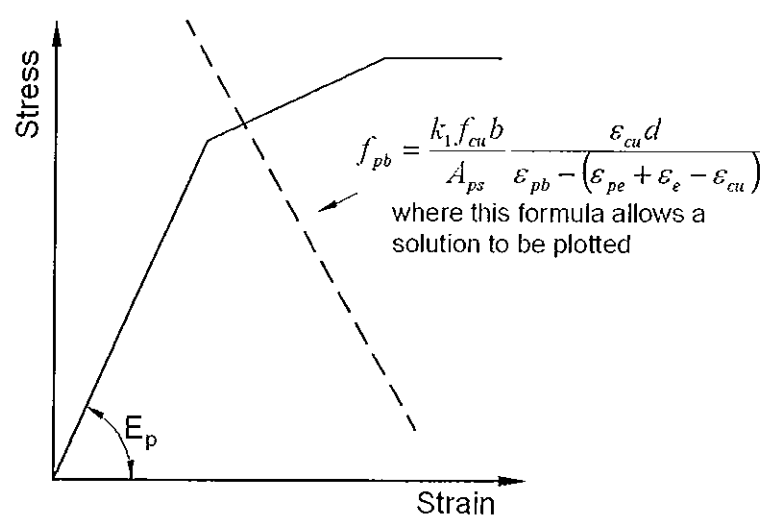

Figure 2.11 possible solution giving 'f_{pb}' and 'ε_{pb}'

The solution provides values for f_{pb} and ε_{pb} in the strands and by substituting the strain value into Equation 2.9, the depth to the neutral axis may be found. The ultimate moment capacity may now be found as both the stress in the strands and the effective lever arm, (d – 0.45x), have been calculated.

$$M_u = f_{pb} A_{ps} (d - 0.45x) \qquad (2.14)$$

A problem arises however where the concrete compression block, whose area is given by A_{cc}, is not rectangular as is the case for hollow core slabs. The simplest method of achieving a satisfactory solution to this is to use an iterative technique. First the equilibrium equation must be developed in general terms as shown in Equation 2.15 which is developed by equating Equation 2.10 and 2.11.

$$f_{pb} = \left(\frac{0.67 f_{cu}}{1.5} \right) \frac{A_{cc}}{A_{ps}} \qquad (2.15)$$

The area of the compression block A_{cc}, is based on the area of concrete that is present above the neutral axis which is obviously less in a voided slab than in a solid slab. However, to comply with the suggested simplified stress block given in the British Standards the depth of the compression block must be reduced to 0.9x. This is shown in Figure 2.10(a) where the shaded area can be seen to show the assumed compression block.

The first step in the iterative process is to assume a value for x from which the area of the compression block can be estimated. Referring to Equation 2.8, the trial value of x assumed can be used to calculate ε_{pb} and then using this value the Young's modulus for the steel may be used to calculate the trial value for the stress in the strands f_{pb}. The value for x taken is then used to calculate the area of concrete in compression. The area of the compression block may then be substituted into Equation 2.15 to produce a second value for the stress in the strands which if found to be within a specified tolerance to that found from the compatibility equation would verify the assumed depth to neutral axis chosen. If the two stress values differ by a value greater than the tolerance then a higher or lower value for x is used and the process repeated. Once a satisfactory convergence is achieved the value for f_{pb} is deemed to be the ultimate stress

acting within the strands. The centroid of the compression block determined earlier is now known and its location is given with respect to the top fibre of the slab. This is denoted by d_c and allows the lever arm, $(d - d_c)$ to be found. As shown in Equation 2.16 the ultimate moment capacity of the slab can be calculated from

$$M_u = f_{pb} A_{ps} (d - d_c) \qquad (2.16)$$

It can be seen that, if a similar ultimate moment capacity check is carried out on a similar slab where the strands are unstressed at casting, the ultimate moment capacity decreases by as little as 20%. However, the deflections would increase greatly and cracking would become critical. This process is shown below in the flowchart in Figure 2.12.

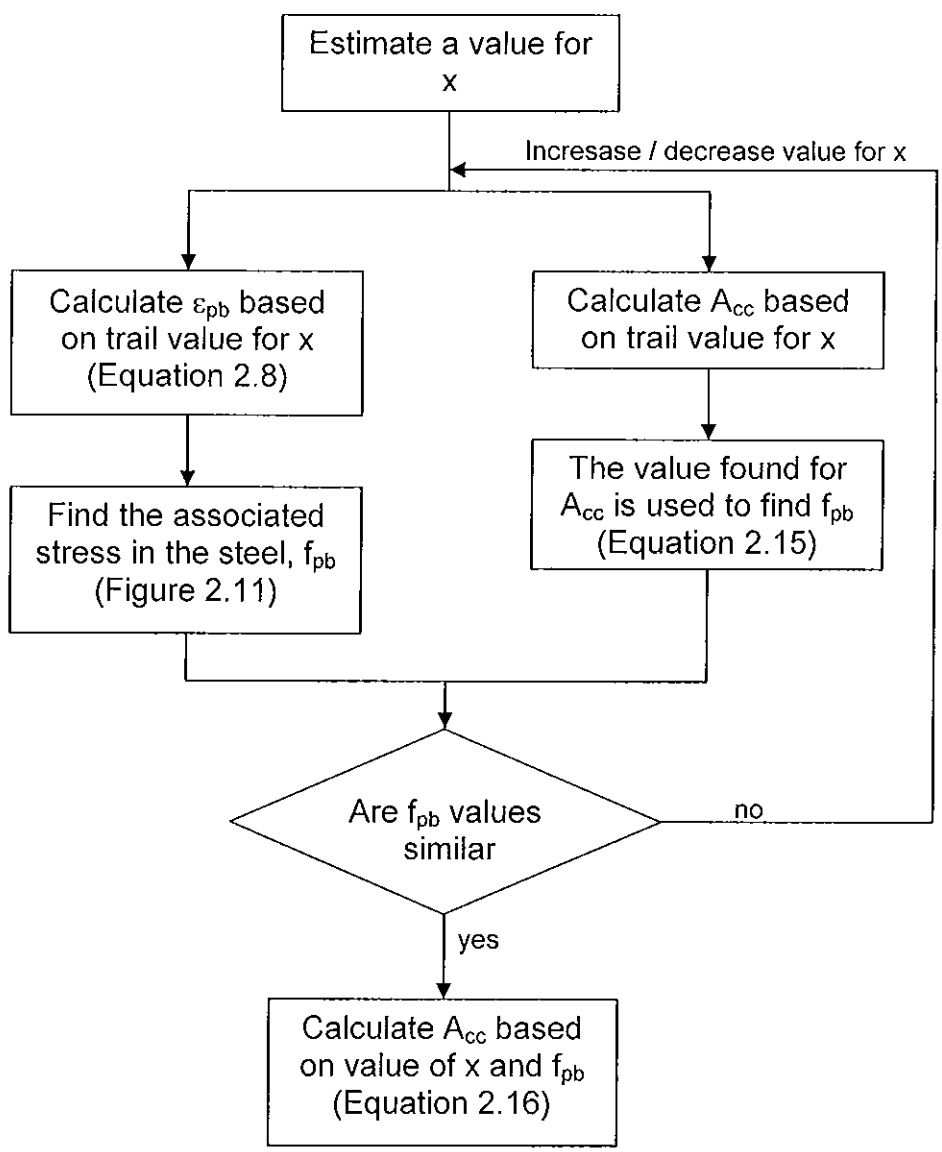

Figure 2.12 Process used for finding ultimate moment capacity

2.2.3.2. Ultimate shear capacity

The ultimate shear capacity of a slab is determined by the aggregate interlock in the concrete and dowel action provided by the strands. The degree of compaction in the concrete is a major factor in the shear capacity of a section. However, it is primarily affected by whether or not the section under consideration is cracked. Unlike a traditional reinforced concrete slab, the soffit of the slab would not be cracked across the full span distance at the ultimate limit state due to the prestressing force. The simple case of a slab resisting a uniformly distributed load demonstrates the requirement for cracked and uncracked portions of the slab to be considered separately. Figure 2.13 shows the bending moment diagram due to imposed loads and also the moments due to the prestressing force.

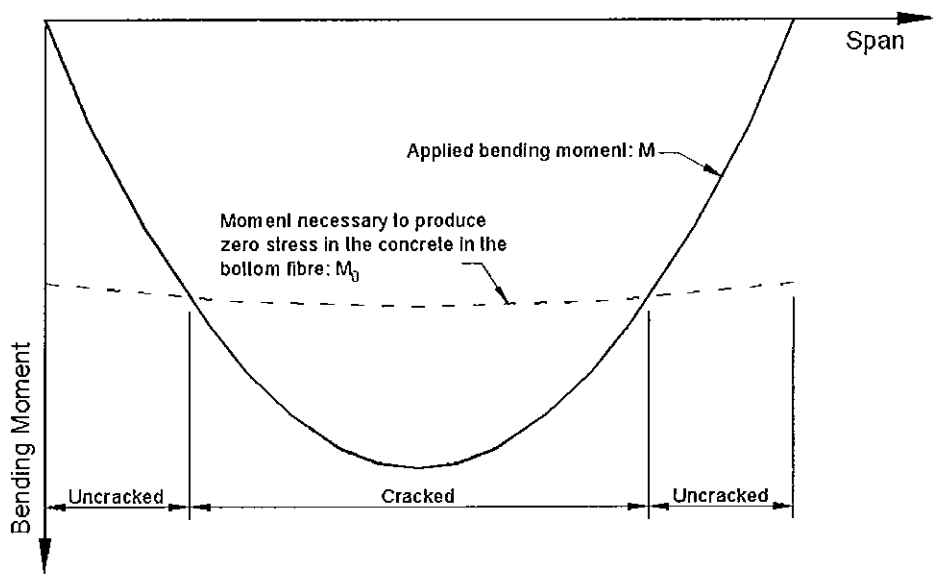

Figure 2.13 cracked and uncracked zones

These moments due to the prestress have the effect of reducing or cancelling the tensile stresses resulting from the gravity loads. The regions where the stresses in the bottom fibre of the slab are either zero or compressive are deemed to be uncracked and therefore the cross sectional area of concrete available to resist the applied shear force is at its greatest. As the centre portion of the slab comes under consideration it can be seen that tensile stresses would occur and therefore the section must be treated as cracked.

The first step in a shear capacity check is to determine which portions of the slab are considered cracked and which are considered uncracked. The moment due to the prestressing force is given by M_0 and shown in Equation 2.17

$$M_0 = \frac{0.8 f_{pt} I_x}{y} \tag{2.17}$$

It is noteworthy that f_{pt}, the stress in the bottom fibre of the slab due to prestress, is derived from the post losses prestressing force. Therefore the value of M_0 can be seen to vary across the span in accordance with the loss of prestressing force as described in Section 2.4. A factor of safety of 0.8 is applied to the bottom fibre stress to account for variances experienced during experimentation and load tests carried out on slabs. The bending stresses due to the applied loads are calculated using loads that are factored in accordance with limit state design. As seen above in Figure 2.12, when the two bending moment diagrams are added to produce the net bending moment diagram the resulting stresses show clearly where the bottom fibre stresses are compressive or tensile and therefore cracked or uncracked.

Uncracked shear capacity

The formula for calculating uncracked shear capacity is obtained by examining the stresses within an element in a region of the uncracked concrete using Mohr's circle analysis. The applied stresses acting on this element are the compressive stresses due to the prestress and a shear stress due to the applied loads. Shown below in Equation 2.18 is the principal tensile stress, f_t, resulting from the compressive stresses, f_c and the uncracked shear strength, v_{c0}.

$$f_t = \frac{1}{2}\sqrt{\left(f_c^2 - 4v_{co}^2\right)} - \frac{1}{2} f_c \tag{2.18}$$

The tensile stress within the concrete is limiting factor with respect to the shear capacity and therefore by reorganising the variables the maximum shear stress is given.

$$v_{c0} = \sqrt{\left(f_t^2 + f_c f_t\right)} \tag{2.19}$$

For a solid rectangular section the shear capacity V_{co}, is given by the following where the area of the section is a function of the overall depth, h, and the effective width, b_v.

$$V_{c0} = \frac{2}{3} b_v h . v_{c0} \qquad (2.20)$$

The more general form of this equation allows slabs with voids of any shape to be considered. This is given by Equation 2.21.

$$V_{c0} = \frac{b_v I_x}{A\bar{y}} v_{c0} \qquad (2.21)$$

The width of section used in this equation, b_v, is based on the cumulative width of the webs of the sections between the voids. It should noted that where the width of the web varies, the narrowest point should be taken as the critical section. Also, $A\bar{y}$, is the first moment of area of the concrete above the centroidal axis.

The British standards recommend that the compression due to the prestressing force value be reduced by 0.8 as a factor of safety. This stress is taken as the average stress at the cross section under consideration given by P/A. The losses in prestress are an important factor in this shear check as the transmission distance where the prestress force varies parabolically from zero to its maximum potential value occurs normally in the region of highest applied shear. The maximum allowable tensile stress in concrete is normally taken as $0.24\sqrt{f_{cu}}$, as suggested by the British Standards. Shown below is the complete equation combining Equation 2.19 and 2.21 to give the shear capacity of the slab in the uncracked region:

$$V_{co} = \frac{b_v I_x}{A\bar{y}} \sqrt{f_t^2 + 0.8 f_c f_t} \qquad (2.22)$$

Cracked shear capacity

The cracked shear capacity of a slab is given by an empirically derived equation as recommended in clause 4.3.8.5. of BS 8110: Part 1: 1997. This is given in Equation 2.23

$$v_{cr} = \left(1 - 0.55\frac{f_{pe}}{f_{pu}}\right) v_c b_v d + \frac{M_0}{M_{ult}} V_{ult} \qquad (2.23)$$

It can be seen that there are two distinct parts to this equation that vary independently as cross sections across the span are considered. For the sake of explanation a uniformly distributed load on a simply supported slab is taken as an example.

In the first part of the equation f_{pe} / f_{pu} is the ratio of the stress in the strands after losses at the cross section under consideration to the characteristic strength of the strands. The design shear stress, v_c, is calculated as in an ordinary reinforced concrete section. It may be noticed that if this part of the equation was applied to an unprestressed section the ratio f_{pe} / f_{pu} would be equal to zero and therefore the formula would simplify to $v_{cr} = v_c b_v d$, which is the same as that given in design codes for reinforced concrete. It is clear therefore that the larger the stress in the strands the smaller the contribution of the first part of the equation to the overall shear capacity. Conversely, in the second part of the equation a larger prestressing force would contribute positively to the capacity of the section. The quantities M_{ult} and V_{ult} are the bending moments and shear stresses calculated at the ultimate limit state. M_0 is given above in Equation 2.17 and as it is a function of f_{pt} will increase as the prestressing force rises at the centre of the span. The two parts of this equation can generally be said to represent the effect of the materials present and the effect of the prestressing force respectively.

The method of manufacturing most prestressed slabs makes it difficult for shear reinforcement to be provided within the slab. If a slab fails the shear check the most likely remedy is to use a deeper section so as to provide a greater area of concrete to resist the shear forces.

Figure 2.14, shows the form that the shear capacity diagram takes. The effect of end anchorage on the shear capacity in the uncracked portions is very clearly visible as is the sudden fall off in capacity in the area where flexural cracking is assumed to occur.

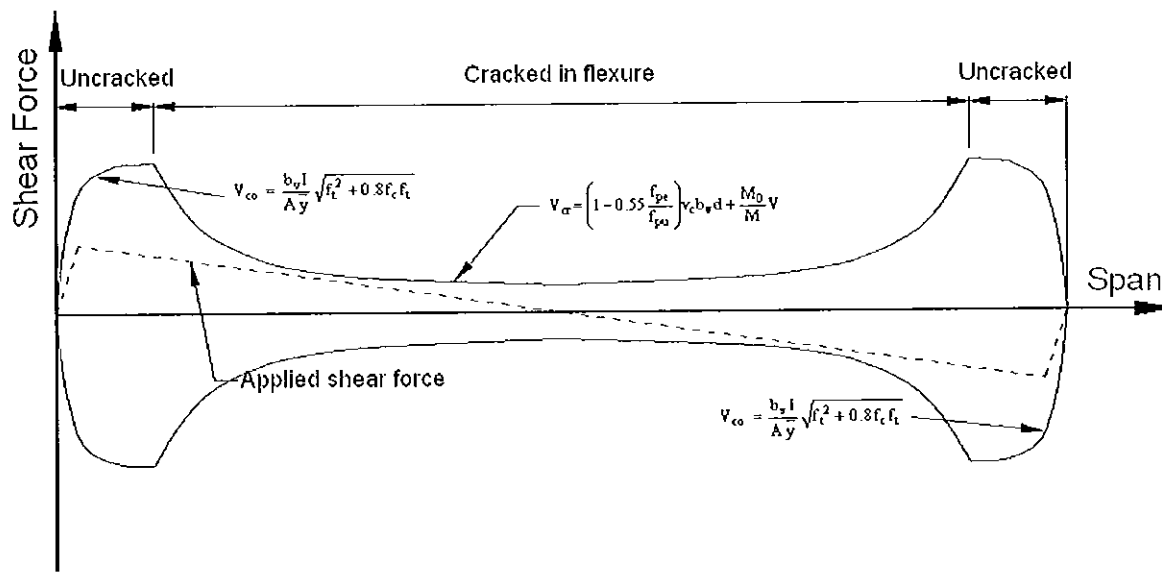

Figure 2.14 shear capacity and applied shear force

2.2.4. Deflection

The process of designing ordinary reinforced concrete beams or slabs predominantly begins with choosing the depth of the slab based on span / depth ratios. This process generally ensures that deflections are within prescribed limits so as to avoid cracking of the internal finishes in buildings, and it also minimises the visual impact of the deflection of the member on the inhabitants of the building. The deflection experienced by prestressed members cannot be simplified to this degree due to the upward camber caused by the prestressing force. Also, as the prestressing force varies with time due to losses, and Young's modulus increases, a short term and long term deflection check is normally carried out. In a limited number of cases a contractor may ask for a deflection calculation for the slab in the unloaded state so as to find the upward camber. This would allow the contractor to more accurately estimate the volume of concrete required for a screed.

2.2.4.1. Short term deflection

There are three components for short term deflection:

1. Upward deflection due to the prestressing force less the initial elastic shortening and relaxation losses. Also the Young's modulus of the concrete is taken as that at transfer.
2. Deflection due to permanent loads causing downward deflection based on the mature properties of the concrete.
3. Live load deflection based on the mature properties of the concrete

The first component of the deflection to consider is the upward cambering due to the prestressing force.

The upward deflection at mid span on a simply supported slab is given as follows:

$$\delta_{prestress} = -\frac{P_t e L^2}{8 E_{ci} I_x} \tag{2.24}$$

This upward camber occurs at the moment of transfer and therefore the Young's modulus at transfer is taken as the appropriate material property. Also, the time dependent losses in the prestressing force will not have occurred and therefore only the instantaneous losses are deemed to have an effect on the prestressing force taken for the camber calculation.

Permanent load deflection which is a function of self weight and the weight of the screed is based on the mature strength of the concrete as a sufficient time will have passed since the casting of the slab to the time when all of the permanent loads are acting. Again, the formula shown here (Equation 2.25) only apply to the simplest case of a uniformly distributed load on a simply supported span. However, for other cases, moment-area theorems can be used for hand calculations. It should be noted however that the geometry and material properties found for the above calculation remain valid for the more complicated cases examined using moment area methods.

$$\delta_{permanent} = \frac{5}{384}\frac{\omega_{perm} L^4}{E_c I_x} \quad (2.25)$$

Semi-permanent loads form the third and final part of the short term deflection. Effectively the semi-permanent loads are any unfactored live loads that may be applied to the slab.

$$\delta_{semi-permanent} = \frac{5}{384}\frac{\omega_{semi} L^4}{E_c I_x} \quad (2.26)$$

The deflections due to permanent and semi-permanent loads are calculated separately so as to allow for comparative deflections to be calculated. This comparison may be called for by a contractor finishing the inside of a building. The case of a studded partition built right up to the under-side of a slab subject only to permanent loads may lead to problems. The semi-permanent loads that would be applied to the slab above during the life time of the structure would lead to further deflection. The slab would bear down on the partition and cause superficial cracking to the plaster.

The maximum and minimum short term deflections are shown below:

$$\delta_{max} = \delta_{prestress} + \delta_{permanent} + \delta_{semi-permanent} \quad (2.27)$$

$$\delta_{min} = \delta_{prestress} + \delta_{permanent} \quad (2.28)$$

2.2.4.2. Long term deflection

Long term deflection is affected by time dependent losses in the prestressing force causing a reduction in the upward camber component of the deflection. Concrete creep also affects the deflection due to the applied moments and the upward camber. It should be noted that in all cases when examining long term deflection the Young's modulus value for mature concrete should be used.

The upward camber is the product of three functions. The largest of these factors is, as before, the upward camber due to the prestressing force at transfer.

$$\delta_{P_i} = -\frac{P_i e L^2}{8 E_c I_x} \tag{2.29}$$

Then as time passes a loss in prestress occurs given by P_{losses} which causes a reduction in the upward camber.

$$\delta_{losses} = \frac{P_{losses} e L^2}{8 E_c I_x} \tag{2.30}$$

Creep has a further effect on the deflection by decreasing the upward camber. The effects of creep are looked at in some detail in Section 2.4.2. As seen in the formula given below this factor is a function of the average prestressing force.

$$\delta_{creep} = -\frac{\phi\left[P_i + \left(P_i - P_{losses}\right)\right]}{2} \frac{eL^2}{8 E_c I_x} \tag{2.31}$$

Therefore, it can be said that the total deflection contribution due to prestressing is as shown in equation 2.32. When δ_{Pi}, δ_{losses} and δ_{creep} are substituted into this formula, equation 2.33 is found. This is simplified as shown in equation 2.34 (Kong and Evans 1997:371).

$$\delta_{prestress} = \delta_{Pi} + \delta_{losses} + \delta_{creep} \tag{2.32}$$

$$= -\frac{P_i e L^2}{8 E_c I_x} + \frac{P_{losses} e L^2}{8 E_c I_x} - \frac{\phi\left(P_i + P_i - P_{losses}\right)}{2} \frac{eL^2}{8 E_c I_x} \tag{2.33}$$

$$= -\frac{P_i e L^2}{8 E_c I_x} \left[\frac{P_i - P_{losses}}{P_i} + \frac{1 + \frac{P_i - P_{losses}}{P_i}}{2} \phi \right] \tag{2.34}$$

From this the following relationship can be extracted where α is the prestressing force loss ratio

$$\alpha = \frac{\left(P_i - P_{losses}\right)}{P_i} \tag{2.35}$$

Equation 2.34 can then be simplified to the following.

$$\delta_{prestress} = -\frac{P_i e L^2}{8 E_c I_x} \left(\alpha + \frac{1 + \alpha}{2} \phi \right) \tag{2.36}$$

The deflection due to all applied loads, permanent and semi-permanent, can itself be divided into two categories, that which occurs instantaneously as the

load is applied and the further deflection that happens due to this load when creep effects occur. The instantaneous deflection due to the loads is given by

$$\delta_{\omega-tran} = \frac{5}{384}\frac{\omega L^4}{E_c I_x} \tag{2.37}$$

After time has elapsed the effects of creep will have occurred and therefore the additional deflection will happen. This is given by:

$$\delta_{\omega-creep} = \frac{5}{384}\frac{\omega L^4}{E_c I_x}\phi \tag{2.38}$$

Equations 2.37 and 2.38 are combined to give the following equation which sums up the downward deflection experienced by the slab.

$$\delta_{\omega-serv} = \frac{5}{384}\frac{\omega L^4}{E_c I_x}(1+\phi) \tag{2.39}$$

As seen in the calculation of short term deflections, the consideration of permanent and semi-permanent loads is often carried out separately so as to allow the range of possible deflections to be examined. The formula given above may be used by substituting in values for $\omega_{semi-permanent}$ and $\omega_{permanent}$. The range of long term deflections due to all loads both internal and external affecting the slab is given by equations 2.40 and 2.41

$$\delta_{\max} = \delta_{prestress} + \delta_{permanent} + \delta_{semi-permanent} \tag{2.40}$$

$$\delta_{\min} = \delta_{prestress} + \delta_{permanent} \tag{2.41}$$

The multitude of factors affecting deflection result in calculations rarely giving an answer that agrees very closely with those measured on site. The final deflection value required a degree of engineering experience to be used. In many cases due to manufacturing techniques the calculated value would differ from actual deflections by an almost constant factor that can only be quantified through experience.

Limits are placed on the deflection due to semi-permanent loads of span / 500 for brittle finishes and span / 350 for non-brittle finishes and in either case not greater than 20mm. In essence this limits the deflection that occurs after the slab is in place with the permanent loads acting on it. A further limit is placed on the overall deflection (downward deflection less upward camber) of span / 1500.

2.3. Materials

The steel and concrete used in prestressed concrete manufacturing is generally of greater quality than that used in other comparable forms of construction. The design philosophy favours increasing the size or number of strands, or the strength of concrete rather than changing section sizes to fit a particular set of design requirements.

2.3.1. Concrete

It is noteworthy when considering concrete as a material that the quality of the wet concrete does not necessarily reflect the performance of the concrete after it has set. The cement used will have been produced to high standards, the aggregate will be of known performance and any admixtures well documented. However, if the concrete has not been adequately compacted or if there has been carelessness on behalf of the staff manufacturing the unit - for example, allowing cold construction joints to form, this will greatly affect the performance of the concrete.

It is generally the case that higher strength concrete mixes are used in prestressed concrete manufacturing. Many manufacturers use machinery to form the slabs by extruding the concrete to form the outline of the slab with circular mandrels forming the voids. This calls for a very dry concrete mix sometimes referred to as 'earth-dry'. This requirement for low slump concrete makes compaction critical for achieving the full potential of the concrete with respect to strength, durability etc. This places demanding requirements on the batching plant operator and mix designer. Typical mix requirements are given in Table 2.1 (Elliott 2002:19)

The early strength of the concrete is of particular interest to the manufacturer. As is shown in the table, grade C50 concrete must reach a transfer strength of at least 30N/mm^2 which is ensured through cube tests carried out on concrete samples taken whilst the slabs were being cast and then cured under the same

conditions. Once the required strength has been reached the slabs can be removed from the casting bed allowing the next production run to begin.

Grade	F_{cu} at 28 days (mm^2)	Demould cube strength (N/mm^2)	Design strength (N/mm^2)	Tensile Strength (N/mm^2)	E_c at 28 days (kN/mm^2)	E_{ci} (kN/mm^2)
C50	50	30 - 35	22.5	3.2	30	27
C60	60	35 - 40	27.0	3.5	32	28

Table 2.1 concrete properties

2.3.2. Steel

The steel used for prestressing concrete in Ireland is generally cold-drawn high strength wire. The wires which range in diameter from 3mm to 7mm are twisted together into strands. The seven wire strand is the most popular configuration, however, five and nineteen wire strands are manufactured. The strength and bond characteristics of the strand are affected by the number of strands present to which the concrete can grip and also the tendency for the straightening of the spun wire within the strand during tensioning. Shown below in Table 2.2 are the properties of seven wire strands (taken from BS 5896: 1980).

Nominal diameter (mm)	Nominal area of strand (mm^2)	Breaking strength (kN)	0.1% proof load (kN)
6.35	23.22	40.0	34.0
7.94	37.42	64.5	54.7
9.53	51.61	89.0	75.6
11.11	69.68	120.1	102.3
12.50	93.00	164.0	139.0
15.70	150.00	265.0	225.0

Table 2.2 steel properties

The stress / strain properties of the high strength steel used in prestressed concrete differs from that used in reinforced concrete. The ultimate characteristic tensile strength of the wire used is approximately 1770 N/mm^2 compared to 460 N/mm^2 for ordinary high yield steel. The value of Young's modulus for this steel is generally taken as 190,000 N/mm^2.The failure strain

tends to fall between 0.04 and 0.06 giving no definite yield point. A proof stress is chosen to give an equivalent yield stress that would not result in an excessive strain and therefore creep. For this purpose a value of 0.1% proof stress is used denoted by '$f_{p,\,0.1}$'. At 0.1% strain a line is draw at an equal angle to the Young's modulus. The point on the graph where the stress / strain curve intersects this line defines where the proof stress can be read. This can be seen in figure 2.15. This stress / strain relationship is simplified in the British standards giving an almost as accurate yet mathematically simple model.

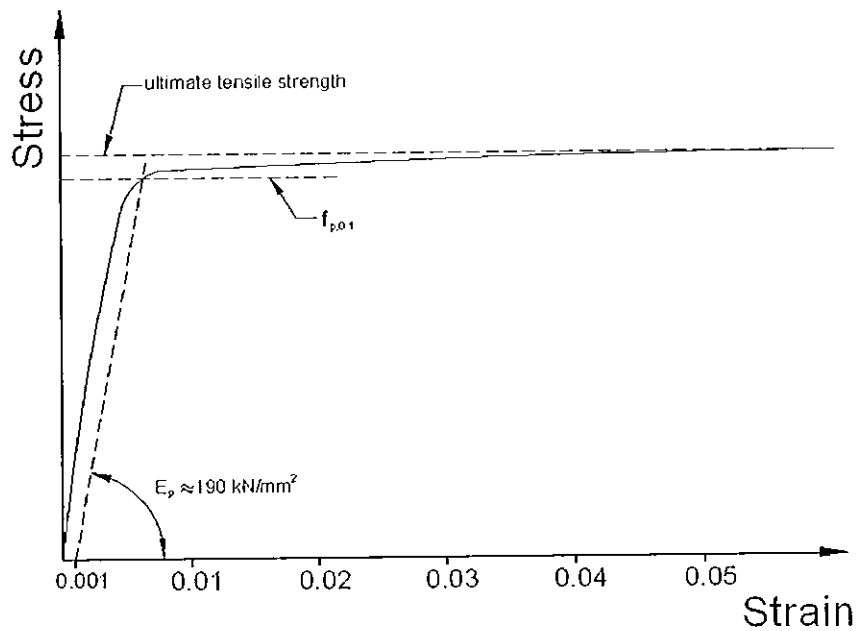

Figure 2.15 stress / strain relationship for steel

The simplified stress / strain relationship is given in BS 8110: Part 1: 1997, Section 2 and is shown in Figure 2.16. Minimum standards for the material properties of the steel are given in BS 5896: 1980.

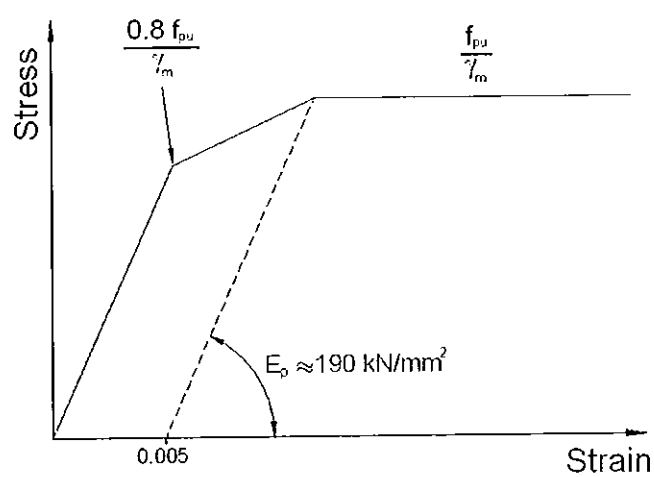

Figure 2.16 simplified stress / strain relationship

Section 3 in BS 5896 relates to strands with table 6 giving details of both the material properties and dimensional requirements.

2.4. Losses

The force applied to the strands is normally 70 – 80% of the ultimate tensile strength of the strands. There are a number of factors affecting the loss of force within the strands. Furthermore, the degree to which these factors affect the prestressing force varies with time. For example, elastic shortening occurs at the moment of transfer, however, relaxation of the steel is assumed to have reached its peak after one thousand hours have passed from the stressing of the steel.

2.4.1. Elastic shortening of the concrete

At transfer, as the strands are cut and the force is transferred into the concrete, the compressive stress in the concrete at the level of the strands is accompanied by strain. As the concrete shortens under the action of the compressive force the strands embedded therein shorten by the same length. The reduction in the strain in the strands leads to a reduction in the prestressing force that is typically in the order of about 5%.

To quantify the reduction of the stress in the strands, the stress in the concrete at the depth where the strands are located must be calculated. The concrete stress 'σ_{cp}' is given by the following formula:

$$\sigma_{cp} = \frac{P}{A}\left(1 + \frac{e^2 A}{I_x}\right) - \sigma_{cg} \qquad (2.42)$$

It is noteworthy that the value taken for the prestressing force is the post-transfer force. The stress due to the self-weight 'σ_{cg}' is relatively small but its presence is beneficial as it partly counters the loss of prestressing force. Most designers will therefore use this. The compressive strain in the concrete that develops at the level of the strands is equal to the reduction in the tensile strain in the strands.

$$\varepsilon_c = \frac{\sigma_{cp}}{E_c} = \varepsilon_s \tag{2.43}$$

And therefore the reduction in steel stress $= \varepsilon_s E_s$ (2.44)

$$= \left(\frac{\sigma_{cp}}{E_c}\right) E_s \tag{2.45}$$

$$= \alpha_e \sigma_{cp} \tag{2.46}$$

The reduction in force in the strand is therefore given by $\alpha_e A_p \sigma_{cp}$

At the moment before transfer the prestressing force is denoted by 'P_0'. It is then clear that the post-transfer prestressing force is given by

$P = P_0$ - reduction in force (2.47)

$P_0 = P$ + reduction in force (2.48)

$$= P + P\frac{\alpha_e A_p}{A}\left(1 + \frac{e^2 A}{I_x}\right) - \frac{\alpha_e A_p M.e}{I_x} \tag{2.49}$$

Finally, when this is rearranged the post-transfer prestressing force is given

$$P = \frac{P_0 + \dfrac{\alpha_e A_p M.e}{I_x}}{1 + \dfrac{\alpha_e A_p}{A}\left(1 + \dfrac{e^2 A}{I_x}\right)} \tag{2.50}$$

It can be seen from this equation that the prestressing force after transfer is amongst other factors, a function of the moment at the cross-section being considered. At transfer the moment acting on the slab is due to the self weight alone and is given by $\omega_{sw} L^2/8$.

2.4.2. Creep

Creep occurs in concrete when it is subjected to a sustained compressive stress over a long period of time. The degree to which creep affects the concrete is a function of the long term stress in the concrete and the atmospheric conditions in which the slab is situated.

The final value for the creep strain 'ε_∞' is in theory only reached after an infinite time has passed. This differs from linear elastic strains by a creep coefficient 'ϕ' which can be estimated from the following formula:

$$\phi = \frac{\varepsilon_\infty}{\sigma_{cp}/E_c} \tag{2.51}$$

This equation can be rearranged to give the creep strain value. From compatibility of strains this allows the strain and therefore the force in the steel to be found. The creep losses can be calculated from the following:

$$= A_p E_s \varepsilon_\infty = A_p E_s \phi \frac{\sigma_{cp}}{E_c} = A_p \alpha_e \phi \sigma_{cp} \tag{2.52}$$

The British Standards recommend the following key factors in estimating the creep factor.

1. Original water content
2. effective age at transfer
3. effective section thickness
4. ambient relative humidity
5. ambient temperature

It the absence of further investigation, BS 8110: Part 1: 1977 gives a value of 1.8 for transfer within 3 days and 1.4 for transfer within 28 days for normal outdoor exposure in the British Isles. If greater accuracy is required with respect to the estimation of ϕ then Figure 2.17 can be used. This is given in BS 8110: Part 2: 1985 Section 7.3 where a more thorough examination of creep is shown.

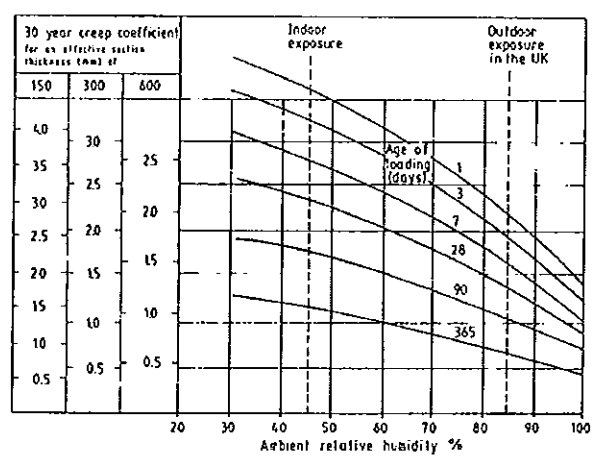

Figure 2.17 creep factor graph

2.4.3. Relaxation of the steel

Relaxation of the strands causes a time dependant loss of prestressing force. The losses due to relaxation of the strands are directly related to the degree to which the strands were initially stressed. Strands stressed to 30 – 40% of their ultimate breaking stress will be prone to virtually no relaxation and therefore the accompanying losses would be miniscule. At a prestressing force of 60% of the breaking force the long term relaxation increases to 1%, however, at 80% of the breaking force the relaxation is of the order of 4.5%. As recommended by the British standards the balance between efficiency and safety is achieved by using a prestressing force of 70% of the breaking force giving a relaxation of 2.5%.

Relaxation of the strands continues to occur over time at an ever reducing rate. For practical purposes it is assumed to have reached its peak value after 1000 hours have passed since the strands were initially stressed. Design codes state the maximum permissible relaxation based on the performance at 1000 hours at a given percentage of the breaking force. Manufacturers also provide similar tables for their own products revising the properties as necessary to reflect improvements in performance. Shown below is an extract taken from Table 6 in BS 5896: 1980 showing allowable relaxation values for the three most commonly used initial prestressing forces for both class 1 and 2 members.

Initial load (% of actual breaking force)	Max. relaxation after 1000 hours	
	Relax Class 1	Relax Class 2
60 %	4.5 %	1%
70 %	8 %	2.5 %
80 %	12 %	4.5 %

Table 2.3 relaxation values

In practice it is assumed that some relaxation will occur before transfer. To reflect this, it is normally taken that 25 % of the relaxation has occurred before transfer. The remaining 75 % is assumed to have occurred by the 1000^{th} hour.

2.4.4. Shrinkage of the concrete

Shrinkage of the concrete is another time dependent source of losses in the prestressing force. The ultimate value of the shrinkage strain is only reached after an infinite time has passed. The factors affecting the degree to which shrinkage would occur are given in the British standards as follows:

1. the aggregate used
2. the original water content of the concrete
3. the age of the concrete at transfer
4. the effective thickness of the concrete
5. the ambient relative humidity

Many of the factors vary greatly according to region and therefore the best estimation of the loss of strain is made through local experience or experimental results. In the absence of local or experimental data the British standards suggest a value of $100 * 10^{-6}$ is taken for outdoor conditions while a value of $300 * 10^{-6}$ is taken for indoor conditions.

2.4.5. Transmission length

The transmission length for a strand is the distance from the end of a length of strand to the point where sufficient anchorage has developed to allow the prestressing force to be transferred from the strands into the concrete. It is clearly the case that at a distance of 100mm from the end of a strand that insufficient surface area on the strand surface to provide anchorage great enough to resist a pullout force in the order of 60 kN. The transmission length is typically of the order of 50 to 160 times the diameter of the strand itself. If a slab has openings or notches that cut the line of a strand then the prestressing force falls off in the same manner as the ends of the slabs.

Guidance on transmission distances is given in BS 8110: Part 1. It suggests again that experience with particular site conditions or experimental data should be used where possible but in their absence gives coefficients that can be used. It lists the key factors affecting the transmission length as follows:

1. the degree of compaction of the concrete
2. the diameter of the strand
3. the concrete strength
4. the surface condition of the strands

The following equation gives an estimation of the transmission length and can be said to be valid for cases where the initial prestressing force does not exceed 75% of the strands breaking force.

$$l_t = \frac{K_t \varphi}{\sqrt{f_{ci}}} \qquad (2.53)$$

Where φ is the nominal diameter of the strand.

f_{ci} is the strength of the concrete at transfer

K_t is the coefficient relating to the surface grip provided by the strands

The two main types of strands used are the seven wire standard or super strand with a K_t value of 240 and the seven wire drawn strand with a K_t value of 360.

2.4.5.1. The rate of anchorage development

The magnitude of the prestressing force varies from zero at the free end of the strand to it full value as mentioned above. BS8110 provides a relationship derived empirically to gives stresses at the centroid of the slab within the transmission length. This formula can be adapted slightly to give the force in the strands themselves. Equation 2.54 shows this relationship with l_t being the transmission length as given above in equation 2.53. 'P_f' in this formula needs to be clearly defined. It is the force in the strand at the end of the transmission length as calculated after all the other sources of losses have been accounted for.

$$P_x = \frac{x}{l_t}\left(2 - \frac{x}{l_t}\right)P_f \qquad (2.54)$$

This relationship gives a convex parabolic growth in the force from the free end of the slab. Figure 2.18 shows the relationship between the stress in the strands before and after transfer.

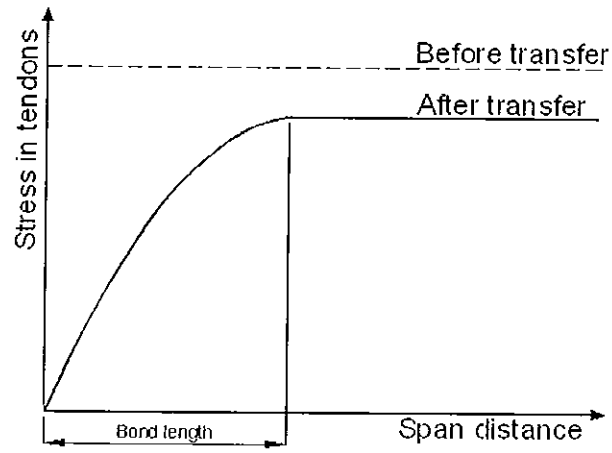

Fig 2.18 development of anchorage

2.4.6. The process of calculating losses

The check for transfer, service and ultimate limit state stress requires careful selection of the appropriate values for the prestressing force. As seen in earlier sections, the slab must be checked for various limiting factors during three distinctly different states transfer stresses, service stresses and the ultimate limit state stresses. Figure 2.19 shows the processes and order in which the losses should be calculated. The two columns on this chart show the sets of values of the prestressing force that must be ascertained as part of a full check.

The transfer losses calculation of relaxation is only 25% of the long term value. This loss affects the value of the prestressing force 'P' used in the elastic shortening check. Also noteworthy is the fact that the moment acting upon the slab during this check is the unfactored self weight.

As concrete creep and shrinkage would have occurred by transfer they are both ignored. Finally the end anchorage values can be calculated based on the previously evaluated forces.

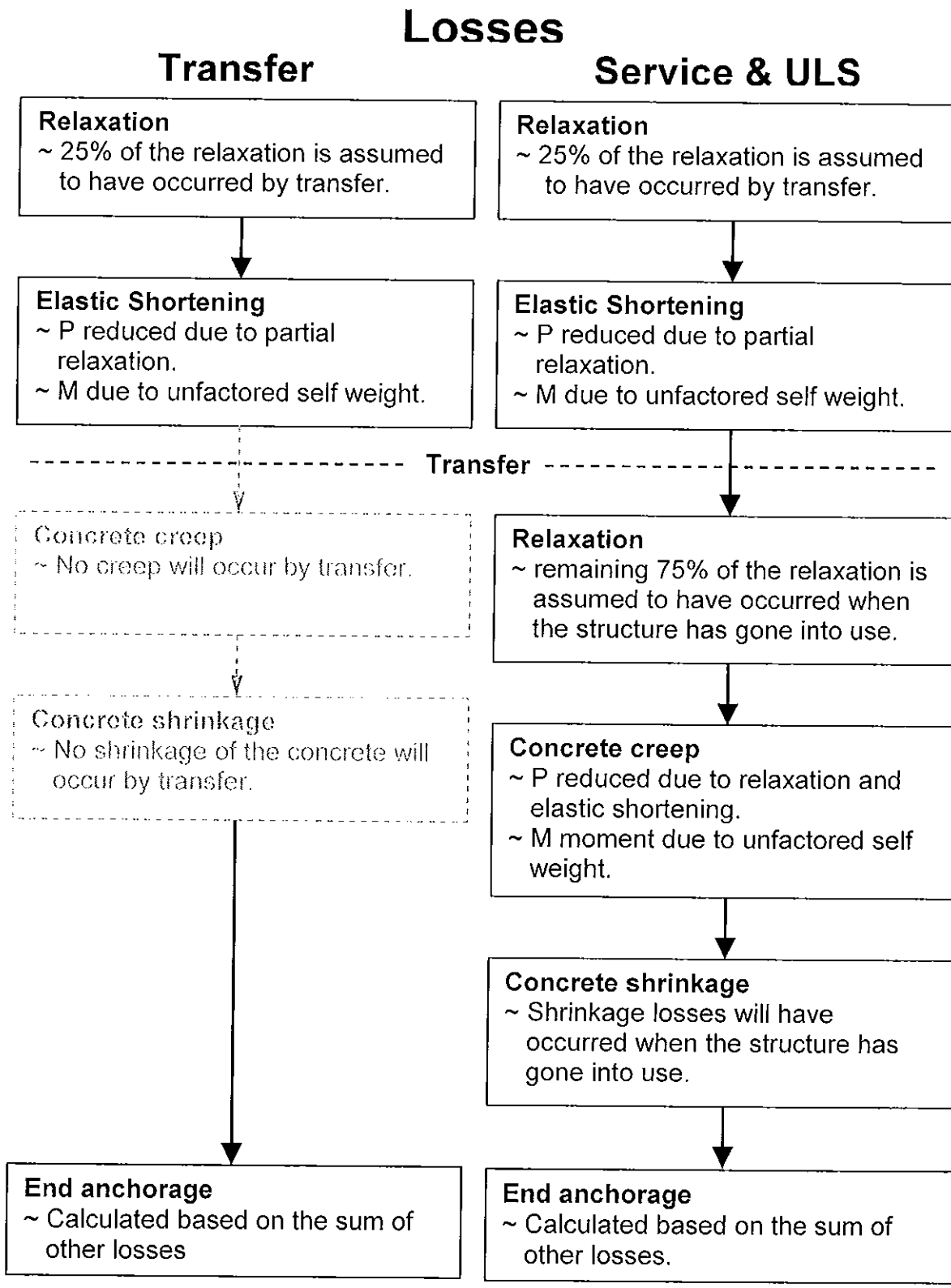

Figure 2.19 loss calculation process

Losses at the service state and the ultimate limit state are the same. Relaxation of the steel will have reached 25% of its final value by transfer, with the remainder occurring post transfer. To calculate the losses due to elastic shortening the prestressing force is the value measured at the jack less the 25% relaxation value. The bending moment values adopted for this calculation are again those due to the unfactored self weight. After transfer, the remaining 75% of the relaxation will occur before the structure goes into service. Following this check creep in the concrete creep is evaluated. This check is based on the state of stresses in the slab after a significant time has passed and therefore it is calculated from the post relaxation and post elastic shortening prestressing force. The bending moment values used are those due to self weigh alone. It may be asked why the imposed loads are not also reflected in the moment values adopted. The unfactored self weight is the only load whose presence is guaranteed to always remain in action. As the gravity loads provide a beneficial role in reducing the elastic shortening losses it would not be prudent to assume that they would be ever-present. Thus to give a conservative design the self weight alone is used. Concrete shrinkage losses are also time dependent and therefore must be carried out after the previously mentioned losses have been accounted for. The final check for end anchorage is again for both cases based on the initial prestressing force less the cumulative losses calculated for the state under consideration.

It is apparent that the creep and elastic shortening losses are a function of the bending moments acting upon the slab. During a very rigorous analysis of a slab the final values of the prestressing forces at both transfer and service may be found. As the applied moments varies parabolically along the length of the slab for even the simplest case, ie the self weight of the slab, theses values must be evaluated at a reasonably large number of intervals along the span. If the losses at each of these intervals are found then a very accurate estimation of the final prestressing force is given. Figure 2.20 show the variation of prestressing force along the length of a slab for the three states that require consideration. The full calculations are shown in Appendix 1.

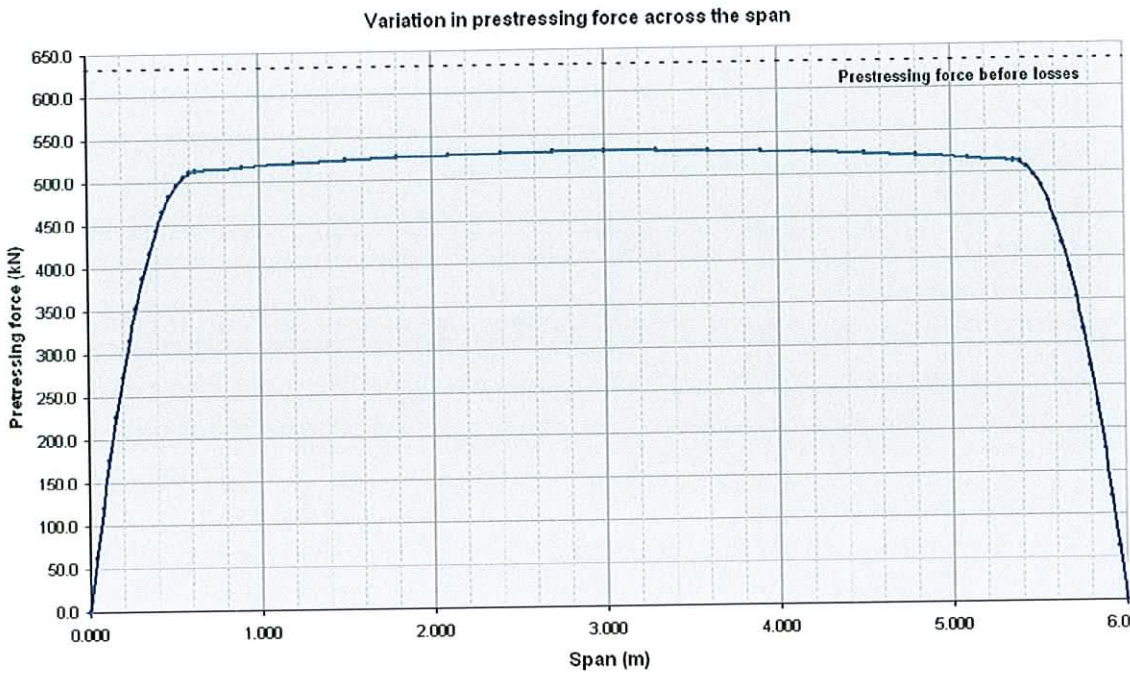

Figure 2.20 example of post losses prestressing forces

Upon examination of this chart the importance of end anchorage becomes clear. The beneficial effects of the gravity load in the elastic shortening and concrete creep calculations are also apparent. Also, excluding transmission distances, the average loss of prestressing force along the span of the slab is of the order of 25%.

2.5. Manufacturing the slabs

All types of prefabricated construction have a number of advantages over in-situ construction. As with any product manufactured under factory conditions, quality control of a higher order than is possible on site is achieved. In most cases the concrete is produced at the same manufacturing facility allowing quality control to also extend to its production. The cement used for producing concrete and steel prestressing strands are manufactured to exacting standards by a small number of companies with their own quality control procedures. The designer can also have greater confidence in the slab being manufactured to the specifications drawn up with respect to the geometry of the cross section, the position of the strands and the location of any notches or openings.

The process of casting prestressed concrete slabs involves six main steps carried out on the factory floor over the course of two days.

1. Preparing the casting beds
2. Stressing the strands.
3. Placing and compacting the concrete.
4. Curing the slabs.
5. Cutting the slabs to the required lengths.
6. Removing the slabs from the casting beds.

2.5.1. Preparing the casting beds

The casting beds used in the production of prestressed slabs are typically one hundred and twenty meters long. At each end of these beds there are large anchorage blocks designed to resist the action of the prestressing force. Between uses, the casting bed must be cleaned and mould oil applied to ensure a clean separation between the casting bed and the underside of the slab.

2.5.2. Stressing the Strands

The strands are positioned according to the design with particular attention to the distance from the strands to the casting bed. However, the designed must also obey certain other constraints such as the minimum cover to the strands for fire protection purposes. The guidance given by the British standards suggests that a minimum cover of 20mm be given for one hour fire resistance with further information given by Table 3.4 in BS8110: part 1: 1997. Similar consideration is given to corrosion where it is deemed to be a problem. A typical slab could have ten 9.5mm diameter stands each with a force of 64.1kN, working with forces of this magnitude requires great care. The jack used for stressing the strands must be calibrated regularly and the sequence in which the strands are stressed involves stressing the centre pair first and the working outwards towards the edge strands in a balanced fashion.

2.5.3. Placing and compacting the concrete

There are a number of machines available for placing and compaction of the concrete all of which accomplish the same goal. As mentioned earlier, the concrete used in the manufacture of prestressed concrete elements is a very dry mix so as to ensure that it will hold its shape after placing. The deeper sections with voids throughout their length require mandrels to give the required void shape. The slip forming process happens relatively quickly as the machine moves along the casting bed on rails. The main difference between the machinery produced by different manufacturers is the shape of the void forming mandrels. As the concrete used sets rapidly, the time from the addition of the water to the mix, to the placing of the concrete is critical. As the concrete begins to set, the task of ensuring that the concrete has been vibrated fully becomes more onerous.

There are a number of modifications that can be made to the standard cross sections produced by the machines. Some factories employ robotic spraying machines to mark the location of notches and openings on the top surface of the slab. This machine follows closely behind the casting machine in order for the team manufacturing the slab to remove the concrete whilst it is still somewhat soft. The spraying machine also marks the ends of the slabs so as to simplify the cutting. Modifications can be made to the cross sectional shape that the machine produces by varying the mould shape or mandrels used. However, this task is somewhat intricate and therefore would not be varied on a slab by slab basis.

2.5.4. Curing the slabs

The process of curing the slabs is greatly helped by the factory conditions in which the slabs are produced. The casting beds upon which the concrete hardens are heated by a system of hot water pipes running below them. In many cases a long tarpaulin sheet is used to cover the slab to keep the heat in. In some of the deeper sections produced, ensuring a uniform temperature

gradient throughout the depth of the slab can become an important issue so as to minimise the possibility of additional stresses being imparted into the slab.

2.5.5. Cutting the slabs to the required lengths

Detensioning of the strands and the process of cutting slabs to their required length can take place once the cube strengths verify that the required transfer strength has been reached. The slabs will also be sprayed with an identification number to ensure that the slab is placed in the correct location within the building when it does reach the construction site.

2.5.6. Removing the slabs from the casting beds

The factories in which the slabs are produced generally have gantry cranes for lifting and moving machinery and slabs. Specialist lifting equipment is required for lifting and moving slabs. Ordinary forklifts cannot be used to lift slabs as lifting a slab around the mid-point would result in tension in the top of the fibres and therefore cracking would occur. To overcome this difficulty, an adjustable length lifting beam is used to pick up the slab by its ends. A great deal of consideration is also given to the order in which slabs are loaded onto the trucks used to bring them to the construction site. By placing the slabs on the truck in reverse order to that in which they are to be placed on site, the need to unload slabs to a storage area on site is removed. As such this allows the slabs to be lifted directly from the truck to their final position.

2.6. Summary

The theory upon which prestressed concrete design is based was examined within this chapter with a view to constructing a software package to calculate the stresses found in prestressed slabs. The stresses at transfer and service states were reviewed and verified from first principles and the logic behinds checking the slabs integrity during these states discussed. Bending moment and shear capacities at the ultimate limit state were both reviewed with particular attention shown to the British Standards. Losses in prestressing force

were due to material and environmental factors and the effect theses losses have on the slabs capacity were reviewed and a sample calculation studied. The deflection characteristics of prestressed slabs and those factors affecting it were studied and this important benefit of prestressed concrete construction shown. Finally, the method of manufacture was discussed and some of the practical aspects of the process highlighted.

3. FINITE ELEMENT ANALYSIS

3.1. Introduction

Finite element analysis was chosen as the best analysis method for the software for two main reasons. Firstly, the accuracy given by a finite element analysis where complex shapes or loads are considered is excellent. Secondly, the processes involved in carrying out this type of analysis are much more easily implemented in a software package than, for example, the Hillerborg strip method or yield line analysis. The finite element model chosen to best suit the requirements of the prestressed slab analysis for normal construction is a plate bending model combined with an in-plane model. The elements to be analysed using this model are two-dimensional rectangles.

This chapter attempts to explain the theory being used and the choices made with respect to applying this theory to prestressed concrete analysis. The theory for the two models to be used are developed independently and then combined in the global stiffness matrix. The application of boundary conditions is discussed and a simple example is used to help explain the process. Finally, the process of solving for displacements and then stresses is outlined.

As stated in Chapter 1, the aim of the research was to produce prototype prescast concrete design software and not a more general study of finite element analysis techniques. At the outset plate bending and plane stress were decided upon as the theories upon which the analysis element of the software would be built. The suitability of these theories will be verified or otherwise in later chapters. The main reference from which the finite element theory was taken was '*The finite element method: a basic introduction for engineers*' (Rockey *et al.* 1983). Elements of theory taken from other sources will be referenced as such.

3.2. The choice of model

In setting up a finite element model the decision must be made as to what degrees of freedom are required to accurately model the element or structure. A '*degree of freedom*' at a node can be defined for this project as '*a deflection perpendicular to a given plane or rotation about a given axis*'. Normal plate bending models have three degrees of freedom, one deflection and two rotations. For a square or rectangular element there are four nodes, one at each corner. Figure 3.1 shows a rectangular element with the degrees of freedom associated with plate bending. At each of the four nodes, loads can be applied in various ways.

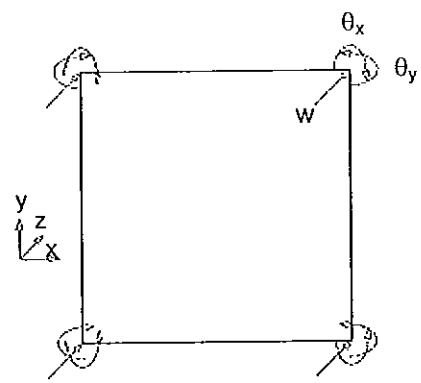

Figure 3.1 plate bending element

A force can be applied normal to the plane of the object denoted by F_z. Moments can also be applied at each node denoted by T_x and T_y.

An in-plane finite element model is incorporated into the program to increase the accuracy of the analysis. This adds two extra degrees of freedom to the model and they are denoted by F_x and F_y. This is shown in Figure 3.2.

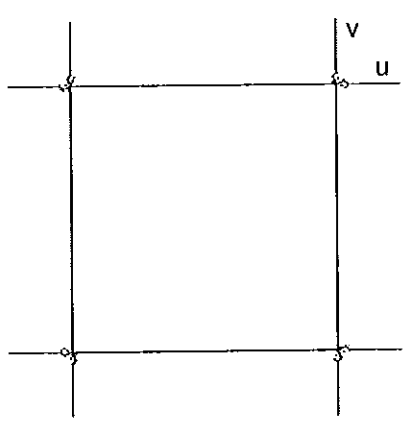

Figure 3.2 plane stress element

It can be seen that the combination of in-plane and plate bending produces a model with degrees of freedom including u, v, z, θ_x and θ_y. There is a possible sixth degree of freedom 'T_z' representing twisting within the plane of the plate, however the plate is extremely stiff in its plane and therefore this degree of freedom can be neglected without any reduction in the accuracy of the overall model.

The loads applied to the slab can be divided into those due to gravity and those due to the presence of the prestressing force. The gravity loads include all types of line load, point loads and uniformly distributed loads including self weight. These loads are applied to the plate bending model via the F_z component. The loading due to prestressing has two components as can be seen in Chapter 2. The prestressing force itself is applied to the F_x component of the plane stress model, whereas the moment due to the eccentricity of the prestressing force is applied to the plate bending model via the T_y component.

3.3. Finite element theory

The forces within an element can be related to the displacement of the element using the following formula:

$$\{F^e\} = [K^e]\{\delta^e\} \qquad (3.1)$$

where $\{F^e\}$ is the nodal forces vector
$\{\delta^e\}$ is the nodal displacement vector
$[K^e]$ is the stiffness matrix

This applies to the plate bending and in-plane methods used in this project. It can be seen that the size of the force and displacement vectors, and also the stiffness matrix, are determined by the number of degrees of freedom used in the model. This will be shown below for both cases

3.3.1. Plate bending

It is assumed that the plate under consideration has a thickness that is small relative to its other dimensions and that deflections are small. These assumptions allow membrane stresses to be neglected as they are deemed to be insignificant.

3.3.1.1. Stiffness matrices

Plate bending elements have three degrees of freedom at each node, two rotations and the deflection normal to the plate itself. The rectangular elements under consideration therefore have twelve degrees of freedom in total. The displacements, and corresponding moments and forces at node one are given by

$$\{\delta_1\} = \begin{Bmatrix} \theta_{x1} \\ \theta_{y1} \\ w_{z1} \end{Bmatrix} \text{ and } \{F_1\} = \begin{Bmatrix} T_{x1} \\ T_{y1} \\ F_{z1} \end{Bmatrix} \qquad (3.2), (3.3)$$

The $\{\delta^e\}$ and $\{F^e\}$ vectors clearly contain twelve terms and therefore the elemental stiffness matrix, $[K^e]$ takes the from of a twelve by twelve matrix.

The following function gives the displacement at any point in plate element

$$\{\delta(x,y)\} = \begin{Bmatrix} \theta_x \\ \theta_y \\ w \end{Bmatrix} \qquad (3.4)$$

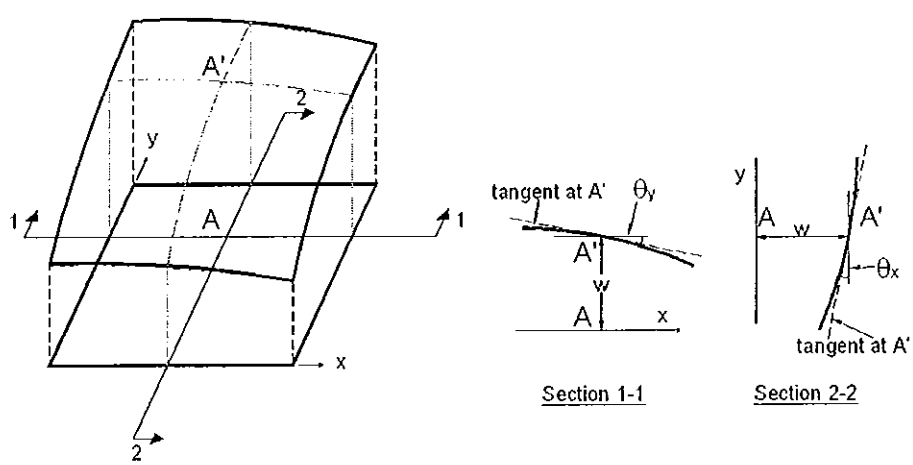

Figure 3.3 element displacements

As is apparent from Figure 3.3, the two rotations, θ_x and θ_y, are related to the deflection at any point in the plate element by the following expressions

$$\theta_x = -\frac{\partial w}{\partial y},\ \theta_y = \frac{\partial w}{\partial x} \qquad (3.5), (3.6)$$

where $w = f(x, y)$ is the vertical displacement function

A displacement function is established to reflect the twelve unknowns corresponding to the twelve degrees of freedom of each element. This function, a polynomial with twelve constants, is shown below in Equation 3.7.

$$w = \alpha_1 + \alpha_2 x + \alpha_3 y + \alpha_4 x^2 + \alpha_5 xy + \alpha_6 y^2 + \alpha_7 x^3 + \alpha_8 x^2 y + \alpha_9 xy^2 + \alpha_{10} y^3 + \alpha_{11} x^3 y + \alpha_{12} xy^3 \qquad (3.7)$$

This equation may be differentiated with respect to x to yield the slope of the plate in the x direction, and differentiated with respect to y to give the slope of the plate in the y direction as shown in Equations 3.5 and 3.6. The three expressions give the general state of displacement within an element. By substituting in the relative co-ordinates of the four corners of the element a matrix with twelve equations and twelve unknowns is obtained. This matrix, [A], is shown in full in Equation A2.13 the derivation carried out in Appendix 2 . However the basic relationship is as follows:

$$\{\delta^e\} = [A]\{\alpha\} \qquad (3.\ 8)$$

And therefore the unknown coefficients in Equation 3.8 can be found using ordinary matrix inversion. Therefore, referring to the general case the following statement may be made:

$$\{\delta(x, y)\} = [f(x, y)][A]^{-1}\{\delta^e\} \qquad (3.\ 9)$$

To relate the strains within an element to the displacements found above, the curvature of the plate in the x and y directions and the twist must be considered. The curvature in the x direction is found by examining the rate of change of the slope in the x direction as shown in Equation 3.10 below. The curvature in the y direction is obtained in a similar manner.

$$-\frac{\partial}{\partial x}\left(\frac{\partial w}{\partial x}\right) = -\frac{\partial^2 w}{\partial x^2} \qquad (3.10)$$

$$-\frac{\partial}{\partial y}\left(\frac{\partial w}{\partial y}\right)=-\frac{\partial^2 w}{\partial y^2} \tag{3.11}$$

The twist is found by considering the rate of change of the slope in the x direction with respect to the y direction.

$$\frac{\partial}{\partial y}\left(\frac{\partial w}{\partial x}\right)=\frac{\partial^2 w}{\partial x \partial y} \tag{3.12}$$

Equation 3.13 gives the general state of strain in an element. The twisting moments acting on the plate act equally along the four edges of the element and therefore it can be that $M_{xy}=M_{yx}$. From this it is apparent that the M_{xy} in Equation 3.13 should be doubled.

$$\{\varepsilon(x,y)\}=\begin{Bmatrix}-\partial^2 w/\partial x^2\\ -\partial^2 w/\partial y^2\\ 2\partial^2 w/\partial x \partial y\end{Bmatrix}=[C]\{\alpha\} \tag{3.13}$$

The complete matrix [C] is shown in detail in Equation A2.14. Substituting for $\{\alpha\}$ in the above equation where $\{\alpha\}$ is found by inverting equation 3.8, the relationship between strains and nodal displacements is obtained.

$$\{\varepsilon(x,y)\}=[B]\{\delta^e\} \tag{3.14}$$

$$\text{where } [B]=[C][A]^{-1} \tag{3.15}$$

The state of bending stresses at any point in the plate bending model can be represented by the three components shown below in Equation 3.16. M_x and M_y are bending moments per unit length while M_{xy} represents the twisting moment per unit length:

$$\{\sigma(x,y)\}=\begin{Bmatrix}M_x\\ M_y\\ M_{xy}\end{Bmatrix} \tag{3.17}$$

Equations 3.17, 3.18 and 3.19 are moment-curvature relationships for plate bending. The action of these moments on a plate element can be seen in Figure 3.4.

$$M_x=-\left(D_x\frac{\partial^2 w}{\partial x^2}+D_1\frac{\partial^2 w}{\partial y^2}\right) \tag{3.17}$$

$$M_y = -\left(D_y \frac{\partial^2 w}{\partial x^2} + D_1 \frac{\partial^2 w}{\partial x^2} \right) \tag{3.18}$$

$$M_{xy} = M_{yx} = 2D_{xy} \frac{\partial^2 w}{\partial x \partial y} \tag{3.19}$$

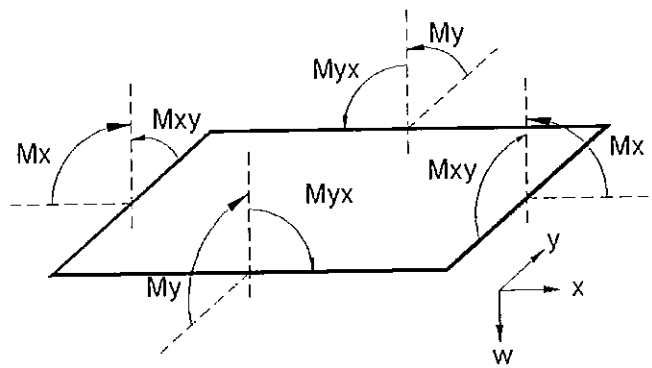

Figure 3.4 element internal forces

The three equations, giving the flexural rigidity of the particular element, can be written in matrix form, denoted by [D]. The elasticity matrix will be discussed in greater detail in the next section. This equation can be further simplified by substituting for $\{\varepsilon(x,y)\}$

$$\{\sigma(x,y)\} = \begin{Bmatrix} M_x \\ M_y \\ M_{xy} \end{Bmatrix} = \begin{bmatrix} D_x & D_1 & 0 \\ D_1 & D_y & 0 \\ 0 & 0 & D_{xy} \end{bmatrix} \begin{Bmatrix} -\partial^2 w/\partial x^2 \\ -\partial^2 w/\partial y^2 \\ 2\partial^2 w/\partial x \partial y \end{Bmatrix} \tag{3.20}$$

$$= [D]\{\varepsilon(x,y)\} = [D][B]\{\delta^e\} \tag{3.21}$$

To obtain the element stiffness matrix the principle of virtual work is employed. The principle of virtual work, as far as the finite element models under consideration in this project are concerned, can be stated as follows: *during any virtual displacement imposed on the element, the total external work done by the nodal loads must equal the total internal work done by the stresses*. This is given by the following Equation 3.22.

$$\sum F\delta = \int_v \sigma\varepsilon . d(vol) \tag{3.22}$$

The external work done at an arbitrarily selected set of nodes is given by Equation 3.23 where $\{\delta^{*e}\}$ denotes the arbitrary set of nodal displacements.

$$W_{ext} = \{\delta_1^{*e}\}\{F_1^e\} + \{\delta_2^{*e}\}\{F_2^e\} + \ldots + \{\delta_n^{*e}\}\{F_n^e\}$$

$$= \{\delta^{*e}\}^T \{F^e\} \tag{3.23}$$

Where $\{\delta^{*e}\} = \begin{Bmatrix} \{\delta_1^{*e}\} \\ \{\delta_2^{*e}\} \\ \vdots \\ \{\delta_n^{*e}\} \end{Bmatrix}$ (3.24)

Equation 3.24 gives the nodal displacements at the arbitrarily selected set of nodes.

The internal work done per unit volume of the same element is:

$$W_{int} = \{\varepsilon(x,y)^*\}^T \{\sigma(x,y)\} \tag{3.25}$$

And therefore the total work done within the entire volume of the element is

$$\int^v W_{int}\, d(vol) = \int^v \{\varepsilon(x,y)^*\}^T \{\sigma(x,y)\} d(vol) \tag{3.26}$$

Referring back to equation 3.14, it can be seen that $\{\varepsilon(x,y)\} = [B]\{\delta^e\}$. However when the nodal displacements given in Equation 3.24 are imposed, this equation becomes

$$\{\varepsilon(x,y)^*\} = [B]\{\delta^{*e}\} \tag{3.27}$$

Substituting Equations 3.21 and 3.27 into Equation 3.26 yields:

$$\int^v W_{int}\, d(vol) = \int^v [B]^T \{\delta^{*e}\}[D][B]\{\delta^e\} d(vol) \tag{3.28}$$

When the internal and external work are equated and the resulting equation simplified the following expression is obtained for $\{F^e\}$.

$$\{F^e\} = \left[\int [B]^T [D][B] d(vol)\right]\{\delta^e\} \tag{3.29}$$

For the particular case of rectangular plate bending elements the volume integral, $\int^v d(vol)$ is replaced by $\int_0^b \int_0^a dx.dy$ to give

$$\{F^e\} = \left[\int_0^b \int_0^a [B]^T [D][B] dx dy\right]\{\delta^e\} \tag{3.30}$$

From which the stiffness matrix is seen to be:

$$[K^e] = \int_0^b \int_0^a [B]^T [D][B] dx dy \tag{3.31}$$

The integral is obviously rather complicated to obtain and the integration is typically carried out using computer software that specialises in symbolic mathematics. The final $[K^e]$ matrix can be found in Equation A2.24.

3.3.1.2. Elasticity Matrix

The elasticity matrix referred to above must be found before the global stiffness matrix can be formed. In the case of plate bending the general form of the elasticity matrix takes the following form:

$$[D] = \begin{bmatrix} D_x & D_1 & 0 \\ D_1 & D_y & 0 \\ 0 & 0 & D_{xy} \end{bmatrix} \tag{3.32}$$

Where D_x and D_y represent the flexural rigidity in the x and y direction respectively, D_1 represents a coupling rigidity and D_{xy} represents the torsional rigidity. For an isotropic plate, the flexural rigidities in the x and y directions are the same and can be evaluated using the following formula:

$$D_x = D_y = D = \frac{Et^3}{12(1-\upsilon^2)} \tag{3.33}$$

$$D_1 = D\upsilon \tag{3.34}$$

$$D_{xy} = \frac{(1-\upsilon)}{2} D \tag{3.35}$$

The coupling rigidity, D_1 allows the effect of Poison's ratio to be modelled. This effect can be observed more readily in thick plates made of materials with a high Poisson's ratio. These plates bend in two directions under load: a concave curvature in the direction of the span, and a convex curvature perpendicular to

the span which produces a saddle-like effect. The coupling rigidity can be evaluated as shown in Equation 3.34

The final element in the elasticity matrix is the torsional rigidity. This is also linked to the flexural rigidity in the y direction and is a function both of this and the shear modulus of the material. This relationship is given by:

$$D_{xy} = G\frac{t^3}{12} \text{ where } G = \frac{E}{2(1-\nu)} \tag{3.36}$$

In the case of orthotropic plates (of which hollow-core, or voided slabs, are both examples) these formulae must be adapted to reflect the reduced rigidities. The adapted forms of the four formulae are shown below (Clark 1983:17).

$$D_x = \frac{E}{(1-\nu^2)} \cdot \frac{I_x}{s_x} \tag{3.37}$$

$$D_y = \frac{E}{(1-\nu^2)} \cdot \frac{I_y}{s_y} \tag{3.38}$$

$$D_1 = \nu D_y \tag{3.39}$$

$$D_{xy} = G\frac{I_y}{s_y} \tag{3.40}$$

The values of I_x and I_y are the second moments of area of the element under consideration with s_x and s_y representing the width of the element in the x and y directions respectively. It must be noted that the centroidal axis varies from element to element due to the presence of strands or voids.

3.3.1.3. Stress-displacement matrix

Once the displacements of the nodes within the plate have been ascertained the vector containing these values may be used to find the stresses within the individual elements.

Referring back to Equation 3.21 it can be seen that

$$\{\sigma(x,y)\} = [H]\{\delta^e\} \tag{3.41}$$

where:

$$[H]=[D][B] \tag{3.42}$$

Equation A2.27 shows the full derivation of the $[H]$ matrix with the nodal coordinates substituted into the $[B]$ matrix for each of the four nodes on the element to give a twelve by twelve matrix.

3.3.2. Plane Stress

Plane elasticity problems refer to plates that are loaded in their own plane. Once again the assumption is that the thickness of the plate is relatively small compared to its other two dimensions.

3.3.2.1. Stiffness matrix

The 2-dimensional model used for analysing rectangular elements subject to in-plane loading has two degrees of freedom per node and therefore eight in total. The displacements at each node in this model are assumed to be in-plane. These displacements and the corresponding forces are shown below:

$$\{\delta_1\}=\begin{Bmatrix} u_1 \\ v_1 \end{Bmatrix} \tag{3.43}$$

$$\{F_1\}=\begin{Bmatrix} F_{x1} \\ F_{y1} \end{Bmatrix} \tag{3.44}$$

For a single element the displacements and forces are therefore as follows

$$\{\delta^e\}=\begin{Bmatrix} \{\delta_1\} \\ \{\delta_2\} \\ \{\delta_3\} \\ \{\delta_4\} \end{Bmatrix} \tag{3.45}$$

$$\{F^e\}=\begin{Bmatrix} \{F_1\} \\ \{F_2\} \\ \{F_3\} \\ \{F_4\} \end{Bmatrix} \tag{3.46}$$

Once again, the equation relating elemental displacements to elemental forces takes the following form where the stiffness matrix, $[K^e]$, is an eight by eight matrix.

$$\{F^e\} = [K^e]\{\delta^e\} \tag{3.47}$$

The following function gives the displacement in the x and y directions at any point within an element

$$\{\delta(x,y)\} = \begin{Bmatrix} u \\ v \end{Bmatrix} \tag{3.48}$$

Two functions are chosen with a total of eight unknowns reflecting the eight degrees of freedom.

$$u = \alpha_1 + \alpha_2 x + \alpha_3 y + \alpha_4 xy \tag{3.49}$$

$$v = \alpha_5 + \alpha_6 x + \alpha_7 y + \alpha_8 xy \tag{3.50}$$

The two displacements can be written in matrix form as shown in Equation 3.52.

$$\begin{Bmatrix} u \\ v \end{Bmatrix} = \begin{bmatrix} 1 & x & y & xy & 0 & 0 & 0 & 0 \\ 0 & 0 & 0 & 0 & 1 & x & y & xy \end{bmatrix} \begin{Bmatrix} \alpha_1 \\ \alpha_2 \\ \alpha_3 \\ \alpha_4 \\ \alpha_5 \\ \alpha_6 \\ \alpha_7 \\ \alpha_8 \end{Bmatrix} \tag{3.52}$$

This relationship can be summarised as shown below to give the general formula for the displacements at a point within an element.

$$\{\delta(x,y)\} = [f(x,y)]\{\alpha\} \tag{3.53}$$

As shown in Equation 3.8 (see Section 3.3.1.1 above), the four sets of nodal coordinates are substituted into the equation relating displacements at a point to the nodal displacements. These nodal coordinates, (x_1, y_1), (x_2, y_2), (x_3, y_3) and (x_4, y_4), are then substituted into Equation 3.52 giving an eight by eight matrix represented by [A], which is shown in full in Equation A2.39.

$$\{\delta^e\} = [A]\{\alpha\} \tag{3.54}$$

and therefore $\{\alpha\} = [A]^{-1}\{\delta^e\}$ (3.55)

This Equation allows the unknown coefficients, $[\alpha]$ to be found and substituted into Equation 3.53 giving the following:

$$\{\delta(x,y)\} = [f(x,y)][A]^{-1}\{\delta^e\} \tag{3.56}$$

The strains at any point within an element can be summarised as shown in Equation 3.57. The strains in the x and y direction are given by ε_x and ε_y respectively, and the shear strain is given by γ_{xy}

$$\{\varepsilon(x,y)\} = \begin{Bmatrix} \varepsilon_x \\ \varepsilon_y \\ \gamma_{xy} \end{Bmatrix} \tag{3.57}$$

These strains are related to displacements using the theory of elasticity to give the following differential equations.

$$\varepsilon_x = \partial u/\partial x \tag{3.58}$$

$$\varepsilon_y = \partial v/\partial y \tag{3.59}$$

$$\gamma_{xy} = \partial u/\partial y + \partial v/\partial x \tag{3.60}$$

The displacements u and v are substituted into Equations 3.58, 3.59 and 3.60. The resulting formula is put into matrix form and is denoted by [C]. The full derivation of [C] is shown in Equation A2.47.

$$\{\varepsilon(x,y)\} = [C]\{\alpha\} \tag{3.61}$$

The vector $\{\alpha\}$ is known from Equation 3.46 and can be substituted into Equation 3.61 to allow strains to be directly related to displacements. This is given in Equation 3.62.

$$\{\varepsilon(x,y)\} = [C][A]^{-1}\{\delta^e\} \tag{3.62}$$

$$= [B]\{\delta^e\} \tag{3.63}$$

The full derivation of [B] is shown in Equation A2.49. The relationship between stress and strain in plane stress problems is given by the following relationship into which Equation 3.63 may be substituted.

$$\{\sigma(x,y)\} = [D]\{\varepsilon(x,y)\} \tag{3.64}$$

$$= [D][B]\{\delta^e\} \tag{3.65}$$

The elasticity matrix will be discussed in the next section in more detail. As seen in Section 3.3.1.1 the principle of virtual work is employed to equate the external work done by nodal loads to the internal work done to give the following integral:

$$\{F^e\} = \left[\int [B]^T [D][B] d(vol) \right] \{\delta^e\} \tag{3.66}$$

From which $[K^e]$ can be extracted as follows

$$[K^e] = \int [B]^T [D][B] d(vol) \tag{3.67}$$

However, since it is assumed that the element under consideration has a constant thickness this integral simplifies to the following

$$[K^e] = t \iint [B]^T [D][B] dx dy \tag{3.68}$$

Once again the matrix multiplication operations are carried out in the usual way before performing the integration over the area of the element. The resulting matrix, $[K^e]$ is shown in full in Equation A2.57.

3.3.2.2. Elasticity matrix

The elasticity matrix for plane stress differs from that of the plate bending model in that the plane stress elasticity matrix only considers material properties and not geometric properties such as the second moment of area.

$$[D] = \begin{bmatrix} d_{11} & d_{12} & 0 \\ d_{21} & d_{22} & 0 \\ 0 & 0 & d_{33} \end{bmatrix} \tag{3.69}$$

where

$$d_{11} = d_{22} = \frac{E}{1-\upsilon^2} \tag{3.70}$$

$$d_{21} = d_{12} = \frac{\upsilon E}{1-\upsilon^2} \tag{3.71}$$

$$d_{33} = \frac{E}{2(1+\upsilon)} \tag{3.72}$$

Referring back to Equation 3.68, the thickness of a given element must be taken as constant; however, within a plate, elements may have different thickness.

3.3.2.3. Stress-displacement matrix

Examination of Equation 3.21 shows that once the displacements at a point have been established, the stresses at that point may then be obtained.

$$\{\sigma(x,y)\} = [D][B]\{\delta^e\} \tag{3.73}$$

$$= [H]\{\delta^e\} \tag{3.74}$$

where $[H] = [D][B]$ (3.75)

The [H] matrix relates to a single point on an element. Substitution of the four sets of relative nodal coordinates into this matrix gives the elemental stress displacement matrix seen in Equation 3.76.

$$[H^e] = \begin{bmatrix} [H(x_1, y_1)] \\ [H(x_2, y_2)] \\ [H(x_3, y_3)] \\ [H(x_4, y_4)] \end{bmatrix} \tag{3.76}$$

The four corners of the element have the following relative coordinates: (0, 0), (0, b), (a, 0) and (a, b). Each of these sets of co-ordinates may then be substituted into the Matrix [H] as found in Equation 3.75. The four resulting 3 * 8 matrices are then assembled into an elemental stress-displacement matrix denoted by $[H^e]$ whose dimensions are 12 * 8. The full derivation of this matrix is shown in Equation A2.61.

3.4. Combined plate bending and plane stress model

The combined plate bending and plane stress model is similar to that sometimes used when analysing shell structures. It can be seen that the two models will be combined into one matrix before the solution stage.

3.4.1. Construction of the Global stiffness matrix

For small deflections the plate bending and in-plane stresses develop independently of each other. The stiffness matrix encompassing both techniques is formed by inserting the corresponding elements from the plate bending and in-plane stiffness matrices. The following are the elemental stiffness matrices for both plane stress and plate bending. Each matrix shows the sub-matrices that form the whole.

$$K^{e,p} = \begin{bmatrix} [K_{11}^p] & [K_{12}^p] & [K_{13}^p] & [K_{14}^p] \\ [K_{21}^p] & [K_{22}^p] & [K_{23}^p] & [K_{24}^p] \\ [K_{31}^p] & [K_{32}^p] & [K_{33}^p] & [K_{34}^p] \\ [K_{41}^p] & [K_{42}^p] & [K_{43}^p] & [K_{44}^p] \end{bmatrix} \tag{3.77}$$

$$K^{e,b} = \begin{bmatrix} [K_{11}^b] & [K_{12}^b] & [K_{13}^b] & [K_{14}^b] \\ [K_{21}^b] & [K_{22}^b] & [K_{23}^b] & [K_{24}^b] \\ [K_{31}^b] & [K_{32}^b] & [K_{33}^b] & [K_{34}^b] \\ [K_{41}^b] & [K_{42}^b] & [K_{43}^b] & [K_{44}^b] \end{bmatrix} \tag{3.78}$$

The sub-matrices on the main diagonal, for example $[K_{11}]$, contribute to the strength of the plate through direct stiffness, while the off diagonal members such as $[K_{32}]$ contribute through indirect stiffness. These sub elements from both elemental stiffness matrices are grafted into the elemental stiffness matrix generated in this combined model as seen below.

$$\{F^e\} = \begin{Bmatrix} F_1 \\ F_2 \\ F_3 \\ F_4 \end{Bmatrix} = \left[\begin{array}{cc:cc:cc:cc} [K_{11}^p] & & & & & & & \\ 0 & [K_{11}^b] & & & & & & \\ \hdashline [K_{21}^p] & 0 & [K_{22}^p] & & & & & \\ 0 & [K_{21}^b] & 0 & [K_{22}^b] & & & & \\ \hdashline [K_{31}^p] & 0 & [K_{32}^p] & 0 & [K_{33}^p] & & & \\ 0 & [K_{31}^b] & 0 & [K_{32}^b] & 0 & [K_{33}^b] & & \\ \hdashline [K_{41}^p] & 0 & [K_{32}^p] & 0 & [K_{43}^p] & 0 & [K_{44}^p] & \\ 0 & [K_{41}^b] & 0 & [K_{42}^b] & 0 & [K_{43}^b] & 0 & [K_{44}^b] \end{array}\right] \begin{Bmatrix} \delta_1 \\ \delta_2 \\ \delta_3 \\ \delta_4 \end{Bmatrix} \tag{3.79}$$

Symmetrical values

where

$$\{F_i\} = \begin{Bmatrix} F_{xi} \\ F_{yi} \\ T_{xi} \\ T_{yi} \\ F_{zi} \end{Bmatrix} \text{ and } \{\delta_i\} = \begin{Bmatrix} u_i \\ v_i \\ \theta_{xi} \\ \theta_{yi} \\ w_{zi} \end{Bmatrix} \qquad (3.80), (3.81)$$

It can be seen from the above that the overall size of each elemental stiffness matrix will be twenty by twenty. The global stiffness matrix may only be formed after the elemental stiffness matrices have been generated for each of the elements in the mesh. The nodes at the corner of the elements must be numbers to assure that the components of the element stiffness matrices are copied to the appropriate cells within the global stiffness matrix. All stiffness matrices in finite element problems are symmetrical and are most heavily populated along the main diagonal. In terms of computing time, the computer expends most of its effort in calculating the inverse of the stiffness matrix. The numbering system used for addressing the nodes determines the bandwidth of the global matrix. It has been found that the least bandwidth can be achieved by numbering the nodes starting along the shortest edge then moving in one row and starting at the node beside the first node in the previous row and numbering in the same direction as before (Rockey et al. 1983:30). This process is continued for all the nodes on the slab. This process is demonstrated in the example show in Figure 3.8

The matrix shown in Equation 3.79 can be summarised as shown in Equation 3.82. Each sub-matrix is a five by five matrix.

$$K^e = \begin{bmatrix} [K_{11}] & [K_{12}] & [K_{13}] & [K_{14}] \\ [K_{21}] & [K_{22}] & [K_{23}] & [K_{24}] \\ [K_{31}] & [K_{32}] & [K_{33}] & [K_{34}] \\ [K_{41}] & [K_{42}] & [K_{43}] & [K_{44}] \end{bmatrix} \qquad (3.82)$$

Upon examining the elemental stiffness matrix shown above a number of important points may be noticed. Firstly, the sub-matrices along the main diagonal relate the effect of a force or moment applied at a corner directly to the

displacement or rotation experienced at that particular corner of the element. The off-diagonal terms give the relationships between applied forces or moments at a particular node and the observed displacements or rotations at any of the other three nodes. For example, sub-matrix $[K_{21}]$ relates the effect that applying a force, or moment to node two has on the displacement or rotation of node one in the element under scrutiny.

3.4.2. An example

A six element plate provides an ideal example of how the global stiffness matrix is constructed. The six elements are lettered from A to F and the nodes at the corners of the elements are numbered from 1 to 12. The node numbering system conforms to the method outlined in the last section to give a global stiffness matrix with the least possible bandwidth.

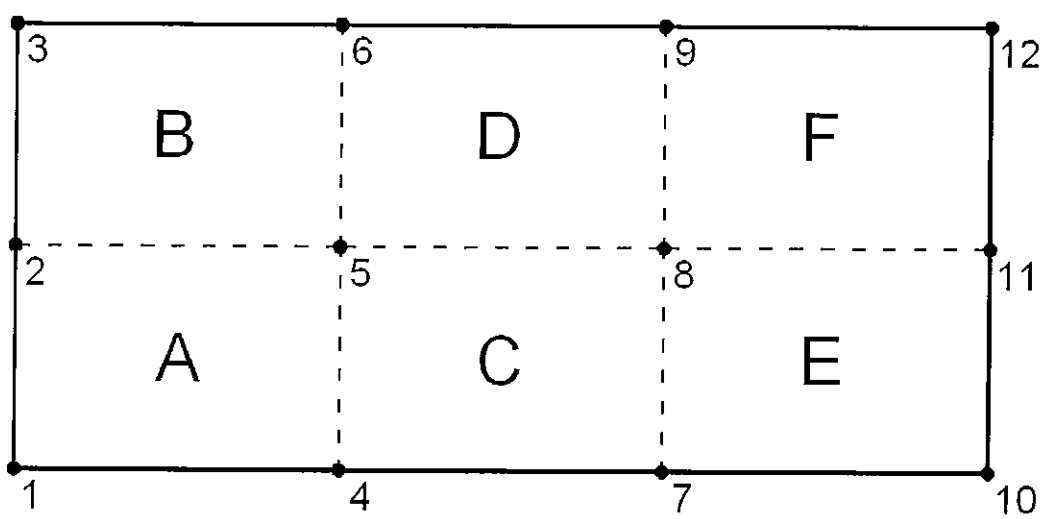

Figure 3.5 six element example

Shown below in Equation 3.83 is an elemental stiffness matrix divided into sixteen sub-matrices. This particular matrix relates to element 'A' from the plate shown above. The rows and columns are numbered according to the numbers assigned to the corners of the element.

$$K^e = \begin{bmatrix} [K_{11}] & [K_{12}] & [K_{14}] & [K_{15}] \\ [K_{21}] & [K_{22}] & [K_{24}] & [K_{25}] \\ [K_{41}] & [K_{42}] & [K_{44}] & [K_{45}] \\ [K_{51}] & [K_{52}] & [K_{54}] & [K_{55}] \end{bmatrix} \tag{3.83}$$

The first element in the plate 'A' has nodes 1, 2, 4 and 5 at its corners. The sixteen sub-matrices from which each elemental stiffness matrix is formed is a five by five matrix. This stems directly from the degrees of freedom chosen for the model used in this project. As is apparent from the numbering of the nodes in Figure 3.5, the numbering of the first and second node and also the third and fourth, is sequential. The difference in the numbering of the first and the third node in an element and also between the second and the fourth node on an element differs by a value equal to the half-bandwidth of the matrix plus one divided by the number of degrees of freedom (DOF) adopted. In the case of the plate shown above the, half-bandwidth is found as follows:

Greatest difference in node numbers: 5 – 1 = 4
Half-bandwidth: number of DOF * (difference in node numbers + 1)
= 5 * (4 + 1) = 25

The cells in the sixteen sub-matrices are copied in block into appropriate cells in the global stiffness matrix according to the numbering assigned to the sub-matrix. This process becomes clearer when the completed global stiffness matrix shown below in Equation 3.84 is studied.

From further examination of the sample plate and the associated global stiffness matrix, elements 'A' and 'B' can be seen to share nodes '2' and '5'. Taking node '2' first, both elements contribute stiffness to the load carrying capacity of this node. The sub-matrices relating to the direct stiffness of node '2' of both elements are added together in the appropriate cells in the global stiffness matrix.

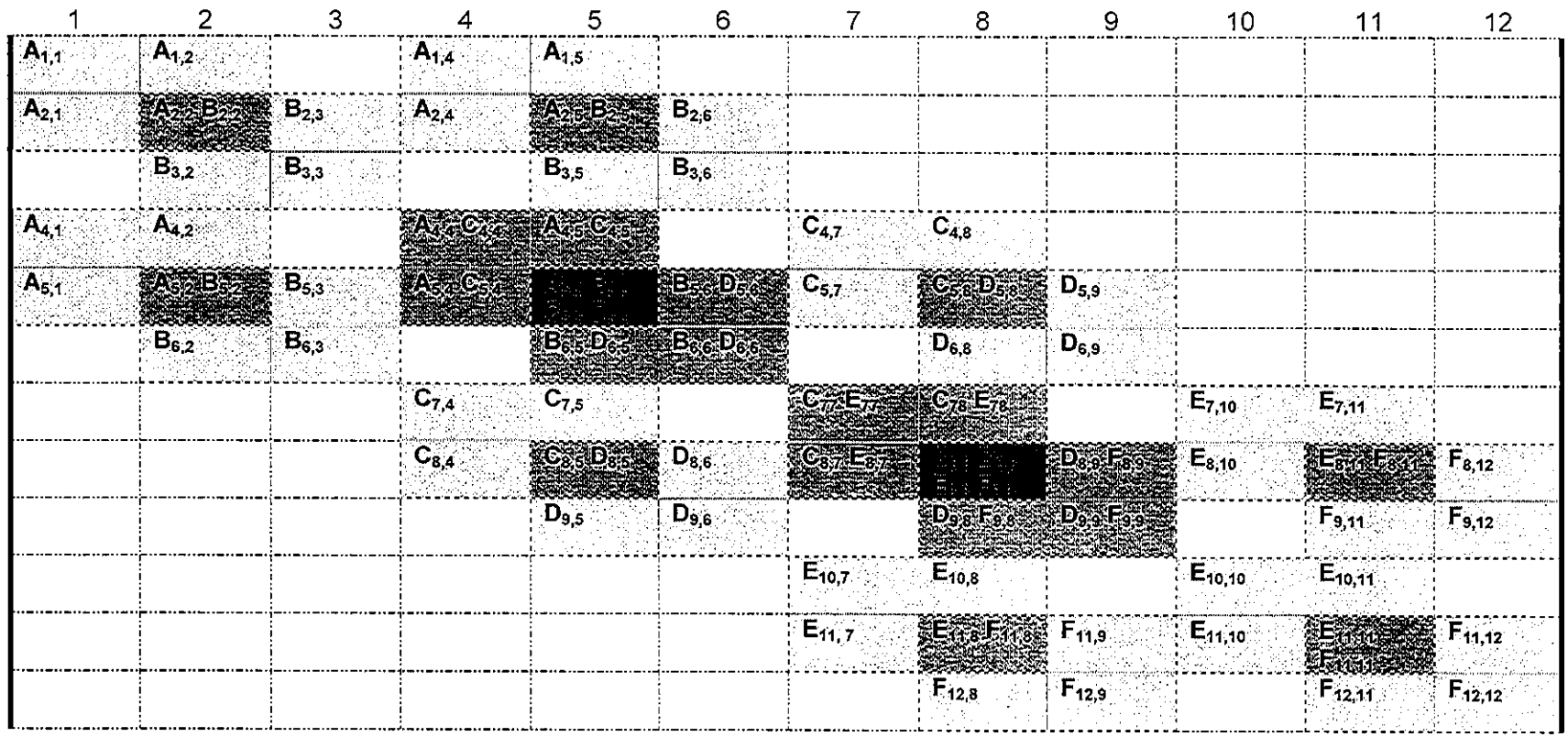
1 2 3 4 5 6 7 8 9 10 11 12
1 A1,1 A1,2 A1,4 A1,5
2 A2,1 A2,2 B2,2 B2,3 A2,4 A2,5 B2,5 B2,6
3 B3,2 B3,3 B3,5 B3,6
4 A4,1 A4,2 A4,4 C4,4 A4,5 C4,5 C4,7 C4,8
5 A5,1 A5,2 B5,2 B5,3 A5,4 C5,4 B5,5 D5,5 C5,7 C5,8 D5,8 D5,9
6 B6,2 B6,3 B6,5 D6,5 B6,6 D6,6 D6,8 D6,9
7 C7,4 C7,5 C7,7 E7,7 C7,8 E7,8 E7,10 E7,11
8 C8,4 C8,5 D8,5 D8,6 C8,7 E8,7 D8,9 F8,9 E8,10 E8,11 F8,11 F8,12
9 D9,5 D9,6 D9,8 F9,8 D9,9 F9,9 F9,11 F9,12
10 E10,7 E10,8 E10,10 E10,11
11 E11,7 E11,8 F11,8 F11,9 E11,10 F11,12
12 F12,8 F12,9 F12,11 F12,12

(3.84)

3.4.3. Applying boundary conditions

The global stiffness matrix is a singular matrix and as such can not be solved as it stands. Boundary conditions are applied to the global stiffness matrix by suppressing the displacements at nodes. In the combined model developed earlier in this chapter has a total of five degrees of freedom. At the support types considered in this project, deflection (displacement of the plate in the z-direction) is always suppressed. In order to yield a stable structure, the plate must be restrained against lateral movement, i.e. the structure has the ability to resist horizontal forces. This is achieved by restraining both horizontal displacements at one of the supported edges of the slab. It must be noted that horizontal movement should only be restrained at one edge so as to produce the ideal model shown in Figure 3.6. Additionally fixed supports could also be modelled by suppressing all the degrees of freedom at a node including the two rotations.

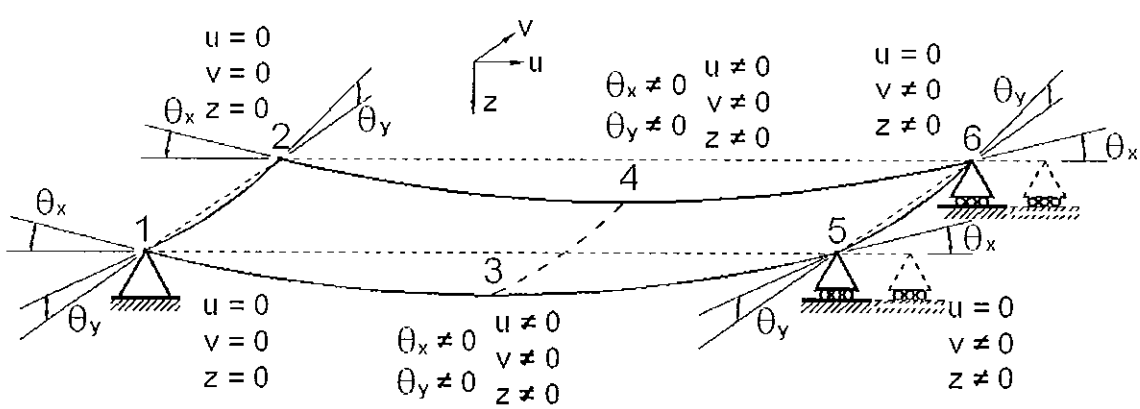

Figure 3.6 sample displacements

As some slabs may be supported on three or more sides it is adequate to restrain lateral movement along only one line of supports.

Once the supports for the slab have been defined these restrictions must be reflected in the global stiffness matrix. This can be accomplished by a number of means. However, the method chosen here involves removing the rows and columns from the global stiffness matrix pertaining to the restrained displacements or rotations. The resulting matrix is commonly referred to as

the restricted global stiffness matrix. The corresponding load vector must also have the rows relating to the suppressed displacements removed.

3.5. Matrix decomposition

The solution stage consumes the greatest proportion of the computational effort in finite element analysis. The two classes of equation solvers are direct solvers and iterative solvers. Direct solvers allow for the stiffness matrix to be decomposed without defining the load vector therefore making the analysis of multiple load cases more efficient than would be the case if iterative solvers are used. Iterative solvers prove more efficient with larger problems involving the solution of greater than fifty thousand degrees of freedom. They are also well suited to problems dealing with non-linear materials (Cook et al. 2002:668). The Cholesky method, a direct solver, was chosen for this project.

The key properties of the matrices generated during finite element analysis are diagonal dominance and symmetry. The symmetrical nature of these matrices means that only half the global stiffness matrix need be generated and stored giving savings in terms of memory space and processor time. Firstly, only half of the elemental stiffness matrix for each element is generated. Given the symmetry of each matrix it is adequate to generate just the lower triangle including the main diagonal. This step reduces the workload by approximately fifty percent and, since a typical analysis may involve many hundreds of elements, there is a considerable time saving. Similarly, since only the lower triangle of the global stiffness matrix is required, the process of assembling the matrix is shortened by approximately a half.

3.5.1. Cholesky decomposition

The Cholesky method in general can only be used for solving symmetrical positive definite matrices. However, the global stiffness matrix generated during a finite element analysis with adequate restraints applied meets these criteria. This method is based on factorisation of the matrix to be solved. The

general case is shown below in Equation 3.85 where {x} is the unknown solution vector. Equation 3.86 shows the form that the decomposition of the matrix [A] would take (Kreyszig 1993:983).

$$[A]\{x\} = \{b\} \tag{3.85}$$

$$[A] = [L][L]^T \tag{3.86}$$

The first step in the matrix solution process is therefore to factorise the [A] as given in the last equation. The $[L][L]^T$ operation is shown in algebraic form in Equation 3.87. The formula used to calculate the specific values in the matrix [L] are shown later in Section 4.10.1.

$$\begin{bmatrix} a_{11} & a_{12} & a_{13} & \cdots & a_{1k} \\ a_{21} & a_{22} & a_{23} & \cdots & a_{2k} \\ a_{31} & a_{32} & a_{33} & \cdots & a_{3k} \\ \vdots & \vdots & \vdots & \ddots & \vdots \\ a_{j1} & a_{j2} & a_{j3} & \cdots & a_{jk} \end{bmatrix} = \begin{bmatrix} m_{11} & 0 & 0 & \cdots & 0 \\ m_{21} & m_{22} & 0 & \cdots & 0 \\ m_{31} & m_{32} & m_{33} & \cdots & 0 \\ \vdots & \vdots & \vdots & \ddots & 0 \\ m_{j1} & m_{j2} & m_{j3} & \cdots & m_{jk} \end{bmatrix} \begin{bmatrix} m_{11} & m_{21} & m_{31} & \cdots & m_{j1} \\ 0 & m_{22} & m_{32} & \cdots & m_{j2} \\ 0 & 0 & m_{33} & \cdots & m_{j3} \\ \vdots & \vdots & \vdots & \ddots & \vdots \\ 0 & 0 & 0 & 0 & m_{jk} \end{bmatrix} \tag{3.87}$$

The factorisation of the global stiffness matrix [A], is carried out independently of the load vector. As will be shown in Chapter 4, this minimises the computation involved in evaluating multiple load cases.

3.5.2. Forward and backward substitution

The next step is the forward and backward substitution of the load vector or load vectors if there is more than one load case to be considered.

Combining Equations 3.85 and 3.86 gives:

$$[L][L]^T\{x\} = \{b\} \tag{3.87}$$

Let $$\{y\} = [L]^T\{x\} \tag{3.88}$$

therefore $$[L]\{y\} = \{b\} \tag{3.89}$$

From this it is apparent that an intermediate vector {y} must be solved for before the displacements in {x} can be found. The matrix $[L]$ obtained from the factorisation of [A], and the load vector {b} allow for an intermediate vector {y} to be found by forward substitution. Back substitution using $[L]^T$ and the

intermediate vector [y] can then be carried out to solve for the displacements in the {x} vector.

3.6. Stresses

Once the displacements have been calculated the results may be scrutinised by the designer. However, it is generally the stresses in slabs that designers are most interested in. Referring back to the main principle on which stress analysis in finite element is based the following can be restated.

$$\{F\} = [K]\{\delta\} \tag{3.90}$$

As seen in Section 3.3.1.3 and 3.3.2.3 stress-displacement matrices link the displacement found above in Equation 3.89 to stresses be the plane stress or plate stresses. A global displacement matrix must be formed with the zero displacements at restrained nodes substituted into the appropriate cells. In order to calculate the stresses in a particular element the displacements and rotations relating to the nodes at the four corners of this element must be gathered into two displacement vectors. The first vector contains the displacements associated with plane stress while the other vector contains the displacements associated with plate bending. These steps can be seen in Figure 3.7 where $\{\delta^{e,\,p}\}$ represents the elemental displacements in the plate associated with in-plane forces, and $\{\delta^{e,\,b}\}$ represents the elemental displacements in the plate associated with the plate bending forces.

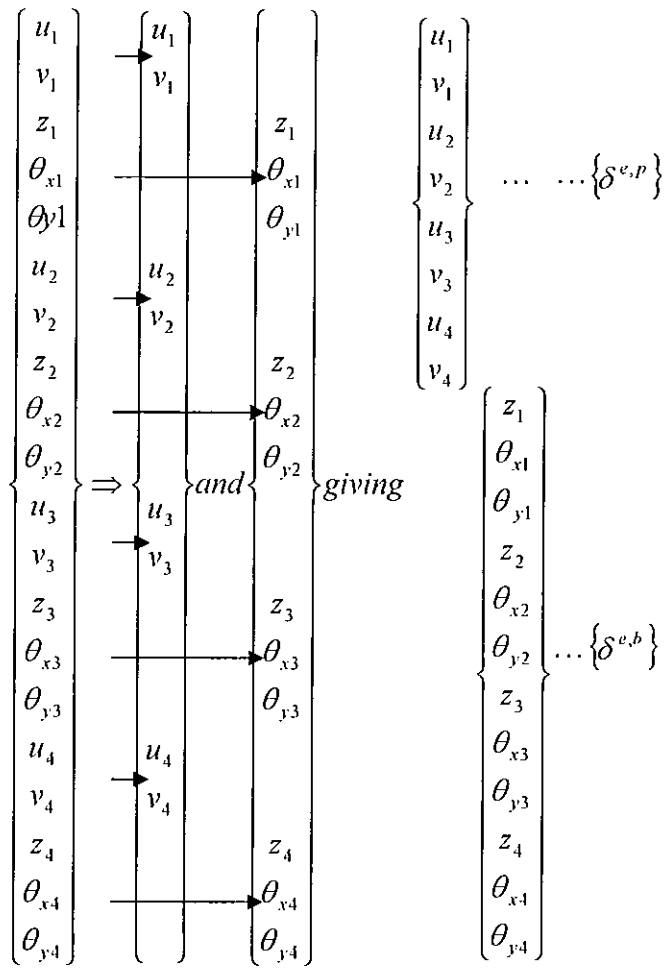

Figure 3.7 division of displacement vector

Once the displacements and rotations for the element have been sorted into their respective vectors, the appropriate stress-displacement matrix is generated and the two stress vectors can be found as shown below in Equations 3.91 and 3.92.

$$\{\sigma\}^p = [H^p]\{\delta^{e,p}\} \tag{3.91}$$

$$\{\sigma\}^b = [H^b]\{\delta^{e,b}\} \tag{3.92}$$

Where $[H^p]$, $[H^b]$ are the stress-displacement matrices for in-plane and plate bending forces respectively and $\{\sigma(x, y)\}^p$, $\{\sigma(x, y)\}^b$ are the stress vectors due to in-plane and out of plane are displacements respectively.

The stresses generated from this analysis can be further processed before presentation. As seen before (see Section 3.3.1.1. and 3.3.2.1.) the stresses from the two models are, once again shown below:

$$\{\sigma\}^p = \begin{Bmatrix} \sigma_x \\ \sigma_y \\ \tau_{xy} \end{Bmatrix} \tag{3.93}$$

$$\{\sigma\}^b = \begin{Bmatrix} \sigma_x \\ \sigma_y \\ \sigma_{xy} \end{Bmatrix} \tag{3.94}$$

The σ_x and σ_y terms in both of the stress vectors may be added to yield the top and bottom fibre stresses in the plate. The shear stress and torsional stresses are not compatible and as such must be presented as other types of stress present in the plate.

3.7. Summary

The plate bending and plane stress theory was developed from first principles with the theory slightly adapted to suit the particular stiffness properties of the hollow core slab examined in this research. The formula for generating both stiffness matrices was developed and the process for constructing the global stiffness matrix shown. The effect of applying boundary conditions is then shown with the global stiffness matrix and load vector being restricted. Matrix decomposition was examined and Cholesky decomposition was chosen for this purpose. The final step examined was the process of using the displacements to calculate the stresses.

4. PROGRAMMING

4.1. Introduction

The previous chapter described the steps involved in setting up the model to be used for analysing the prestressed slabs. It is clear for even the simplest model that computerisation of the process is essential. The simplest possible solution to this would involve constructing an elaborate spreadsheet in Microsoft Excel. However, the user would quickly find that this solution requires a vast amount of work most of which would require modification if a design is changed. Therefore the most flexible option was to write software tailored for the purpose.

The Delphi programming language was chosen as the preferred environment within which to develop the software. The primary reason for this compiler being chosen was that an existing body of expertise in this programming environment had already been accumulated by one of the project supervisors. It could therefore be said with relative certainty that the language was versatile enough to allow the task to be achieved. Delphi is an object orientated Pascal based programming language. The benefit of the object oriented nature of this language is the ability to compartmentalise pieces of code that accomplish different tasks. This helps to simplify the task of debugging code as the error can be tracked to within a relatively small fragment of code. This also allows the programmer to organise the code very easily into logical divisions on work which lends itself to the reuse of sections of code. The Delphi compiler also allows software to be easily linked to other existing packages which, as will be seen in the next section, is essential for a simple user interface. Delphi 7 was the version of the compiler used for this project. Throughout this chapter reference is made to particular sections of code contained in Appendix 3 where the parts of code for the software can be found.

Figure 4.1 shows a brief outline of the processes carried out by the software. Detailed descriptions of these processes are given later in the chapter and a more detailed flowchart of the processes is shown at the end of the chapter.

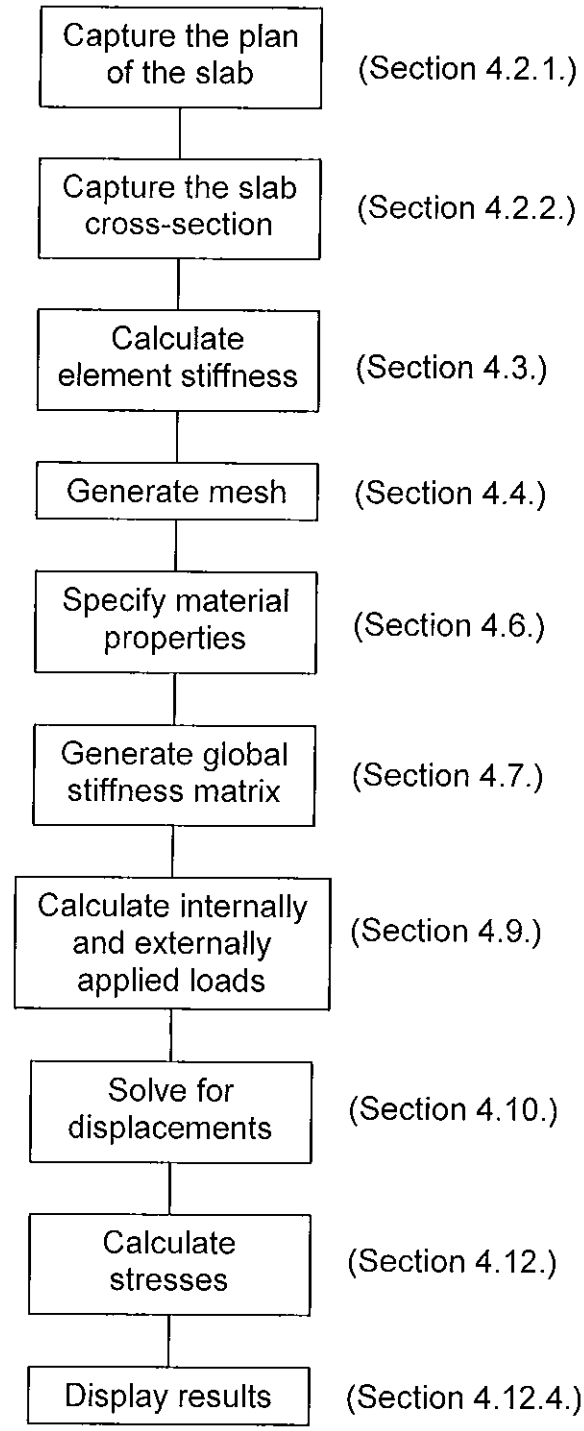

Figure 4.1 outline of processes carried out by the software

4.2. The AutoCAD Interface

A good user interface is one of the more crucial elements required for a software package to be used by engineers without a finite element background. The geometry of the slab, both the cross section and plan shape, are the key

sets of data required to lay out the basic analysis problem. This data is communicated to designers through drawings that are almost always computer generated and distributed electronically through e-mail. There is a limited number of drawing packages used for generating drawings in civil and structural engineering detailing, with Autodesk's AutoCAD, and Bentley's Microstation being the leaders. The AutoCAD package is considerably more popular in Ireland and is used by consulting engineers, architects, contractors and their suppliers and is therefore the most obvious choice of drawing package to link to the analysis software. Linking the analysis package to AutoCAD for the purpose of extracting the geometry of the slab to be analysed provides great convenience and removes a potential source of error from the process.

4.2.1. Capturing the plan of the slab

The floor area to be constructed using precast concrete slabs is also captured from AutoCAD. The area to be slabbed would most commonly be obtained from architect's or engineer's general arrangement drawings. These drawings contain other superfluous information that must be filtered out to prevent errors from occurring. The method chosen to accomplish this end was to filter all lines other than '*polylines*' out of the selection. In the AutoCAD environment, a '*polyline*' is a set of lines treated as a single entity. A '*polyline*' may be draw from known co-ordinates, traced over an existing drawing, or lines and arcs on an existing drawing may be converted to '*polylines*' and then joined together. Figure 4.2 shows the plan of a typical slab with a sizable opening present, and the cross section of a standard 150mm deep slab drawn in AutoCAD.

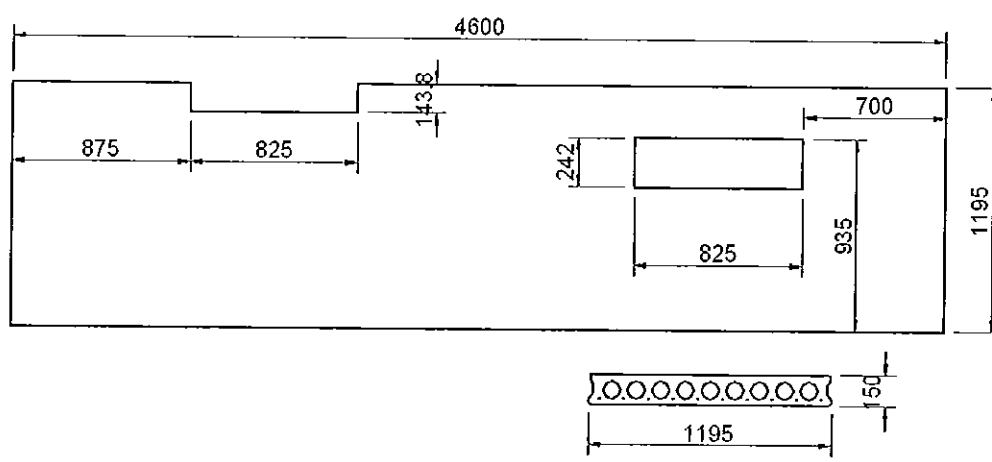

Figure 4.2 slab outline in Auto-CAD

Selecting the shape of the slab in plan is the starting point for the analysis. The slab outline is the first item to be selected. The techniques used as standard to select the items on screen in AutoCAD such as using the 'window selection method', 'crossing selection method' or clicking directly on the item itself may be employed to capture the slab outline. These selection operations are managed by AutoCAD and therefore implement the filters that, for example, prevent the same item being selected twice. The user can also add or remove items from the selection using standard AutoCAD commands. Once the selection of the outline has been confirmed, the main form reappears on screen and generates a scaled down graphical representation of the slab. The user is then is presented with the option to capture any openings in the slab which must be included in the design. Again, as the openings are selected, the graphic on screen representing the slab is updated to indicate the presence of these openings on the slab. This allows the user to verify selections as they are made. Figure 4.3 shows the graphic generated for inspection by the user. The software code relating to the processes outlined above are contained mainly in the unit titled '*Unit_main*' on page 238 in the procedure named 'Get_polyline'.

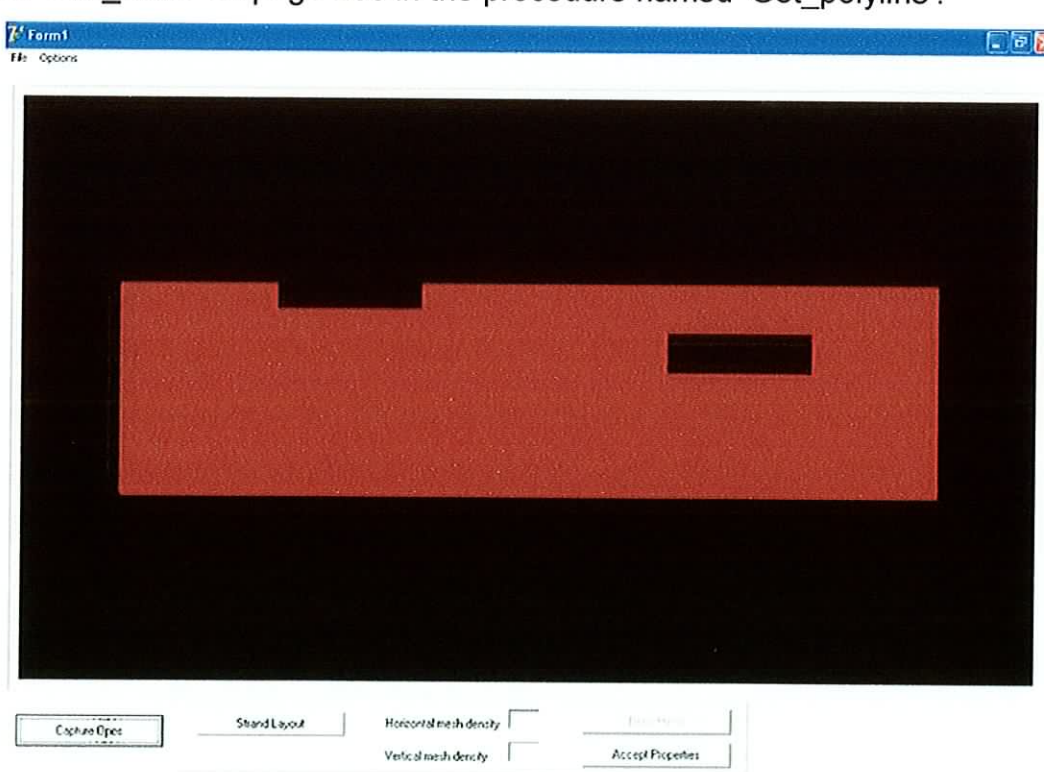

Figure 4.3 slab outline as displayed in the software

4.2.2. Capturing the slab cross-section

The slab cross section including strand locations and sizes is established next. A new form is presented for the purpose of gathering and displaying this information. The selection of the data from the AutoCAD drawing is similar to that for plan shape of the slab however lines, arcs and circles are not filtered out so as to allow the profile of the voids and the location of the strands to be captured. The four different slab cross sections that the software has been designed to capture are shown below in Figure 4.4. In essence there are actually only three cases to be programmed for. The cross sections shown in Figure 4.4(a) and (b) differ only very slightly. The distance from the bottom of the slab to the centres of the top and bottom arcs which make up the longitudinal voids is the first difference and the slightly modified edge profile and deeper cross section is the second. The software deals with both of these two cases in the same manner removing the requirement for extra code to be written. Figure 4.4(c) and (d) shows the circular voided slab and solid slab respectively.

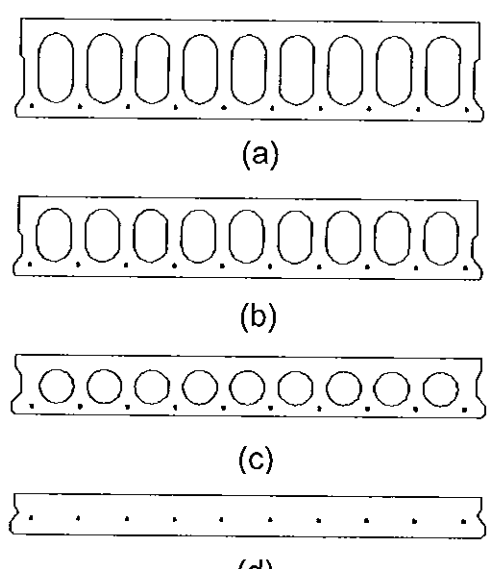

(a)

(b)

(c)

(d)

Figure 4.4 slab cross sections

The shape captured is displayed in the form and the user is then prompted to select a number of key properties relating to the strands diameter and the prestressing force and also factors affecting the losses in prestressing force. All of these fields have values already present that are relatively standard. The

strand diameter is selected from a list of standard sizes whose areas are known from the British Standards relating to prestressing strands. This form is shown in Figure 4.5.

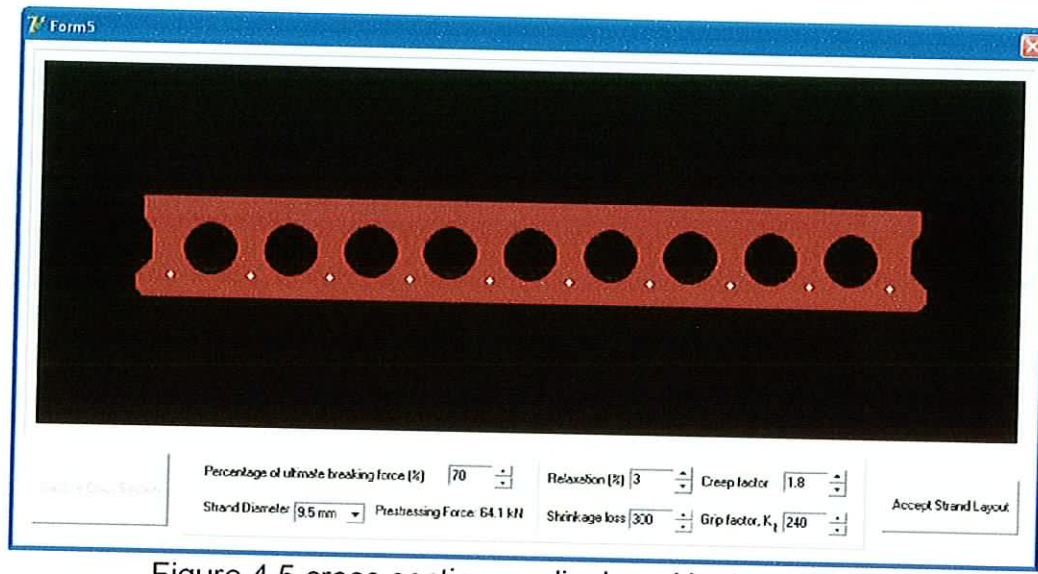

Figure 4.5 cross section as displayed in the software

The value taken for the prestress force as a percentage of the ultimate breaking force is, as standard, 70%; however this may be varied if a designer so chooses. This value along with the strand area is used to calculate and display the prestressing force per strand. The force is calculated based on an ultimate steel strength of 1775 N/mm^2; however this value and other such properties of the steel can be changed through the options menu on the main form before capturing the cross section.

The geometry captured is then processed to extract the relevant data from it. The number of strands and their positions, the number of openings and their positions and the geometry of the perimeter of the cross section are extracted from the data set. All the co-ordinates are reduced based on an x axis that is co-linear with the bottom of the slab cross section and a y axis intersecting the left most point on the slab. The width and depth of the chosen section is established and also the slab type: solid, circular voids or elongated voids. The user then exits this form by clicking on the button to accepting the data displayed. The software code executing this can be seen in the unit '*UO_Strands*' on page 336 and '*UO_shapedata*' on page 325.

4.3. Element stiffness

The geometry of the slab has now been established and at this point some of the engineering properties of the slab can be ascertained. The relationship between the second moment of area of a slab about both the x axis and y axis and the plate bending elastic matrices is given in Section 3.2.1.2. It can clearly be seen from both equations that the flexural rigidity of an element in either plane is a function of the material properties of the element and its geometry.

$$D_x = \frac{E}{(1-\nu^2)} \cdot \frac{I_x}{s_x} \tag{4.1}$$

$$D_y = \frac{E}{(1-\nu^2)} \cdot \frac{I_y}{s_y} \tag{4.2}$$

The second part of each equation, relating to the geometry, gives a quantity found by dividing the second moment of area of the element in the direction under consideration by the width of the element in that direction. As such this quantity could be described as the average second moment of area of the element per unit width.

4.3.1. Selecting element sizes

The choice of element size is based on the cross sectional shape of the slab in the span direction. Another key consideration is the aspect ratio of the element in plan as the best results are given by elements with an aspect ratio of approximately one. Therefore, if the standard element width is halved to help improve accuracy the number of elements to be analysed would increase by a factor of four. The knock on effect in terms of computer processor time must be weighed up against the payback in accuracy. As the calculation of the second moment of area of the elements is complex it is desirable to minimise the variety of element shapes to be analysed, however the values produced must still give significantly accurate results. Figure 4.6(a) and (b) show two potential element arrangements. The element layout shown in figure 4.6(a) has one element type for all the internal elements with the requirement for a second special case to be developed for the edge elements. The element arrangement

shown in Figure 4.6(b) requires two different types of internal elements to be considered together with the special case of the edge element.

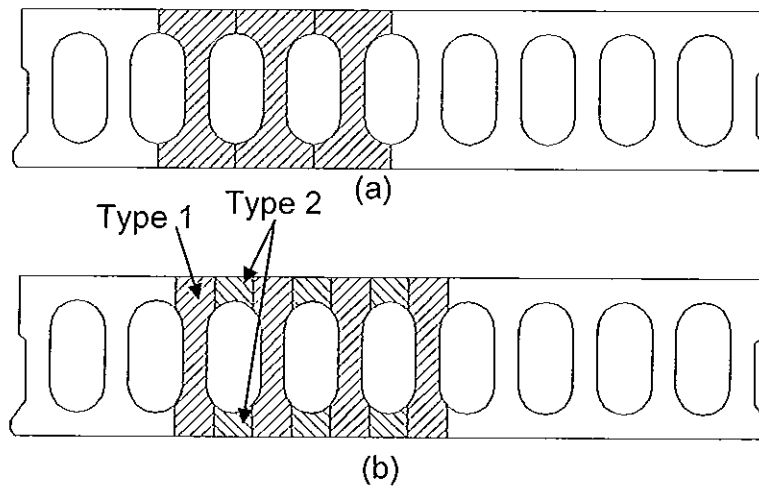

Figure 4.6 possible element divisions

To fully understand the implications of choosing either element arrangement the flexural rigidity equations must be examined. As stated earlier, the second part of these equations gives the average second moment of area of the element per unit width. When this is applied to the 'I-beam' shaped elements given by Figure 4.6(a), it is apparent that the average second moment of area value would differ significantly from values calculated for the individual unit wide strips of the element. Conversely, when the same considerations are applied to either of the two main element types shown in Figure 4.6(b), the average value can be seen to be much closer to the actual value calculated for an arbitrarily selected unit wide strip. The two element types show in Figure 4.6(b) are the narrow I-shaped element composing of the material predominantly between the voids (Type 1) and the element formed from the material above and below the voids (Type 2). Type 1 elements are approximately rectangular with thin, predominantly rectangular slices removed from each side. It must be noted that the portions removed are close to the centroid and therefore have a minor effect on the average second moment of area of the element.

As stated earlier, halving the width of the standard elements approximately quadruples the work load for the computer at the solution stage. However, the time taken to form the global stiffness matrix and solve for the displacements was seen to be reasonably short (10 – 30 seconds) and therefore the increased

accuracy brought by increasing the number of elements was considered to be justified.

The selection of element size also affects the results of the plane elasticity analysis. In the case of a simple isotropic plate, the area per unit width of the element is required. For an element with a solid rectangular cross-section this value is the same as the thickness of the plate. In the case of an orthotropic plate the value that is taken is the average thickness of the plate. Again, if the size and shape of the elements is chosen carefully then the average thickness of an element should not vary greatly from the actual value.

4.3.2. Calculation of the second moment of area

The second moment of area of all the elements must be found as a first step towards establishing the flexural rigidities of the elements. The full set of data required for each element is: the first moment of area in the x-direction and y-direction, the cross sectional area of the element in both directions and the distance from the bottom fibre to the centroid in both directions. As is the norm when finding the second moment of area of a complex shape, the area and distance to the centroid are found as part of the calculation.

To understand this point, the 250mm deep slab is taken as an example. Figure 4.7(a) shows a typical Type 1 element in 3D. From this, the computation process for the second moment of area of the elements becomes clearer. The second moment of area in the x-direction 'Ix', is calculated based on this somewhat complicated 'I-beam' shaped cross section. In the y-direction the 'Iy' is based on a simple rectangular cross section. In Figure 4.7(b) a Type 2 element is shown from which it can be seen that the 'Ix' value is based on a cross section consisting of a top and bottom rectangle with circular segments removed. In the 'Iy' direction, the cross section to be examined consists of an upper and lower rectangle

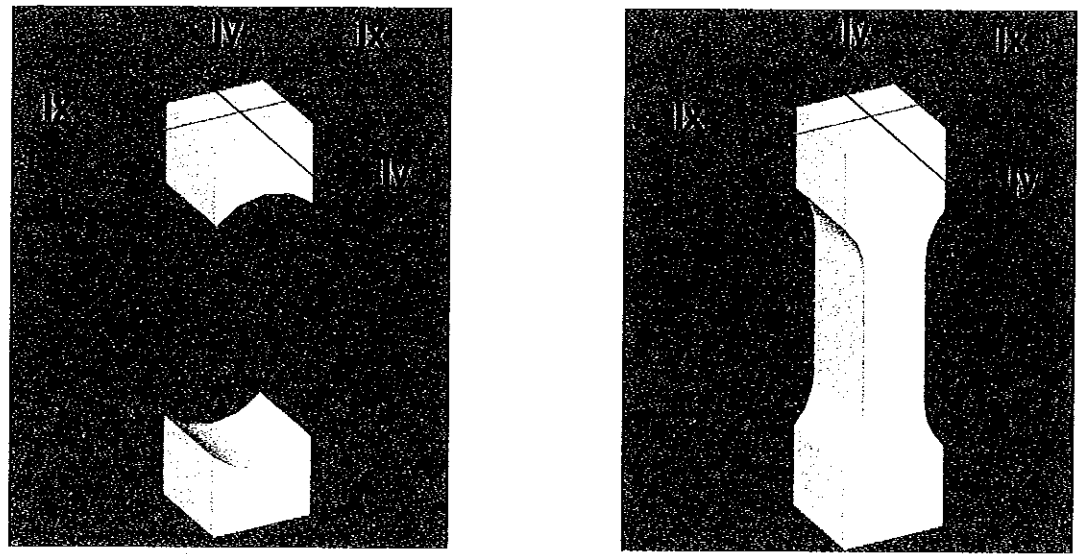

(a) Type 1 (b) Type 2

Figure 4.7 3D display of elements

The actual process of obtaining the second moment of area of the voided slabs involves many steps as can be seen from the partial example shown below in Figure 4.8

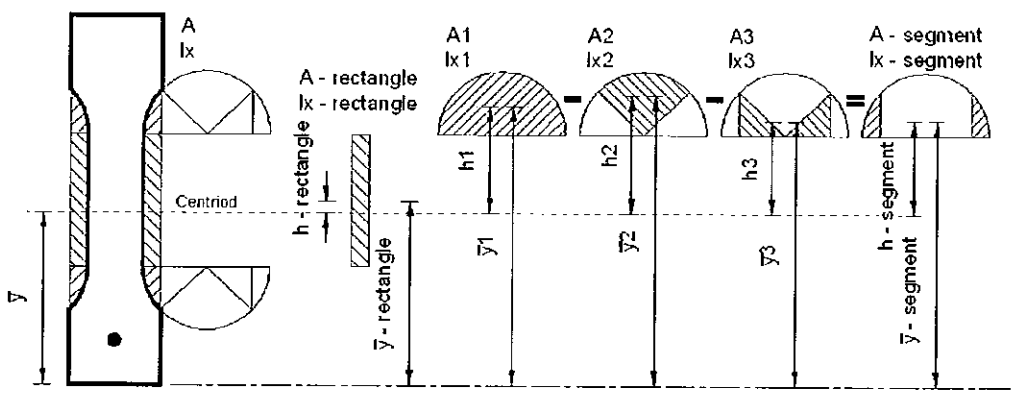

Figure 4.8 calculation of second moment of area

The method used for ascertaining the second moment of area of this section involves finding the value for the hatched areas on either side of the element and subtracting these from that found for the rectangle bounding the cross section and hatched areas combined. The second moment of area of the rectangular section can be found once the distance to the centroid of the overall cross section has been found using the parallel axis theorem. Finding the properties of the segments involves a number of steps. The segmental shape shown by the hatched area can be derived by subtracting an arc and two right angled triangles from a semi-circle. The second moment of area of these three

shapes must be found relative to their own centroids and only then may these values be found relative to the centroid of the element itself again using the parallel axis theorem.

The stiffness contribution of the prestressing strands will effect the second moment of area value of the slab in the direction of the span in a positive manner. The presence of the strands in the bottom of the slab will raise the level of the centroid somewhat and also increase the second moment of area of the element. Despite the relatively insignificant cross sectional area of the stand, when the transformed section is formed, the modular ratio can be seen to increase the effective area of the strand.

The size of the edge elements is found through simple geometry. This is shown in Figure 4.9(a) and (b).

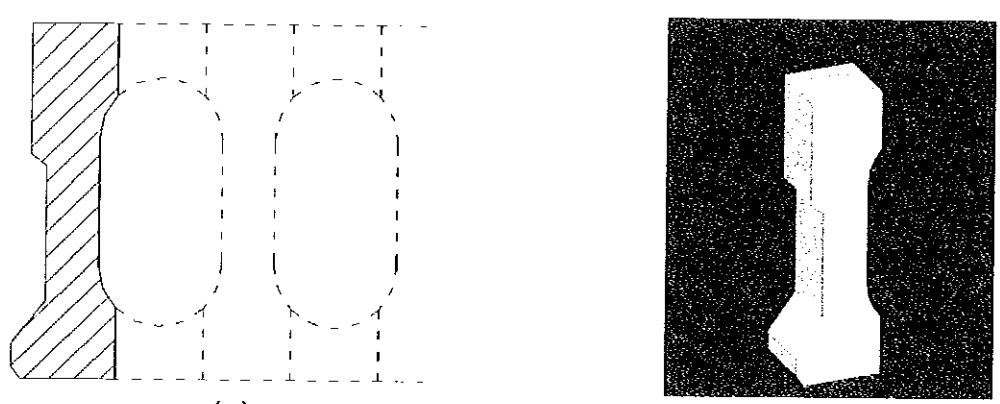

(a) (b)

Figure 4.9 Edge element shape

The elements at the outer edges present a special case in terms of calculating stiffness. The complex shape of edge of the slab, shown on the left side of Figure 4.9(a), requires that an alternative approach be taken to calculating its second moment of area. The method chosen to accomplish this was to calculate half the second moment of area of a standard Type 1 element and to use the Greene's theorem to find the second moment of area of the irregularly shaped outside edge of the first and last element in the cross-section of the slab. The code implementing this is found in *'UO_DArray'* on page 260.

4.4. Mesh Generation

A detailed study of mesh generation is beyond the scope of this research however at a basic level it must be employed in the software. A possible extension to the research could include the application of shape functions to allow denser meshes to be used, for example, near corners or openings.

As seen in the last section, the mesh density perpendicular to the direction of the span of the slab is determined by the shape and number of voids. In the span direction openings and notches in the slab affect the layout of the mesh.

4.4.1. Element Shape

As stated in Section 4.3.1. an aspect ratio of less than 2 for the elements is desirable with square elements being best. The standard element width is found by examining the cross section. The width of the cross section to be meshed with either Type 1 or Type 2 elements of whatever size is found and divided by the number of such elements to be found in the cross section. This process can be seen in Figure 4.10.

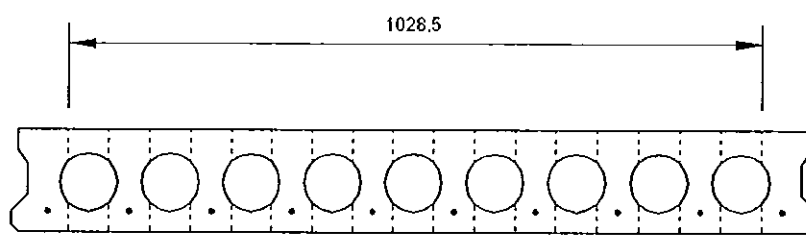

Figure 4.10 cross section through the mesh

In the case of the slab shown the standard element width would be 60.5mm (1028.5 / 17). It is unlikely that exact multiples of the standard element size found above would fill out the distances shown below in Figure 4.11, and therefore a number of element sizes must be developed to meet this requirement.

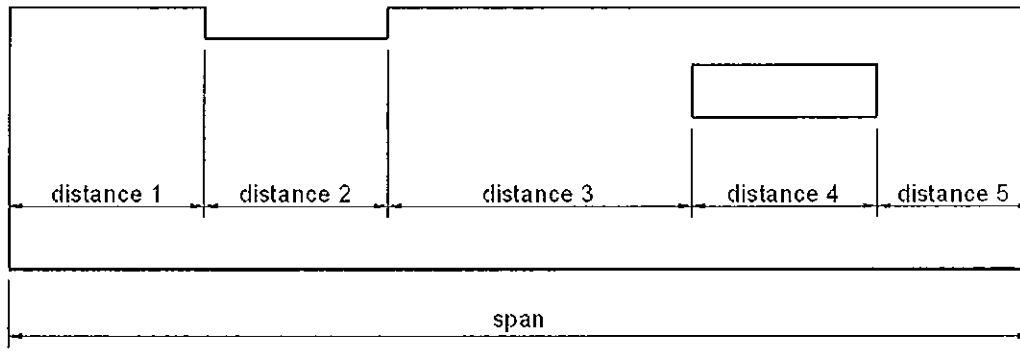

Figure 4.11 division of area for meshing purposes

An array of distances within which identical elements sizes are required is constructed. From these distances the number of columns or rows of standard elements that will fit within the region is found. However, to ensure that the elements fit exactly within the bounds of the region being meshed, a whole number of elements must be used. The number of elements to be used in each of these regions is found by rounding the number of partial elements and adjusting the element sizes so as to create a perfect fit. It can be seen that this process ensures that the aspect ratio of the elements is kept within the desirable range. The process used to generate the array of element sizes is shown in Table 4.1.

	Length (mm)	Length / Average Element size	Number of Elements	Exact Element Size (mm)	Aspect Ratio
Distance 1	950	15.70	16	59.375	1.019
Distance 2	825	13.64	14	58.929	1.027
Distance 3	1300	21.49	21	61.905	1.023
Distance 4	825	13.64	14	58.929	1.027
Distance 5	700	11.57	12	58.333	1.037

Table 4.1 sample meshing calculation

The geometry of the edge elements is such that their aspect ratio is greater that the other elements, typically up to 1.5, however this is below the upper limit and therefore does not present a problem. In the case of a small distance where the (Length / Average Element size) calculation rounds down to zero then one column of elements is inserted at this location with an element width equal to the distance itself. Refer to '*UO_Mesh*' on page 299.

4.4.2. Location of the elements

The presence of an opening on a simple level involves removing elements from the mesh so as to negate their contribution to the stiffness of the overall body. The procedure to achieve this involves two steps. Firstly, a test is carried out on all of the nodes in the mesh to determine whether they lie on the surface of the slab or not (in a notch or opening). From this a 2D Boolean array is formed. In Figure 4.12 the nodes that have been found to lie on the slab are denoted by a solid black dot with the remaining nodes left blank.

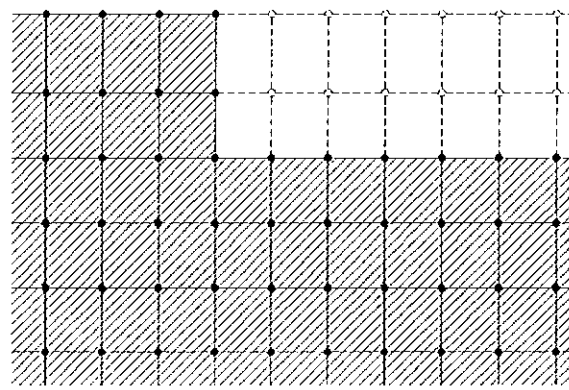

Figure 4.12 removing elements from a mesh to create an opening

The second step entails examining each rectangle in the mesh by counting the number of nodes on its perimeter and denoting it as an element if all four nodes are inside. Again, a Boolean array is formed to store this data for every element in the mesh.

The mesh generated within the software is generated on the display in the main form. The mesh is superimposed over the plan of the slab shown in Figure 4.3 to allow the user to verify mesh generated by the software. This is shown in Figure 4.13. The user then clicks to accept the geometry and properties material properties of the elements.

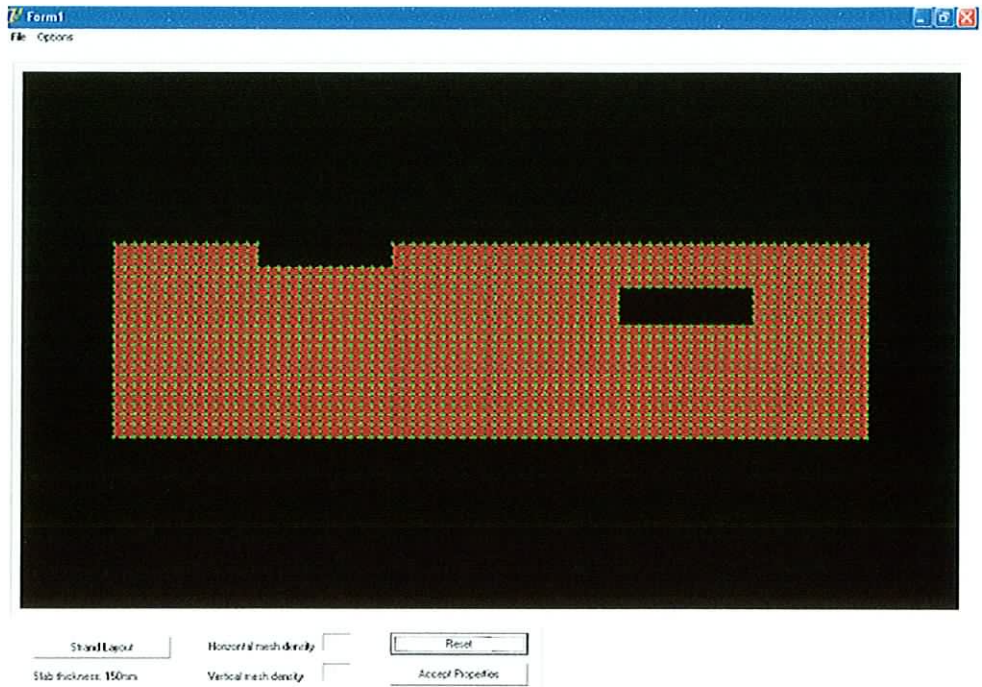

Figure 4.13 meshed slab as displayed in the software

4.5. Service and transfer condition stress checks

In the last chapter the requirement to check both transfer and service stresses was shown. The key differences between the transfer and service checks are the concrete strengths used, the magnitude of the gravity loads and the effect of time dependant losses in prestressing force. As will be seen in the next section, the Young's Modulus of the concrete at transfer is significantly different to the long term value used for the service stress checks. Referring back to the finite element theory outlined in Section 3.2.1.2 and 3.2.2.2., the elasticity matrices are a function of the Young's modulus of the concrete. Those elasticity matrices are in turn used in the formation of the global stiffness matrix. This results in the requirement for two global stiffness matrices to be formed and solved.

The process of solving for the stresses at both transfer and service conditions also involves generating a pair of load vectors to reflect the different loading present at these two conditions. At the transfer stage the only gravity loads present are those due to the self weight of the slab. The prestressing force at this stage is affected only by losses that occur almost instantaneously at the moment of transfer. These losses are detailed in Section 2.4. The second load vector required contains the total effect of all gravity loads acting on the slab

such as the self weight, uniformly distributed loads and patch loads. The prestressing forces within this load vector are assumed to have been reduced by all the losses including those that are time related. Following the two sets of analyses outlined above, two sets of results would be displayed to the user.

4.6. Material Properties

As stated earlier the material properties to be used during the analysis are either those that are preset when the software was written or if the user so chooses a custom set of values may be used. The preset values would be considered to be the standard values used in a lot of design work and so may not require alteration. The option does however exist to change the steel and concrete material properties.

The steel properties form, shown below in Figure 4.14 is the form on which the steel properties are defined. The idealised stress / strain graph, discussed in some detail in Section 2.4.2, is shown. The user may decide to change the 'f_{pb}' or 'E_s' values presented on the form. The graph updates itself automatically to reflect these new values.

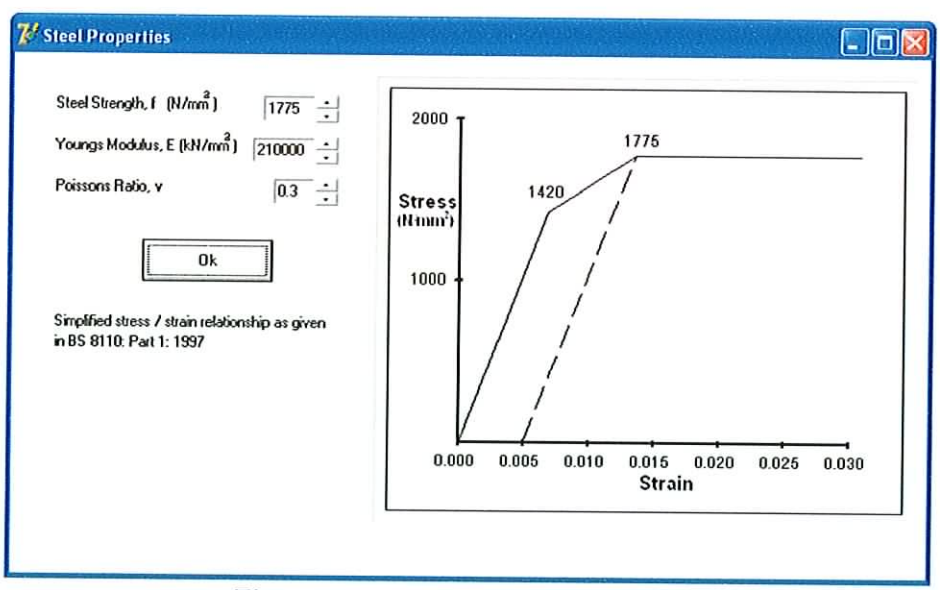

Figure 4.14 Steel properties form

The properties of the concrete can be changed through the concrete properties form. Once again a set of values are presented that the user may choose to

accept. Figure 4.15 shows the form on which the changes to the standard properties may be made.

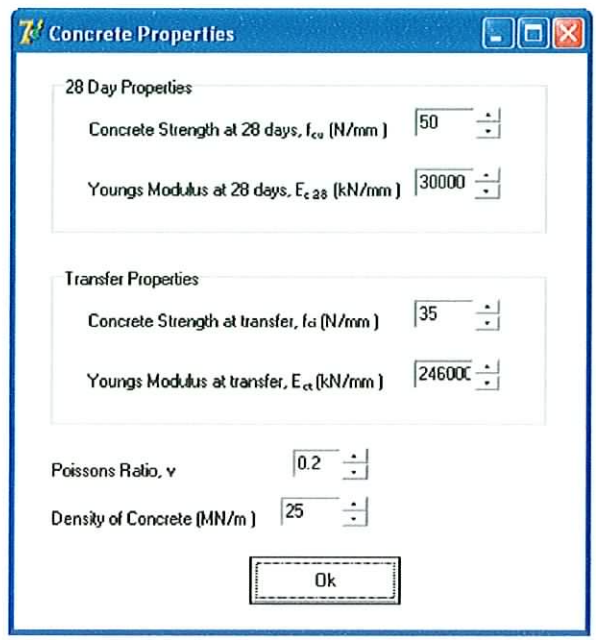

Figure 4.15 Concrete properties form

If the user changes the 28 day strength the value of the 28 day Young's modulus changes to reflect these changes. As a relationship exists between the 28 day strength and the Young's modulus at transfer, any changes to the 28 day strength will affect the value shown for the Yong's modulus at transfer. However this does not preclude the user from manually selecting a value based on experience or experimentally found values. It can also be seen that changing the value for the concrete strength at transfer also affects the displayed value for the Young's modulus at transfer. The concrete density used for calculating the self weight of the slab may also be changed. The Poisson's ratio value presented is standard but again the option is there for the user to modify it. The units titled '*UO_MaterialProperties_Concrete*' on page 287 and '*UO_MaterialProperties_Steel*' on page 290 perform the tasks outlined above.

4.7. Filling the global stiffness matrix

It is now possible to construct the global stiffness matrix based on the data collected. The theory outlining this procedure is discussed in Section 3.4.1 however whilst programming this section it became apparent that it would be critical to consider optimising the assembly and storage of the global stiffness

matrix. As this software was being assembled, the standard quantity of RAM memory sold with computers was between 512Mb and 1024Mb. Whilst assembling and solving a large matrix, the operating system attempts to carry out the operation whilst storing the pertinent data in RAM. However, if the available RAM memory is insufficient then the computer will move some of the data to virtual memory which is hard disk based. The problem then arises that data stored in the hard disk takes approximately 30 times longer to access.

4.7.1. Bandwidth optimisation

As a rule there will always be a greater number of columns of elements in the span direction than rows in the lateral direction. This enables the matrix with the least possible bandwidth to be formed following the rule of thumb stated in Section 3.4.1. Once the half-bandwidth has been found it is then possible to minimise the storage space required for the global stiffness matrix. This is achieved by creating storage space for a rectangular array of numbers as opposed to the square array required to store the entire matrix. Figure 4.16(a) shows the general form taken by a global stiffness matrix generated for a body divided into a 4 * 3 element mesh

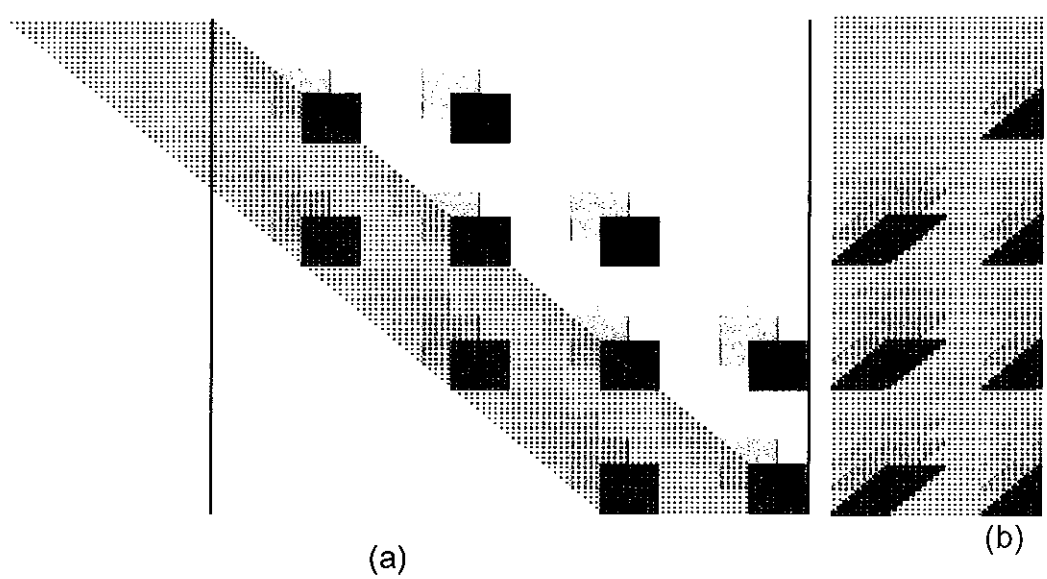

Figure 4.16 storage method for global stiffness matrix

The rectangular array is shown in Figure 4.16(b). The square array in this case contains 10,000 numbers whilst the rectangular array contains 3,500. The savings in terms of memory space increase greatly as the matrices get bigger.

For example, if the plate being considered above was divided into a 4 * 4 element mesh the square array would have 15,625 numbers whereas the rectangular array has 4,375 numbers. Whilst these numbers are relatively small if a small slab with a span of 4m were considered, a 19 * 64 mesh would be formed. The square array formed for this would contain 42,250,000 numbers whilst a rectangular array would require 715,000 numbers. As the spans get larger, and therefore, the matrices bigger, the percentage saving in terms of memory space increases when using the rectangular storage technique.

The rectangular arrays discussed above result in a relatively small number of cells at the top left of the global stiffness matrix, as seen in Figure 4.16, effectively being wasted. It proved a simpler solution to accept this wastage so as to simplify the code governing the formation and assembly of the global stiffness matrix. In the case of the 19 * 64 mesh discussed above the number of unused cells in the triangle at the top of the array would be 4851 or 0.7% of the total array size. The unit '*UO_Ke*' on page 278 carries out the formation and optimisation discussed above.

4.7.2. Elemental stiffness matrices

The individual elemental stiffness matrices must be formed before copying the individual cells into the global stiffness matrix. This process begins with a loop that systematically works through the mesh, determining, from the Boolean array (discussed in Section 4.4.2) whether or not an element exists in the particular location. If an element does exist at the location under consideration, then the geometry of the element is established and the plane stress and plate bending elasticity matrices for the particular element are used to generate the stiffness matrix for the element. This matrix is also symmetrical and therefore only the lower triangle is formed. The individual elemental stiffness matrices are destroyed after its cells are copied into the global stiffness matrix so as to free up memory space.

4.7.3. Openings and Notches

The first step taken when constructing the global stiffness matrix within the software is to create an array large enough to store the data. The initial storage array gets its size from the numbers of rows of elements multiplied by the number of columns of elements by the number of degrees of freedom. This is the size of the global stiffness matrix assuming that the slab is solid. However, the presence of notches or openings in the slab results in nodes effectively being removed from the solid mesh. It was deemed simpler to write a piece of code to fill the oversized matrix and then after this is complete remove the rows and columns pertaining to the defunct nodes. Referring back to the 4 * 3 element mesh from Section 4.5.1, it can be seen that the rows and columns corresponding to the degrees of freedom at the nodes excluded from the mesh remain empty. Figure 4.17(a) shows a plate with four elements removed.

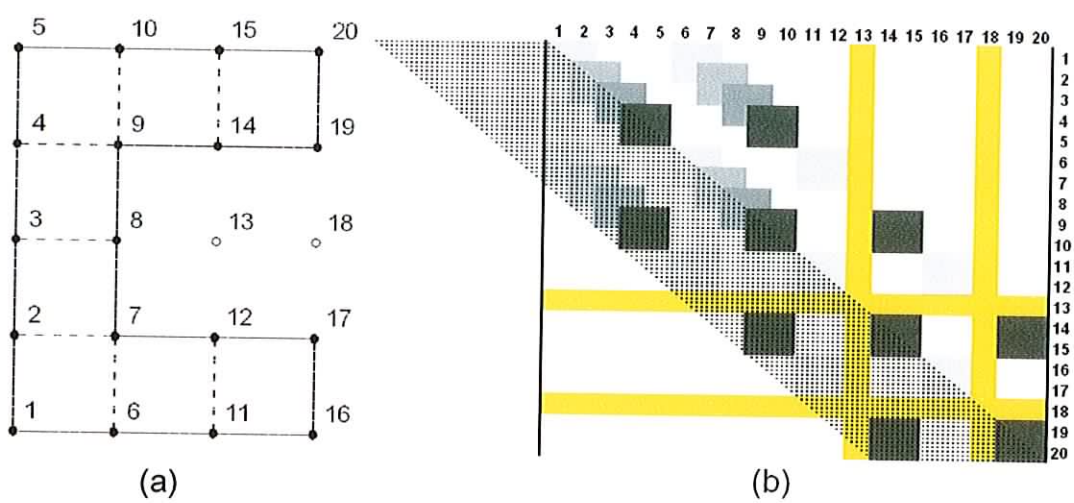

(a) (b)

Figure 4.17 example of global stiffness matrix storage

The diagram shows that two nodes, 13 and 18, are obsolete and therefore their equivalent rows and columns must be removed from the global stiffness matrix. The effect that this has on the global stiffness matrix can be seen in Figure 4.17(b) with the rows and columns to be removed shown in yellow. These rows and column are removed after the global stiffness matrix has been populated by all the elemental stiffness matrices. The resized global stiffness matrix for the above example is shown in Figure 4.18.

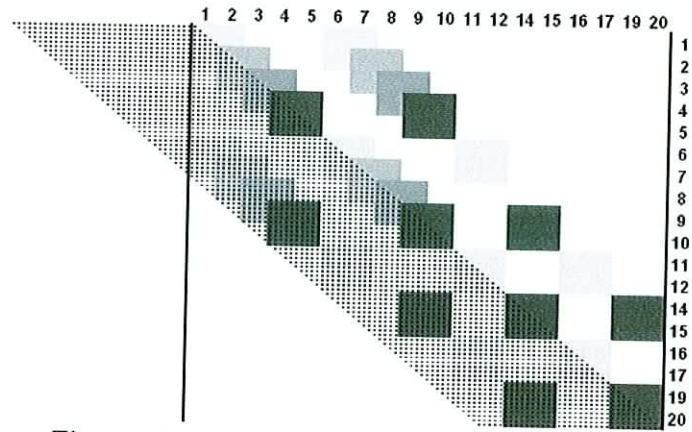

Figure 4.18 resized global stiffness matrix

4.8. The application of boundary conditions.

The global stiffness matrix generated using the steps given thus far in this section is, in theory, a singular matrix, whose variables can not, as things stand, be solved for. In mathematical terms, the determinant of the matrix is zero and therefore no solution exists. In real terms, attempting to solve for displacements without specifying the supports makes little sense as infinite displacements would occur.

The next step for the user is to define the supports for the slab. An assumption is made that all supports defined will be found at the perimeter of the slab. To ensure that an adequately restricted structure is defined, all horizontal movement as well as vertical movement is restrained at the first supported edge selected, thereafter any supports selected are roller supports. To define a supported edge the user simply hovers the arrow over the edge to be supported. As seen in Figure 4.19(a), a white line appears under the arrow.

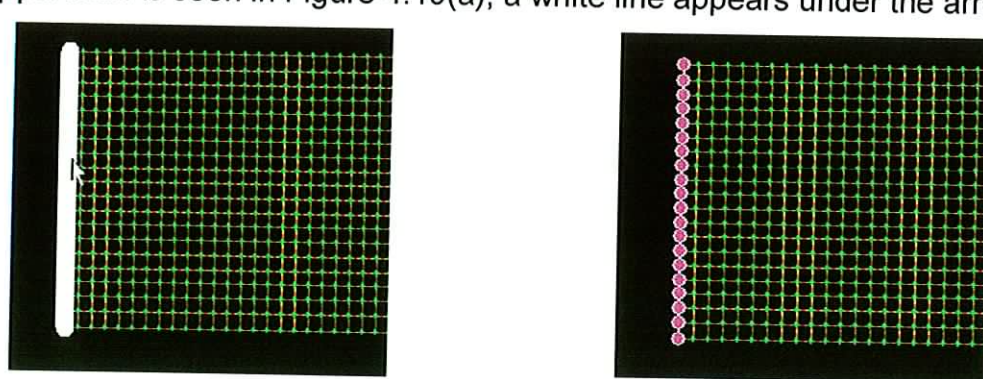
(a) (b)

Figure 4.19 applying supports in the software

The user then verifies the selection by clicking on the white line. As the user does this the white line disappears and pink dots appear on the nodes indicating the selection. As each support has been selected a database of the supported nodes is formed with the exact nature of the support recorded (fixed or pinned). The user then moves to the next support and the process is repeated. A further precaution is taken to ensure that adequate supports are provided by preventing the user from proceeding to the next step in the process until at least two supported edges have successfully been defined. The software code for this is given in '*UO_Support*' on page 356.

4.8.1. The restricted global stiffness matrix

The data collected must then be used to restrain the global stiffness matrix as such forming a second 'restricted' global stiffness matrix. Figure 4.20 shows the plate for which the global stiffness matrix was developed in Section 4.5.3. The diagram shown below has supports defined along the top and bottom. Nodes 5, 10, 15 and 20 are pinned supports whilst nodes 1, 6, 11 and 16 are roller supports.

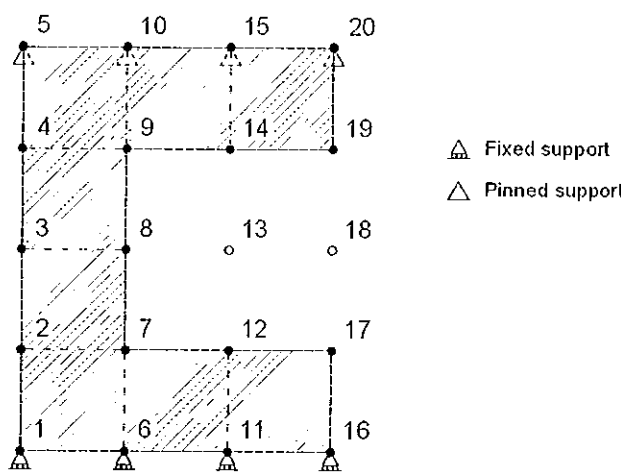

Figure 4.20 sample plate with supports

The restricted global stiffness matrix is formed by suppressing the relevant row and columns in the global stiffness matrix. This process is similar to that shown Figure 4.17, however instead of eliminating all rows and columns relating to the nodes in question, the rows and column removed relate to certain degrees of freedom at these nodes. As seen in Section 3.3.1 the first, second and third degrees of freedom at a node relate to movement in the horizontal x and y

directions respectively, and vertical deflection in the z direction. The fourth and fifth degrees of freedom relate to rotations about the x and y axis. Therefore, in order to restrain a node at a pinned support the first three degrees of freedom must be suppressed and also, to restrain a node at a roller support only the third degree of freedom would be suppressed. Figure 4.21 shows the rows and columns in yellow that must be suppressed in order to correctly restrain the plate shown above in Figure 4.20.

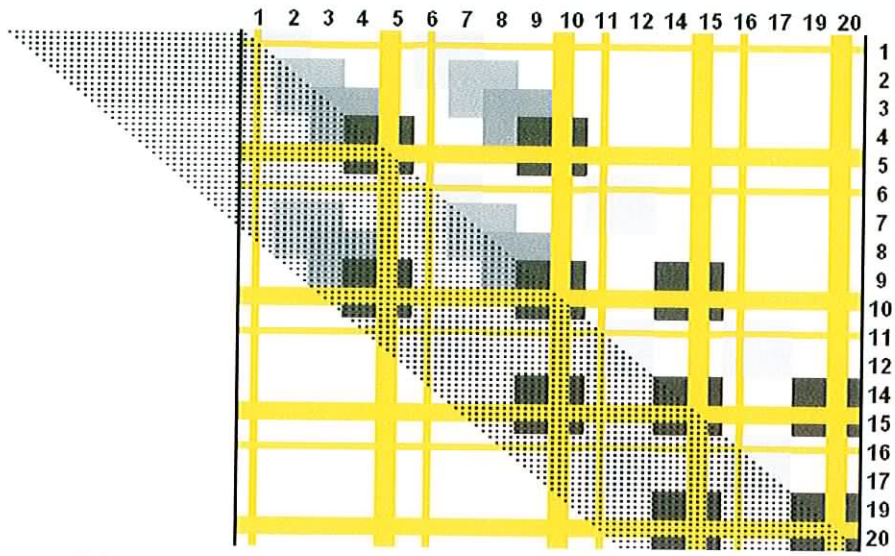

Figure 4.21 global stiffness matrix with restricted rows and columns

Again, a new resized array must be formed to hold the values contained in the restricted global stiffness matrix. Figure 4.22 shows the reconstructed restricted global stiffness matrix.

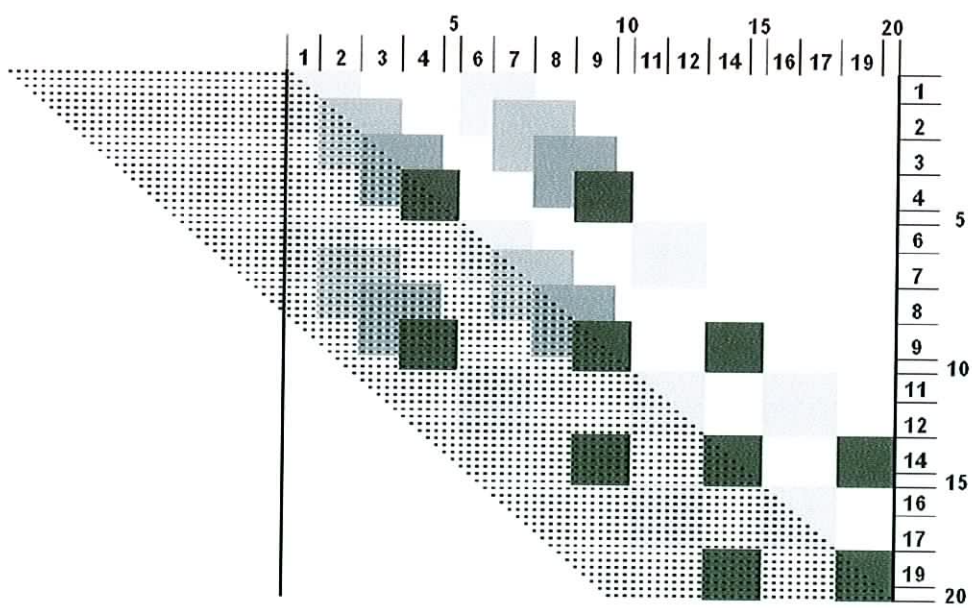

Figure 4.22 restricted global stiffness matrix

4.9. Loading

The loading applied to an element acts on the structure through the nodes at the corners of the element under examination. A node located inside the perimeter of a structure and away from openings or notches would potentially receive loading from all four surrounding elements. To this end, the procedure used to produce the load vector was to examine the elements, an element at a time, determine whether it was loaded and if so how much loading, and then distribute the load evenly to its four corner elements.

4.9.1. Externally applied loads

The application of externally applied loads is relatively simple. The two most common loads, a uniformly distributed load and the self weight, are applied by clicking on a tick box. In the case of the uniformly distributed load, its magnitude must also be defined. The patch load is selected using selections made with the mouse as opposed to specifying coordinates.

4.9.1.1. Self Weight

The self weight of the slab is the one ever present load and therefore by default is included in the calculations to find the load vector. The option to remove the effect of the self weight from the load vector is however presented, as this may be required occasionally for testing or calibrating the software.

In Section 4.3.2. the process used to determine a number of properties was outlined including the cross sectional area of the elements. The cross section taken in the x direction is a true cross section for any plane along the length of the element in the x direction. Therefore, from this cross sectional area and the length of the element in the span direction, the volume of the element can be found and then from this the weight of the element. Section 4.3.1. shows that the mesh will typically be made up from three different element cross sections, the two standard internal element types and the special element shape required at the sides of the slab. The Type 1 and 2 internal elements are symmetrical in

the x and y direction and therefore their self weight can be said to be carried evenly by all four corner nodes. This is not the case for the edge elements as they are clearly asymmetrical in the x direction. Upon visual inspection of the three edge element shapes it was deemed to be close enough to symmetrical to allow the distribution of quarter of the self weight to each node to stand. The pay off in terms of the accuracy of writing code to find a more accurate distribution was deemed to be inefficient.

4.9.1.2. Uniformly distributed loads

The loading applied to an element acts on the structure through the nodes at the corners of the element under examination. Therefore if an element has a uniformly distributed load applied (udl) to its entire surface area it can be said that each of the four corner nodes is carrying a quarter of the load. The user must specifically choose to apply this load as it is not included by default. The magnitude of the load is preset at 2 kN/m^2.

4.9.1.3. Patch loads

Patch loading may be used to simulate a number of potential loading patterns that may be applied to slabs. Line loads due to walls being constructed or point loads due to columns bearing onto the slab may also be simulated. To achieve this, the user must increase the intensity of the patch load which is given in kN/m^2 in order to replicate the effect of a wall load which would be calculated in kN/m run based on a wall width of 100mm to 150mm. A limitation in the software is found here as the exact boundaries of the patch load must coincide with the mesh as generated earlier. However, it should be considered that since the elements are generally about 60mm in width and length, this approximation should not lead to a large error.

4.9.2. Internally applied loads

The information gathered thus far allows the prestressing forces at the required intervals along the span of the slab to be calculated. The unit of code which

carries out this function is triggered once the externally applied loads have been defined.

4.9.2.1. Calculating losses in the prestressing force

Once again the theory underlying this process is dealt with in Chapter 2. However the methods used to implement this theory in the software itself are shown here. The first step in this process is determining the length of the sections of strands in the slab. This is accomplished by considering the rows of elements containing strands. Starting from the left most element in a particular row, the width of the element in the span direction, is copied to a 1D array of values. This process continues along the strand moving across the slab in the direction of the span until either a notch or opening is encountered or when the end of the row of elements is reached. A new array is formed to store the width values for the next section of the strand if such a section exists. At the end of the row a number of arrays may exist, one for each unbroken section of the strand. The data is copied into a record structure before the next row is considered. An example is used to demonstrate the method adopted and the data structure generated in the process. Figure 4.23 shows a typical slab with a notch and opening present. The elements of interest, i.e. those containing the strands, are shown lightly hatched. Each row containing a strand is numbered. The individual sections of strand are also numbered in the order in which they are scrutinised.

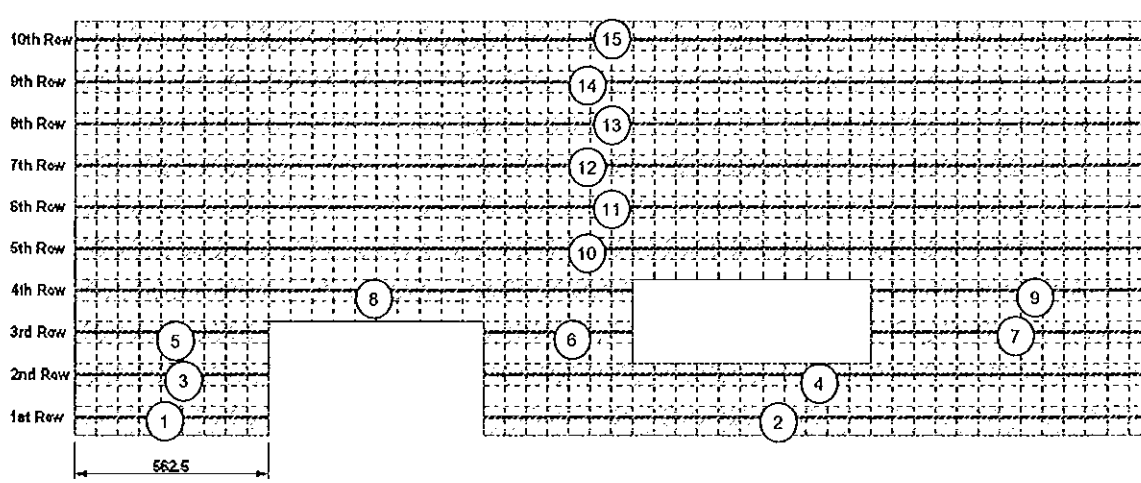

Figure 4.23 slab outline with strands

The first row of elements containing a strand is divided by a notch in the slab and following the procedure laid out above it can be seen that two arrays of element widths are required. These arrays are represented by (1) and (2) on Figure 4.23. Once the entire row has been considered the resulting arrays may be copied into the overall record structure, the first half of which is shown in Figure 4.24.

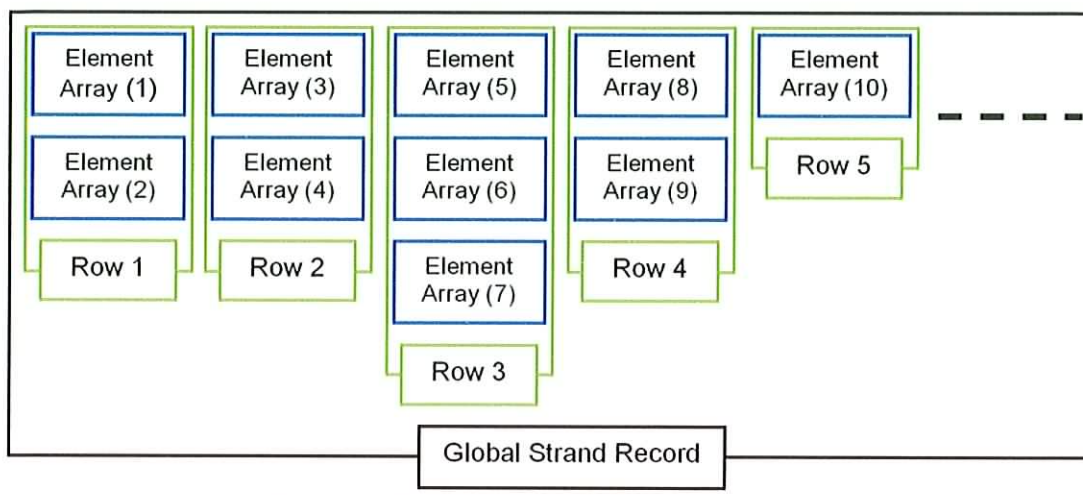

Figure 4.24 record structure for strand data

The two arrays are copied into a subsection of the overall data structure created to hold data pertaining to the first row of elements. The next row of elements is examined in a similar manner producing two arrays, (3) and (4), which are again copied to the appropriate address in the overall data structure. The third row of elements is broken up by both the notch and opening and therefore three element arrays are generated. Rows 5 to 10 are unbroken along their length and therefore only one element array is required for each row.

As seen in Section 2.4 both elastic shortening and creep are a function of the stress in the concrete at the level of the strand, σ_{cp}. Also, this stress was seen to be a function of the self weight bending stresses and the stress due to the prestressing force. The next step carried out by the software is to find the self weight bending stresses. The self weight of the individual elements can be found as shown in the same manner as outlined in Section 4.3.2. The simplest possible case where self weight stresses are calculated is along the length of an unbroken section of strand whose length is that of the span. Referring back to the slab in Figure 4.23 the self weight bending moments for the strands in

rows 5 to 10 would be of the order shown by Figure 4.25. These moments are calculated in the same way as a simply supported beam with a UDL applied.

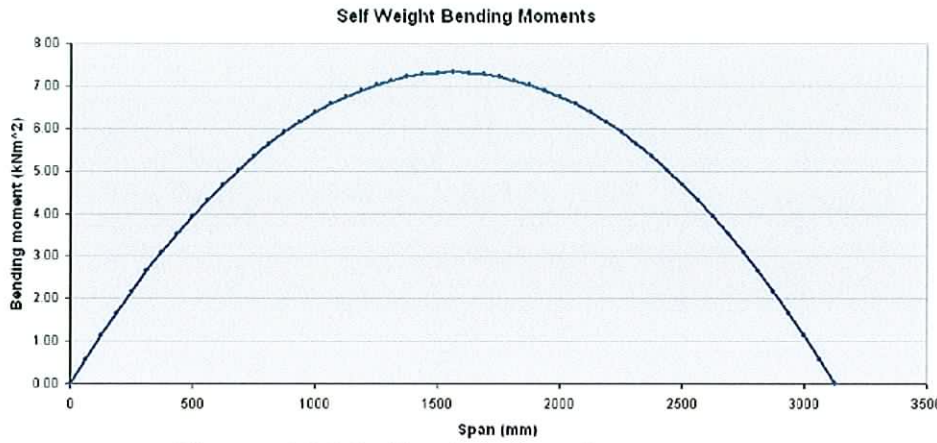

Figure 4.25 Self weight bending moments

The rows numbered 1 to 4 are complicated by the presence of the opening and/or notch. An accurate estimation of the actual bending stresses due to self weight could only be found by adding another finite element analysis step to the process. It was deemed that such a step would add significantly to the workload without a significant payoff in terms of accuracy. As was seen in Section 2.4, the addition of stresses due to gravity loads to the overall state of stress in the concrete at the depth of the strand was a small but beneficial contributor to the prestressing force. Therefore, any estimation of self weight bending stresses that understates the stresses would lead to a conservative design. The approach taken was to assume that the stresses in each section of the strand vary as if the concrete encasing that section of the strand is simply supported beam supported at the ends of the section of strand. Shown in Figure 4.26 is a plausible bending moment diagram for the full length of row 3 in Figure 4.23.

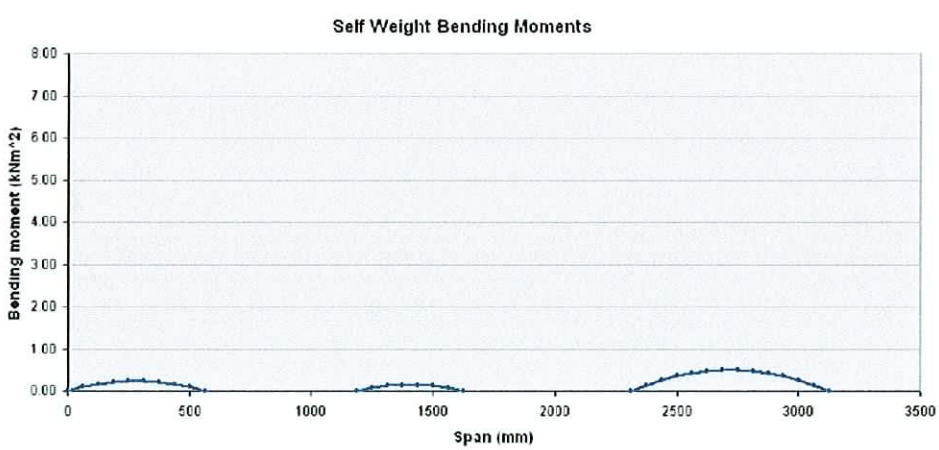

Figure 4.26 self weight bending moments for a non continuous strand

The stresses can be seen to be much smaller than would be expected had a more rigorous analysis been carried out.

Transfer prestressing forces

The force to which the strands are actually stressed before the concrete is placed is calculated next. An array of strand forces is formed to store the prestressing force values at distances equal to those stored in the global strand record found earlier. The structure of this array is identical to the global strand record. From these initial values all loses will be deducted. The loss in prestress force due to the 25% relaxation that occurs before transfer is the first loss to be calculated. This loss affects the full span of the stand uniformly and therefore is subtracted from every value in the current array. The losses due to elastic shortening must be found next. This process is slightly more involving as the magnitude of the loss varies across the span. The reduction in prestressing force is largely affected by the initial prestressing force before elastic shortening occurs with the minor relieving effect due to the self weight bending moments calculated earlier. The array of forces produced must now be altered to allow for the development in anchorage of the prestressing force that occurs at the ends of the strands.

The anchorage distance is found as shown in Section 2.4.5. The situation will normally arise where the anchorage distance calculated does not correspond exactly to any of the distances at which the prestressing forces were found for the array developed in the last paragraph. Linear extrapolation is used to find the peak force value at the end of the anchorage distance. With this information it is now possible to ascertain the development curve for the prestressing force within the anchorage distance at each end of the strand. Figure 4.27 shows the nature of the reduction in force that must be applied to the end of both sections of strand.

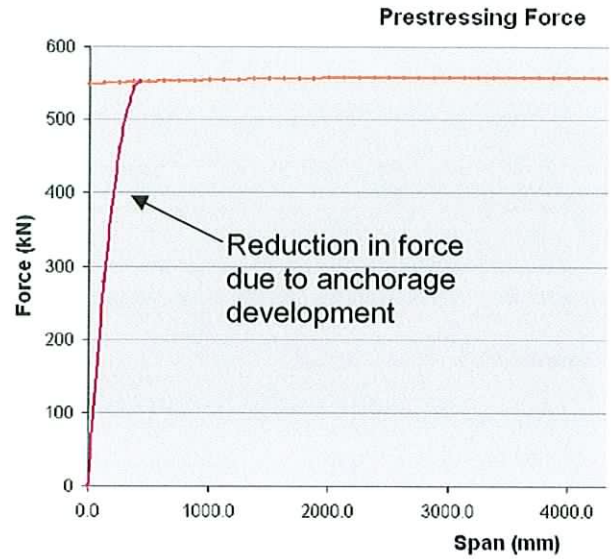

Figure 4.27 reduction in force due to anchorage

A case may arise where the length of a section of strand may be shorter than twice the anchorage distance. Where this occurs the force will not develop to the peak value at the end of the transmission distance as insufficient anchorage distance exists to resist the opposing force. Figure 4.28 shows the idealised development in the prestressing from either end of a short section of strand. From this it is assumed that the actual maximum force occurs at the mid point of the strand and that the anchorage develops as before.

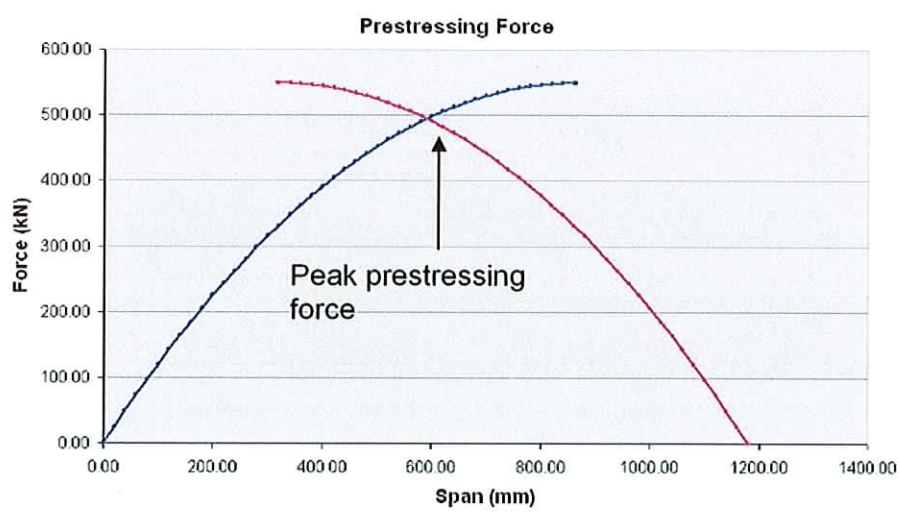

Figure 4.28 reduction in prestress force in a short section of strand

A new data record is formed to hold the force values at transfer after anchorage losses are accounted for as the post elastic shortening forces are required for the calculation of the forces at the service stage. The functions written to

calculate anchorage distances and the development of the forces in this region are used after both the transfer and service losses have been found.

Service prestressing forces

The remaining work involves the calculation of the prestressing forces found at the service condition. The remaining 75% relaxation is the next loss applied and again its effects are uniform across the span. The creep losses are a function of a number of factors including the stress in the concrete at the level of the strands. Again the arrays of self weight moments in conjunction with the post relaxation prestressing forces are used in calculation of these stresses. In a manner similar to that used to calculate elastic shortening, these stresses are used along with the creep factor, strand area and modular ratio to find the losses. Shrinkage losses act uniformly across the span and therefore once quantified are merely subtracted from each of the post creep force values. Finally, this resulting array of forces is passed to the functions to reduce the forces at the ends of the strands to account for anchorage. The process of calculating the prestressing force is carried out in '*UO_prestress*' on page 310.

4.9.2.2. Applying nodal prestressing forces and moments

The contribution to the load vector due to the internally applied loading is found next. In the last section the force in the strands at locations corresponding to the horizontal distances from the end of the slab to the nodes at the element corners were found. However, the forces in the strands must be distributed to the nodes at the corners of the elements.

Taking an arbitrary element at some point along the strand the forces acting on the left and right sides of the element are given by 'F_i' and 'F_{i+1}'. This arbitrary element is shown in Figure 4.29.

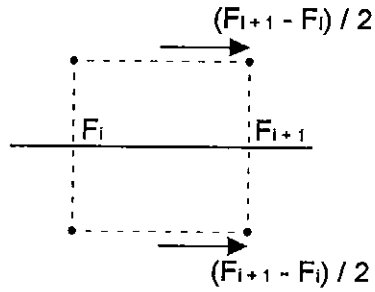

Figure 4.29 applying nodal forces

x (m)	Force (kN)
0.000	0.0
0.063	52.5
0.126	101.6
0.189	147.3
0.252	189.6
0.315	228.4

Table 4.2 Sample strand forces

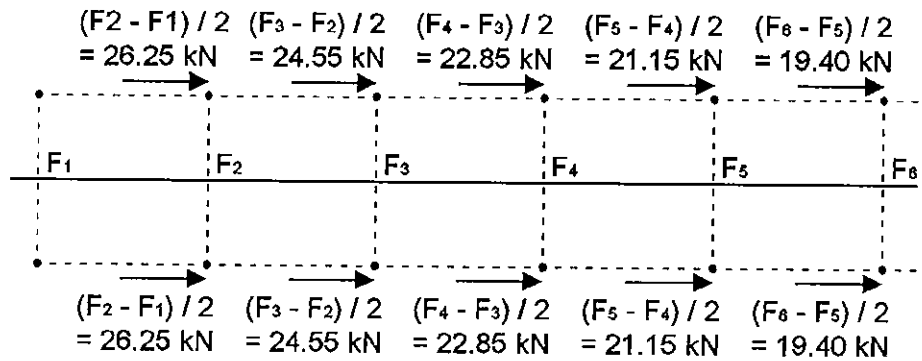

Figure 4.30 example of the application of forces

Once the nodal forces have been found the moment values are found immediately and also stored. The distance to the centroid from the bottom of the slab is known for each element as is the cover from the bottom of the slab to the strands themselves and therefore the eccentricity itself is easily found. Finally the moment applied at each node is a function of the nodal force found above by the eccentricity.

4.9.3. The load vector

Initially two separate load vectors were formed, the first for transfer and the second for service stress conditions. For each case, the first load vector formed contains the gravity load data and the second load vector contains prestressing force data. In turn, both gravity and prestress load vectors are restricted using the support condition data gathered earlier. The final restricted load vector is found by simply adding both load vectors together. Once again the units of code written to carry out these processes are used in an identical manner for both transfer and service load vectors.

4.10. Solving for displacements

The restricted global stiffness matrix for the structure must now be decomposed as a first step towards solving for displacements. Cholesky decomposition is used in the software to achieve this task. A brief introduction to Cholesky decomposition is given in Chapter 3. As mentioned, one of the strengths of this method for this type of calculation is that the decomposition is carried out on the restricted global stiffness matrix and is completely independent of the load vector. This allows a considerable portion of the calculation work to be carried out only once even if multiple load cases are to be considered. This allows the software to be written so as to permit the user to change the applied gravity loads, for example, to analyse a number of slabs whose geometry is identical but with differing loads. It should be noted, however, that two different load vectors would be required when considering transfer stresses and service stresses as the Young's modulus at the service stage is greater than that at transfer, a second global stiffness matrix must be considered thereby doubling the calculations.

4.10.1. Decomposition of the half-bandwidth matrix

The restricted global stiffness matrix seen in Figure 4.22 is stored as a rectangular array of numbers as given below in Figure 4.31. The cells shown in red are those created to simplify the storage structure however no values will have been assigned to any of these cells.

Figure 4.31 portion of matrix to be decomposed

The section of code containing the decomposition function is designed to avoid carrying out any computations based on these cells. There are three formulae used in the process of decomposing the restricted global stiffness matrix. These are given below:

$$m_{11} = \sqrt{a_{11}} \tag{4.3}$$

$$m_{jj} = \sqrt{a_{jj} - \sum_{s=1}^{j-1} m_{js}} \qquad j = 2, \cdots, n \tag{4.4}$$

$$m_{jk} = \frac{1}{m_{kk}} \left(a_{jk} - \sum_{s=1}^{k-1} m_{js} m_{ks} \right) \qquad j = k+1, \cdots, n; k \geq 2 \tag{4.5}$$

These three equations can be used to find all of the values in the decomposed matrix. Equation 4.3 is employed to find the first value on the main diagonal whilst Equation 4.4 is used for every subsequent value on the main diagonal. Equation 4.5 is employed in the case of every other cell. From examining Equations 4.4 and 4.5 it is apparent that the cells in the decomposed matrix must be filled in a systematic fashion, from left to right in a given row before proceeding downwards to the next row. As mentioned in Section 3.4.1, the decomposed matrix is a triangular array of numbers. Therefore there is one calculation involved in filling the first row, two for the second, three in the third row and so on. The order in which the values in the decomposed matrix must be found and the shape of the matrix is given in Figure 4.32.

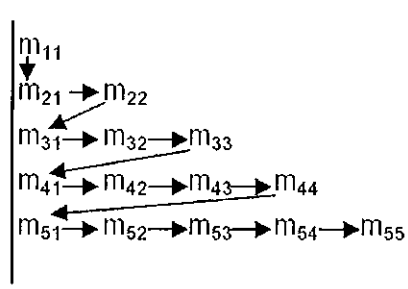

Figure 4.32 order in which solution is carried out

However the storage structure designed to minimise the required memory complicated the looping in the section of code carrying out the decomposition. Once this problem was overcome the resulting code dealt with the decomposition process much more efficiently. The software code executing this is show in '*UO_matrix*' on page 295.

4.10.2. Displacements

The forward and back substitution process was again designed with due cognisance shown to the minimised storage structure used through out the software. The displacement vectors generated for both transfer and service conditions could as such be called restricted displacement vectors. These vectors are modified by reinstating zero values into the vectors for restrained displacements. This simplifies all further processes involving the displacement vectors.

4.11. Displaying displacements

The displacements, in particular the upward camber and downward deflection, are found in the two load vectors. As seen in Section 3.3. for each node in the structure, five displacements are found for each node. The first two displacements give the horizontal movement of the nodes which whilst necessary for calculating the accompanying stresses is of little value to a designer. Similarly, the following pair of displacements, both rotations, will be later used in the calculation of stresses but are again of little interest. The final displacement given for each node is the displacement in the z direction. This quantity is traditionally sought by designers and therefore in parallel with its usage in the calculation of stresses, it is used to form a displaced shape diagram.

The outline of the slab and the mesh that is displayed over it are shown in plan. The problem that arises stems from the fact that whatever deflection occurs will move the node points out of the plane of the slab almost perpendicular to the original position of the node. Displaying the deflected shape in plan therefore would not produce a clear displaced shape diagram. To overcome this difficulty the deflection is displayed distorted downwards in the south – south – east direction. The distance that each node is transposed is proportional to the deflection experienced by the node. The user may also change the scale factor by which the deflection is exaggerated. Figure 4.33 demonstrates how these principles operate.

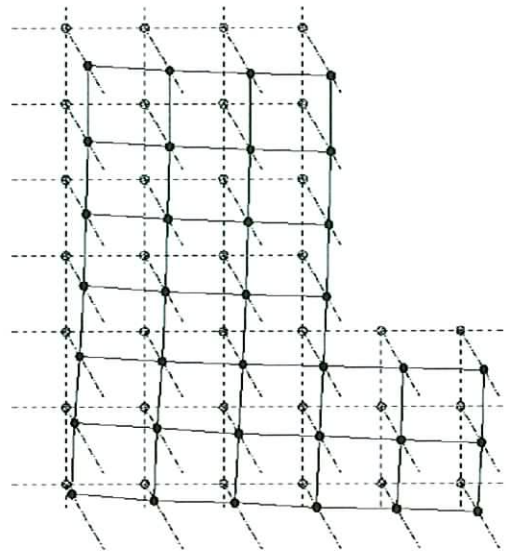

Figure 4.33 deflection display method

Shown in Figure 4.34 is a screen shot of the deflected shape diagram for a slab. The user may switch between the deflected shape diagrams produced for the transfer and service conditions.

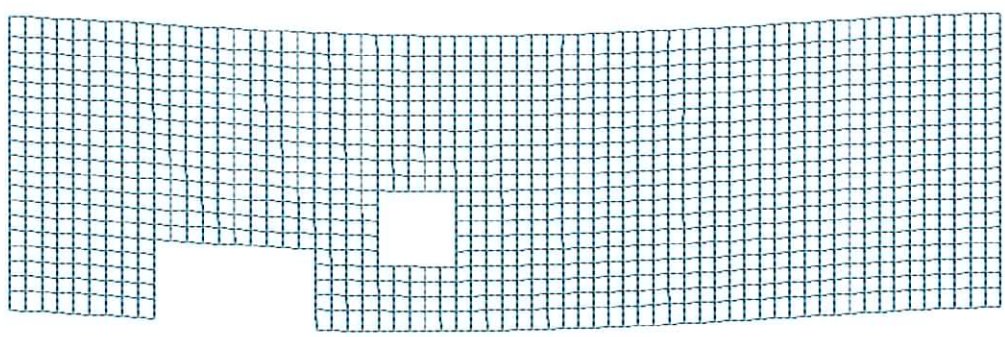

Figure 4.34 displaced shape diagram

The deflections displayed above were generated using plate bending theory. However, as seen in Section 2.2.5. the estimation of the deflection in prestressed slabs is a relatively complicated process. The deflections shown here are calculated based on maximum loads and with no consideration given to creep as shown in Equations 2.38 and 2.39. However these values do allow the deflected shape to be shown and the location of the maximum deflection to be identified.

4.12. Stresses

The next step involves finding the stresses due to the combined model. The predominantly compressive stresses due to the prestressing force was modelled through the use of the plane stress theory, whilst the plate bending theory was used to model stresses arising from the internal moments which occur due to the eccentricity of the prestressing force. Once these stresses have been found they may be combined to yield the complete state of membrane stresses in the slab.

4.12.1. Plane Stresses

With all displacements found, and the displacement vector altered in order to give the global displacements (including the displacements that were restrained due to support conditions) the process of finding stresses may begin. The plane stresses are solely a function of the displacements in the x and y directions and therefore an array of in-plane displacements must be formed from the global displacement vector. This concept is shown in Figure 3.6 in the previous chapter.

The components that must be brought together to find the plane stresses in each element are the elemental displacement vectors, the elasticity matrices and the geometry of the element. The elasticity matrix was seen in Chapter 3 to contain terms that only referred to the material properties of the element. However the properties of the materials in the slab are uniform throughout and therefore this elastic matrix is universally applicable to a slab with particular material properties. The process of calculating the stresses in the slab involves considering each element sequentially, i.e. forming the stress-displacement matrix, gathering the appropriate displacements and multiplying these together to find the elemental stresses.

The elemental displacements for the corners of each element must be copied into an 8 * 1 array. This is carried out by identifying the node numbers for the four corners of the element and then using these numbers to access the correct

cell address in the global displacement vector from which to copy the values. The stress-displacement matrix for the element under consideration must be formed using the height and width of the element and the elasticity matrix mentioned earlier are used to generate this matrix. It should be noted that due to the size of this matrix (12 * 8), and due also to the fact that in excess of one thousand of such matrices would be formed during an analysis, the matrix is created, used and destroyed before proceeding to the next element.

The stresses at each of the four corners of the element are found by multiplying the stress-displacement matrix by the displacements. These values are then stored in a global plane stress array.

4.12.2. Plate bending stresses

The process of calculating stresses due to plate bending is similar to that found in the last section. The relevant displacements are copied into an elemental displacement vector, the stress-displacement matrix is formed and the multiplication of the two results in the determination of the stresses. However, the process of constructing each stress-displacement matrix is more complicated because the elasticity matrices generated in plate bending theory vary from element to element as they are a function of each element's second moment of area. Once again the array storing the elemental elasticity matrices is consulted for these values. The height and width of each element is also required for the construction of the stress-displacement matrix as before.

Once the vector and stress-displacement matrix have been formed they are multiplied together to give an array that contains moment values. These moment values, M_x,M_y and M_{xy}, are actually moments per unit width of the element. The stresses resulting from M_x and M_y are given by Equations 4.6 and 4.7.

$$\sigma_x = \frac{M_x y}{I_x} \text{ and } \sigma_y = \frac{M_y y}{I_y} \qquad (4.6), (4.7)$$

The twisting moment, M_{xy}, gives rise to vertical shear in the elements however this research is focused on examining transfer and service stresses and not shear stresses which are examined at the ultimate limit state. This can be examined further in '*UO_Stress*' on page 343.

4.12.3. Combined stresses

The stresses calculated above may now be combined to give the final state of transfer and service stresses in the slab. The stresses in the top and bottom fibres of the slab are found by adding or subtracting respectively the bending stresses to/from the plane stresses. The stresses found from the plane stress model may be combined with their equivalent from the plate bending analysis as shown in Figure 4.35. The vertical shear stress due to M_{xy}, the twisting moment, is shown in the figure for completeness however this result is not used in the software itself.

Plane stress		Plate bending		Total stress
σ_x	+	σ_x		σ_{x-top}
σ_y	+	σ_y	=	σ_{y-top}
τ_{xy}				τ_{xy-top}
		τ_{xz}		τ_{xz}
σ_x	-	σ_x		$\sigma_{x-bottom}$
σ_y	-	σ_y	=	$\sigma_{y-bottom}$
τ_{xy}				$\tau_{xy-bottom}$
		τ_{xz}		τ_{xz}

Figure 4.35 combining plate and plane stresses

Once the stresses at the nodes in the corners of the elements have been found the next step involves finding the average stress in the quadrants of each element. The stress values calculated for each node may be significantly higher or lower than the average stress in that quadrant of the element. Figure 4.36(a) shows a plan view of a typical element. The hatched areas represent the

quadrants for which the average stress is sought. Figure 4.36(b) show the same element in 3D with the magnitude of the stresses being displayed on the vertical axis rising from each corner node.

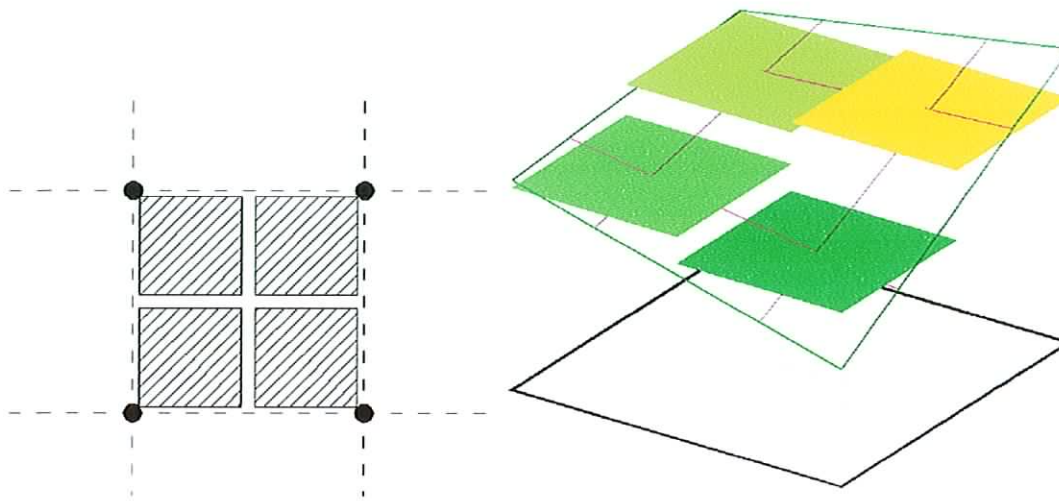

(a) element in plan (b) stresses show in 3d

Figure 4.36 variation of stress within an element

The construction lines on this diagram help to explain how the average height (and therefore stress) of any particular quadrant could be found. A mathematical formula was found to calculate stresses according to this method numerically. This is given in Equation 4.8 where σ_a is the stress at the nearest node to the quadrant under consideration, σ_b and σ_c are the stresses at the nodes at the two near corners and σ_d is the stress at the furthest node from the quadrant.

$$\sigma = \frac{1}{16}\left[(9*\sigma_a)+(3*\sigma_b)+(3*\sigma_c)+(1*\sigma_d)\right] \qquad (4.8)$$

This equation is employed in the four quadrants for σ_x, σ_y and τ_{xy}. It should also be remembered that this must be repeated for top and bottom stresses for both the transfer and service stresses.

These results give stresses in their respective directions which are most likely not the maximum stress present in these elements. To get the maximum values the principles stresses at each node is found for the top and bottom fibres. These stresses represent the final state of stresses and the next task is to

display them graphically to the user. As is commonly the case in prestressed concrete design, compressive forces are shown as positive whilst tensile stresses are shown as negative.

4.12.4. Presentation of results

The method chosen to present the results is a colour coded plan of the slab. The maximum and minimum stresses are found and twenty even divisions of the difference are found. The lowest stress value in the slab is shown in green, with each 5% increase in stress of the total range warranting a colour change. Figure 4.37 shows a stress plot produced by the software. This plot shows the top fibre stresses in the x-direction produced by the combined effect of the plate bending stresses and plane stresses.

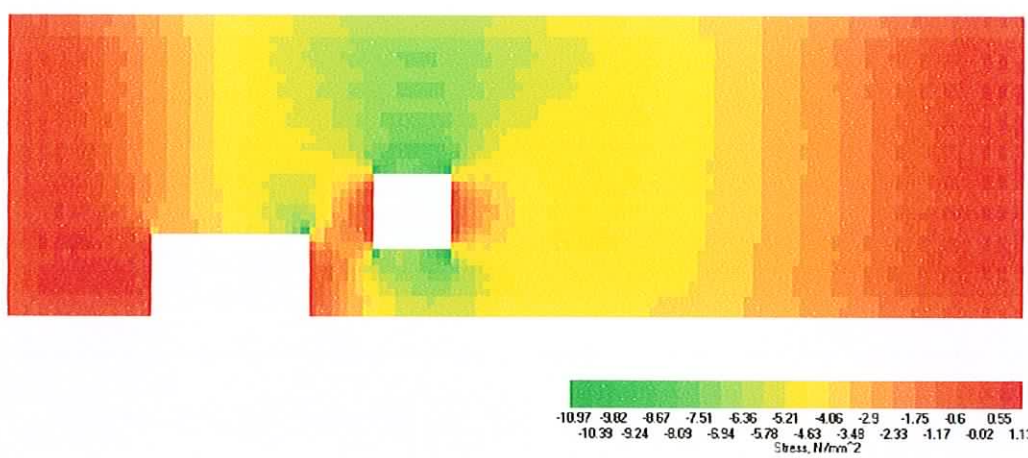

Figure 4.37 top fibre x – direction stresses

The deflections may also be shown in a contour plot in this section of the program as given in figure 4.38.

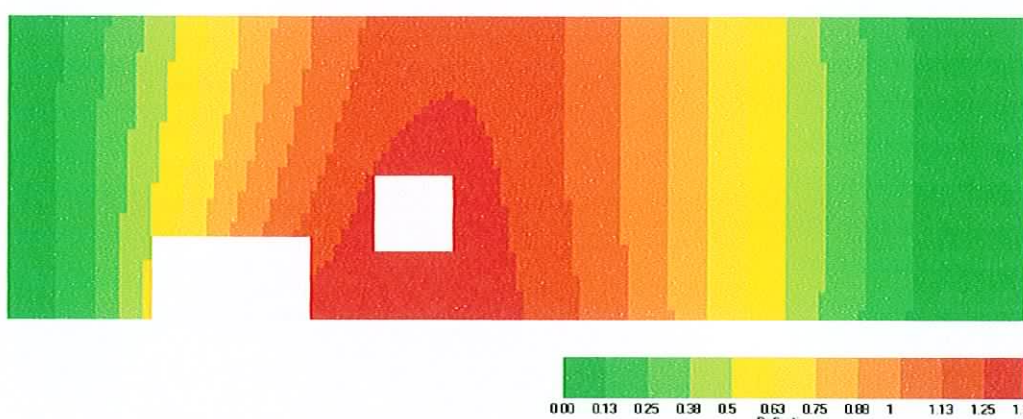

Figure 4.38 deflection plot

It should be noted that the deflection values do not account for such factors as creep as mentioned in Section 2.2.5. This area was not examined as the number of types of deflection examined in a typical study of slab design check is considerable and was therefore deemed to be outside the scope of this research.

Shown below in Table 4.3 shows the various stress and deflection data sets that may be displayed in this part of the program. These results may also be exported to Microsoft Excel for further examination.

Plane stress	x - direction y - direction
Plate stress	Top fibre: x - direction Top fibre: y - direction Bottom fibre: x - direction Bottom fibre: y - direction
Combined stress	Top fibre: x - direction Top fibre: y - direction Bottom fibre: x - direction Bottom fibre: y - direction
Principal stress	Top fibre: p1 Top fibre: p2 Bottom fibre: p1 Bottom fibre: p2
Deflection	Displacement in y - direction

Table 4.3 results shown by contour plot

4.13. Ultimate shear and bending moment capacity

Upon completing the transfer and service stress design checks, the author examined the possibility of extending the software to carry out the stress checks at the ultimate limit state. Having examined the theory underlying ultimate moment capacity and ultimate shear capacity in Section 2.2.3. and studied programming techniques before constructing the software detailed earlier in this chapter it was decided that the programming required to add these checks

would be very substantial and therefore it was not carried out. The largest factor impeding the extension of the software to cover ultimate limit state checks relates to the finite element theory used. The theory outlined in Chapter 3 suits transfer and service stress as the concrete is assumed to be acting in the elastic region. At the ultimate limit state the concrete is assumed to be acting outside the linear elastic region and therefore the finite element theory used in this project could not be applied to this check.

4.14. Summary

In this chapter the process of constructing the software was detailed. It shows how the theory examined in the first two chapters was used to build the software. The link to AutoCAD is explained and it's benefits shown. Some discussion is made relating to the generation of the mesh and subsequent calculation of element stiffness. A large amount of time was spent on the construction of the global stiffness matrix in a manner that minimises the storage space required. The process of generating the load vector was shown including the detailed calculation of losses at intervals along the span. The process of restricting the global stiffness matrix and load vector was discussed followed by the matrix operations such as inverting the restricted global stiffness matrix and the forward and back substitution to find the displacements. Finally the methods used to calculate and display the stresses and the deflection are shown.

A flowchart display of theses processes is shown over then next three pages in Figure 3.39.

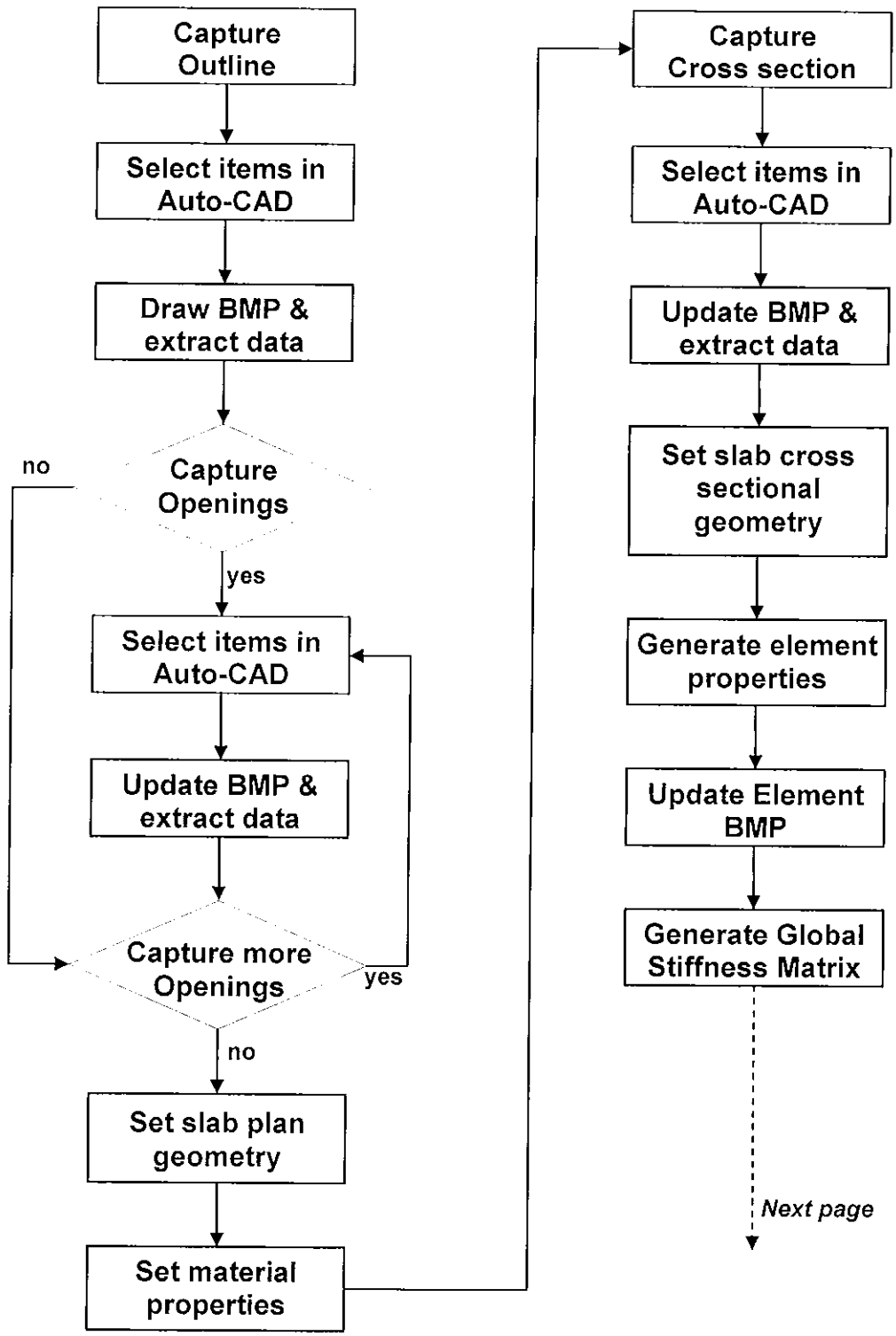

Figure 3.39 Flowchart of process

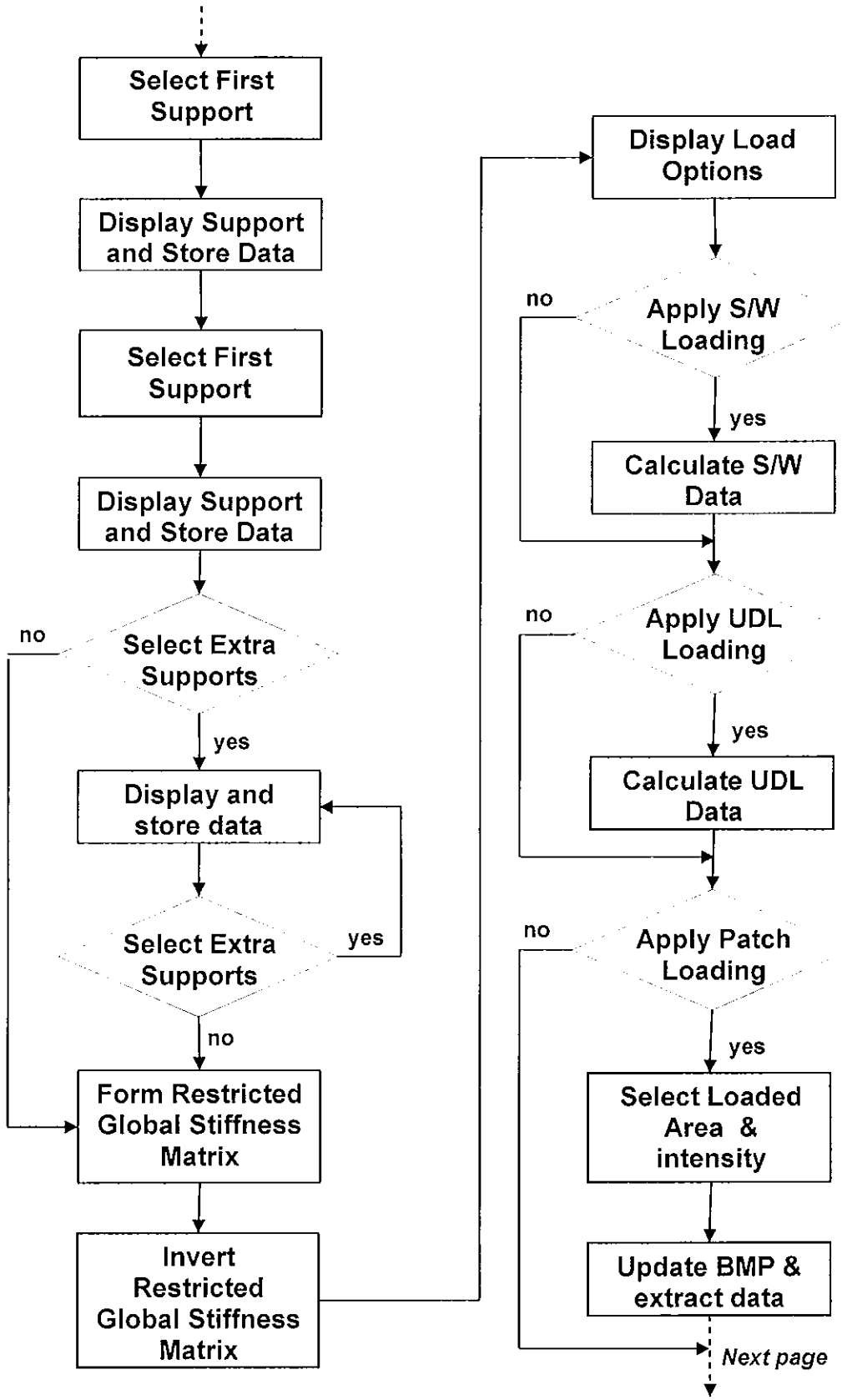

Figure 3.39 Flowchart of process (continued)

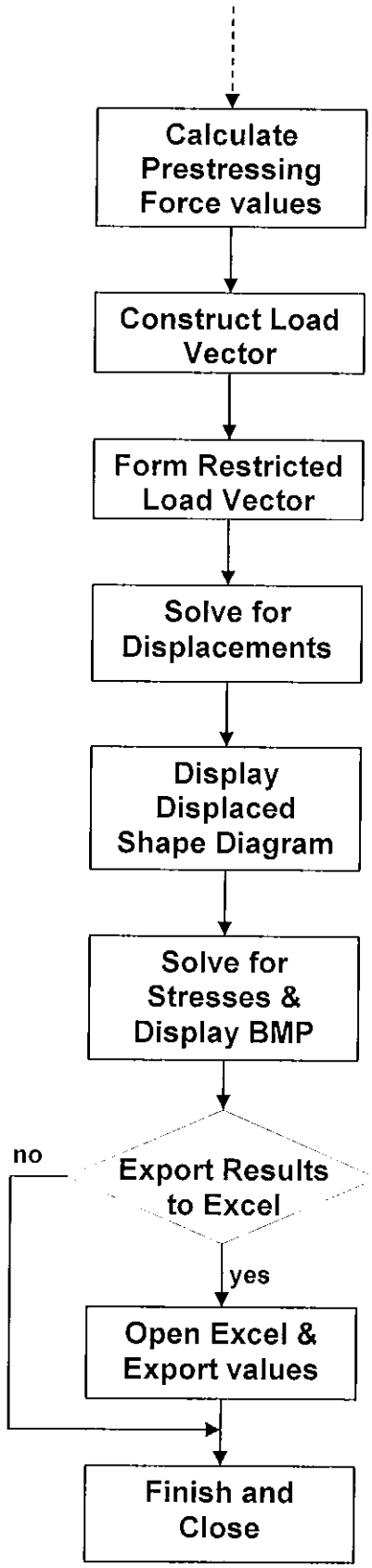

Figure 3.39 Flowchart of process (continued)

5. VALIDATING RESULTS

5.1. Introduction

The quality of the results given by the software written must be verified in order for confidence to be gained in the package. There are three main reasons why the results given by a software package, such as that produced during the course of this project need to be checked. The first is related purely to the errors that creep in during the writing of the software such as incorrectly specifying the size of an array of numbers, or the incorrect use of components or routines. The second source of errors rests in the formula used to perform a function. Such errors may be caused by a typing error or even a misprint in source material. The final main reason for inaccurate solutions would lie with the assumptions that were made when employing the formula. The methods used to attempt to eliminate these errors are debugging, comparative calculations in Excel spreadsheets and Ansys modelling of similar problems.

5.2. Locating errors

Great care was taken whilst writing the software and the theory was researched and in some cases derived from first principles. Aside from the complexity of the formulae that were employed, there are approximately 15,000 lines of code in the software. During the preparation of such a large body of work, mistakes would occasionally be made. These errors fall into the first two categories mentioned in the introduction. The process of debugging the code will catch many of the errors relating to poorly chosen functions or incorrectly sized arrays.

5.2.1. Debugging

A number of mistakes were be located by the debugging features in the Delphi 7 compiler or by range checking which occurs during looping. As the hundreds of steps in the development of the code were added the compiler was used to search for errors. A number of errors made during the development of this

software were spotted as a result of graphic displays that were mainly included to allow testing. Break points strategically placed within the code allow intermediate results not normally displayed to the user to be checked by stopping the program temporarily and displaying the result of the particular line of code.

An example of this type of error can be seen by examining two similar but different functions. These functions '/' and 'div' serve the purpose of dividing a number, however the results given may differ slightly. The '/' function divides a number and returns a real number. However, the 'div' function divides a number and returns a value rounded down to the nearest integer. This type of error can clearly be seen to lie solely in the choice of function as opposed to an error in the execution of the function. Whilst this type of error would not be ring fenced by the debugging features in the compiler, breakpoints may be employed. Shown below in Figure 5.1. is a breakpoint being employed to expose the value assigned to an array at a particular point in a loop.

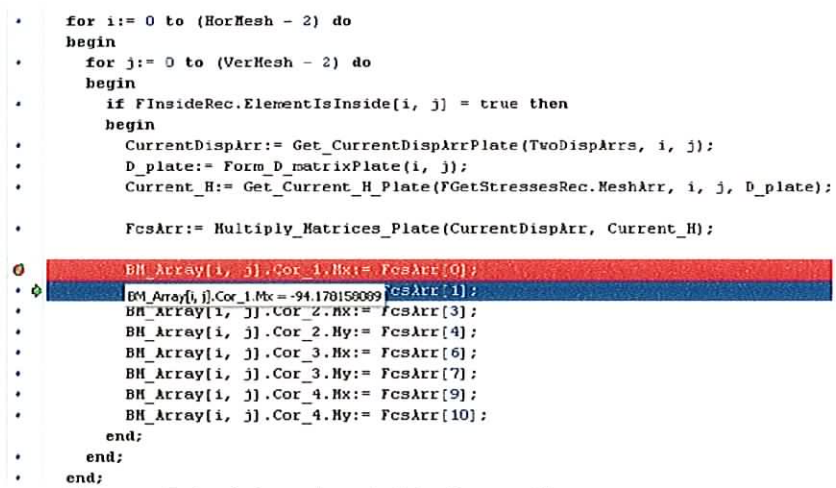

Figure 5.1. A breakpoint in the software

The debugging features in the compiler eliminated simple spelling errors made when calling functions contained with the Delphi software itself. As such, this could be described as checking the spellings within the code at run time.

5.2.2. Excel Spreadsheets

The second type of error that occurred within the code relates to formulae that have been incorrectly typed. An example of this type of error could be as simple

as typing a '+' instead of '-' in a formula. The compiler would not find a software error in this type of mistake and therefore would execute the program without flagging it as an error. This type of error was found through the use of comparative calculations mainly performed in Microsoft Excel. Spreadsheets were used at many stages throughout the writing of the software to verify intermediate results.

For example, the section of code written to find the losses in prestress at intervals along the strands was compared with a spreadsheet written to assist the checking process. This type of check was employed to verify the results of the simplified finite element model before adding more detail. The simplified model was checked by examining a test case with no prestressing force or reinforcement, with a uniformly distributed load applied, taking a solid cross-section with no openings or notches along the slab length and the assumption (only taken for the purpose of testing) that the material properties of concrete are isotropic. The deflections and rotations calculated by the software could then be easily compared with a relatively simple spreadsheet developed with the same parameters. The increments across the span taken in the spreadsheet were purposely defined to be identical to those generated by the software.

The subsequent comparison of results provided a level of confidence in the software. Whilst the results found were not identical, they were generally within 2-3% of those given by the simple spreadsheet model. It should also be noted that the spreadsheet model paid no regard to the effect of Poisson's ratio, which could be seen within the software to cause a saddle-shaped effect on the deflection of the slab. This spreadsheet was further expanded to calculate moments which could then be compared with the results of the next phase of the software. Within the software, a stress-displacement matrix was generated for each element and then multiplied by the displacements found earlier to yield the moments in the x and y directions and the twisting moments at each of the four corners of the element. Finally from these moments, the corresponding stresses may be found. In many cases these checks were most usefull to verify that units were converted correctly. A number of errors were isolated in this

manner when results produced by the software were noticed to differ from those in the spreadsheet by a factor of ten, a hundred or a thousand.

5.3. Ansys

The checks described above were employed to as great a degree as possible at every stage. These particular checks will not, however, guarantee accurate results, as the assumptions upon which the theory was employed may be incorrect or have certain limitations. Therefore, in an attempt to verify the overall soundness of the assumptions made and the reliability of the software itself some comparative finite element modelling was carried out. Ansys was chosen for this purpose. Once again, the choice as to which software to use was greatly influenced by the fact that this particular package was widely used throughout the college and a number of people with expertise in the use of this package were available.

5.3.1. Ansys Classic versus Ansys Workbench

Initially Ansys workbench was chosen for the purpose of generating comparative results. The advantage of using the Workbench as apposed to the classic version relates to its user friendly graphic interface. The first attempts at producing a set of results was carried out using Ansys Workbench, with the geometry of the slab being generated in a separate software package named Solid Edge. However, the limitations of this package became evident after some experimentation, as outlined below, and therefore Ansys Classic was ultimately used.

5.3.1.1. Solid Edge

Solid Edge is described as being '*a computer-aided design system for mechanical assembly, part modelling, and drawing production*'. Solid edge provided a means of rapidly generating the geometry of both the slab and the strands. This data could then be saved to a format recognisable in Ansys Workbench. Within the solid edge environment the user generates 'parts' which

are 3-d volumes extruded from shapes drawn on a selected plane. Once two or more parts have been generated, they may be brought together in an 'assembly' to give the completed body. This feature was of interest as the prestressed slabs under consideration were comprised of the concrete slab part and up to ten steel strand parts.

5.3.1.2. Ansys Workbench

The slab assembly was saved in a jointly compatible format and then imported into Ansys Workbench. In the simulation environment the user can see the list of parts in the imported assembly. The display in which the slab is shown and the surrounding menus would prove very recognisable to experienced Microsoft Windows users. The user can use very straightforward options menus to create materials, specify their properties and assign them to particular 'parts' of the assembly shown on screen. Applying support parameters through the user interface is made simple by the filters that allow the user to choose whether the item to be selected is a vertex, edge, face or body. Pressure and gravity are also similarly applied. In the case of gravity, the user only needs to specify the direction in which gravity acts, and for pressure loads the user selects the face on which the pressure is acting and then specifies its magnitude.

Bolt Loads

Initially, the '*bolt load*' feature within Ansys Workbench was selected to be the means by which the prestressing force would be applied. The nature of the contact between the strands and the concrete within which they are embedded could be set to bonded to accurately model the conditions found in reality. The bolt load option however is based on similar theory to the PRETS179 element type from Ansys classic meshed in a particular manner. Details on this particular element type can be found in the Ansys help menu. This is shown in figure 5.2, where it can be seen that the tension or compression in the bolt is applied through a ring of elements at a distance approximately half way along the shank of the bolt. As a result the prestress is only transmitted through to the concrete between the nodes of the ring of 'special' prestressing elements. This

is due to the bond between the nodes on elements in the strands to the corresponding elements in the concrete. It is noteworthy that the bolt load discussed could be used in the modelling of post tensioning where there is no bond between the strand and concrete.

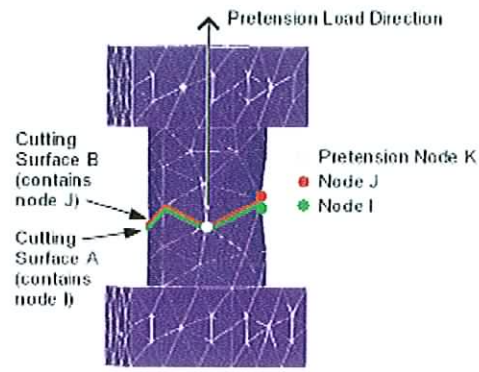

Figure 5.2. bolt load (taken from the Ansys help documentation)

Meshing

The meshing tool in the Ansys Workbench attempts to mesh a given volume with an automatically generated mesh using elements deemed suitable to meet the demands of the particular situation. The mesh generated for the strands includes tiny elements in order to mesh the cylindrical cross-section, as the diameter of the strands is between 6.4mm and 15.7mm. The density of the mesh in the strands is such that the number of elements required in the surrounding concrete to provide adequate linkage to the nodes on the strands surface is typically huge. However, it should be noted that the stresses in the concrete are the results that are sought, while the stresses in the strands are of secondary interest. The strands are of interest only in that they impart the prestressing force into the concrete. The mesh in the concrete in the region surrounding the strands is far denser than that required to give reasonable results.

The mesh produced utilises the uniformity of the cross section along the length of the slab by meshing an end face and then extruding the mesh along the length of the slab. Based on Ansys guidelines on the aspect ratios permitted,

the number of divisions along the span length is calculated and the mesh extruded to fill the volume.

5.3.1.3. The limitations of Ansys Workbench

The user-friendly nature of the Ansys Workbench comes at a price as the options presented to the user at each step in the analysis are limited. In many other cases the options presented to the user are more than adequate to perform the analysis required. However, as seen in the last two sections the two critical aspect of the analysis of a prestressed slab, meshing and prestressing, can not be controlled adequately therefore making Ansys Workbench unsuitable for the purposes of this project.

5.3.2. Ansys Classic

Ansys classic offers the user far greater control over every aspect of the analysis than is possible with Ansys Workbench. This, however, comes at the expense of considerably greater complexity and a less well developed user interface. The user will often find two or more ways of executing any command in this version of Ansys. The main method employed during this research was the use of the 'Ansys Main Menu' which is ever present on the left side of the screen. This contains a huge number of options compacted into a 'Tree View' format in which commands performing similar functions are grouped together with subcommands shown in logical hierarchical of subheadings. This allows the user to intuitively find the desired commands with little effort. An example is shown in Figure 5.3 where the primary commands for creating the geometry of the model are displayed.

Some other commands were most easily accessed through the utility menu across the top of the screen. Finally, some users of Ansys prefer to utilise the 'Ansys Command Prompt' to execute commands. For example, if the user wishes to add sub volumes together to create a single volume, the 'VADD' command could be typed followed by the names attached to the volumes concerned. Referring back, to the main menu, the user could have achieved the

same objective by moving through the following path to the same command: '*MainMenu – Preprocessor – Modeling – Operate – Booleans – Add – Volumes*'. The Command prompt was not used during this research.

Figure 5.3 Ansys Main Menu

5.3.2.1. Setting up the pre-processor

Before creating geometry, the user may define a number of properties such as element types, material properties and real constants. Firstly, it is advisable to set the Preferences option to '*Structural*' so as to allow Ansys to filter out commands from the options presented down the line that bear no relevance to the analysis being carried out. For example, the fluid, thermal and electromagnetic options are removed from most menus presented later in the analysis.

The element types used in this analysis are chosen by selecting add elements. Three elements types are required to set up the model, these are:

1. MESH200 – This element type is used solely for creating a mesh on a surface which would later be extruded into a different element type. This is termed as 'not solved' as its presence is ignored once the solution stage begins. In the options menu relating to this element type the user must specify that the element shape required is a 'Quad 8-node' so that once the elements are extruded a 20-node brick is formed. This is shown below in Figure 5.4

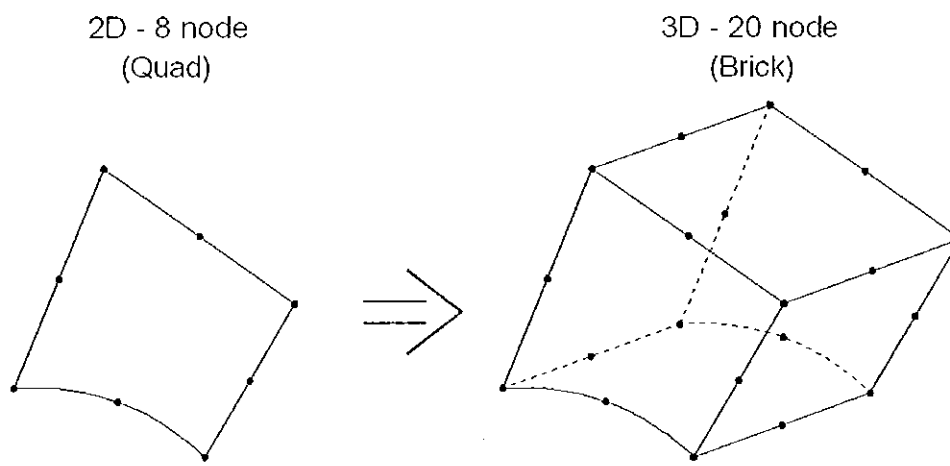

Figure 5.4 transposing an 8 node element to a 20 node element

2. SOLID186 – This element type is the 20 node brick that is used to fill the volume when the MESH200 elements are extruded into 3D elements.
3. BEAM4 – The choice of element used to model the effect of the prestressing force was determined by requirement that the element type in question must have the capability to have a prestress or prestrain applied. This element type is normally used for modelling beams within larger structures with real constants such as second moment of area, torsional moment of inertia and shear deflection constants for beams being optional inputs for the user. For the purpose of this analysis the prestrain constant was of interest.

The real constants relating to the BEAM4 elements can now be set by adding the set of real constants that relate to this element type. Once the user correctly selects BEAM4, only the options relating to it will appear. The user must give at the very least, information relating to the cross sectional area of the strands and

also the prestrain accounting for losses relating to relaxation and concrete shrinkage as detailed in Chapter 2. Furthermore, to increase the accuracy of the overall model, the user may also include data relating to the second moment of area of the strand and its thickness.

Material properties are then set by selecting the '*Material Model*' option. The user must at this point decide on the units to be used through-out the analysis. Obviously, the geometry of the slab would be defined in metric units, which, in the case of this project, were millimetres. However, the user may define the material properties in terms of N/mm^2 or in Mpa. Once again the units through-out this research were N/mm^2. The first material defined, concrete, would typically have an assumed Young's modulus of between 28,000 N/mm^2 and 32,000 N/mm^2 with a Poisson's ratio of between 0.20 and 0.25. The density of the concrete is then specified so as to allow self weight bending stresses to be quantified during the analysis. The density of concrete is typically taken as 2.5 Mg/m^3. The properties of prestressing steel are almost universally taken as 190,000 N/mm^2 for Young's modulus and 0.3 for Poisson's ratio. Since the weight of the concrete contributes to greater than 99% of the weight of the slab, the density of the steel is ignored.

5.3.2.2. Creating geometry

In a manner similar to that used in Ansys Workbench, Ansys classic allows geometry generated using other software packages to be imported. However, It was decided that creating the geometry from scratch in Ansys was desirable in order to remove a potential source of errors.

There is a large array of methods that can be employed to generate geometry in Ansys all of which can be accessed through the Modelling sub-option found in the Preprocessor heading in the Ansys main menu. Generally, the user's ultimate goal within this section is to create a volume which may later be meshed, loaded, etc. To create a simple volume the x, y and z dimensions of the cube may be specified in a window that appears once the '*Create Volume*' command is executed. The user may create other volumes and Add these to

the main volume to create geometry. Similarly, a volume may be created which partially co-habits the same space as another volume, allowing the Subtract command to be used to remove the common space from the main volume. This is commonly referred to as creating the geometry from the top down. The other main technique employed for creating geometry is referred to as creating geometry from the bottom up. This was the method used in this project as it best suited the creation of the cross-sectional shape of the slab.

The technique involves creating single coordinates in space called '*keypoints*'. Once at least two keypoints have been created a line may be formed connecting them. Building upon this, lines may then be used to construct an area. This may only be accomplished once a sufficient number of lines have been created to enclose the area itself. Again, once a sufficient number of areas have been created, the volume that these areas enclose can be defined. Figure 5.5 shows the four steps from defining kepoints, linking them to create lines, defining the areas by lines and finally using the areas to define the volume itself.

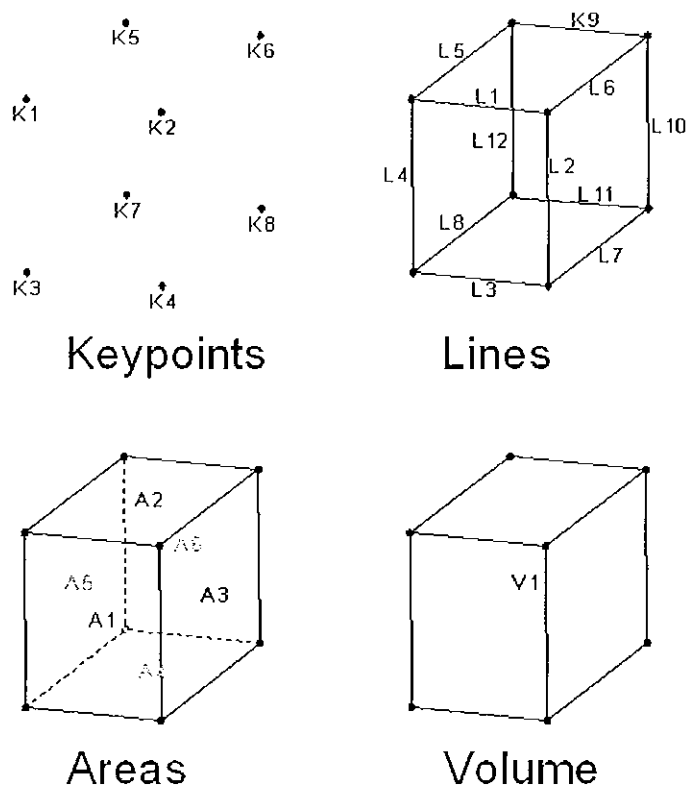

Figure 5.5 building volumes from the bottom up

It is also possible however to create an area and extrude it in a specified direction to create the volume. There are a large number of options available for

geometry creation allowing the user to decide through experience as to which technique best suits the geometry being created. For example, in the case of the geometry required for modelling hollow core slabs, creating the cross sectional area of the slab and extruding it back was the most efficient way of producing this geometry.

The process used to generate the hollowcore slab cross section is shown in Figure 5.6. The first step involved creating the keypoints from the 2D co-ordinates of the cross section and then linking the appropriate keypoints with lines as shown in Figure 5.6(a). These lines may then be used to define the outline area of the slab as shown in Figure 5.6(b). The '*Solid Circle*' command directly creates a circular area which allows the user to skip the process of creating a keypoint and circle in order to define the area. All nine cores are created in this manner, simply specifying the coordinates of the centres of the circles and radius as given in Figure 5.6(c). Finally, the Boolean '*Subtract*' command is used to subtract areas from each other. In the example given, areas A 2 to A 10 are subtracted from the base area, A 1. This yields the completed cross sectional area shown in figure 5.6(d).

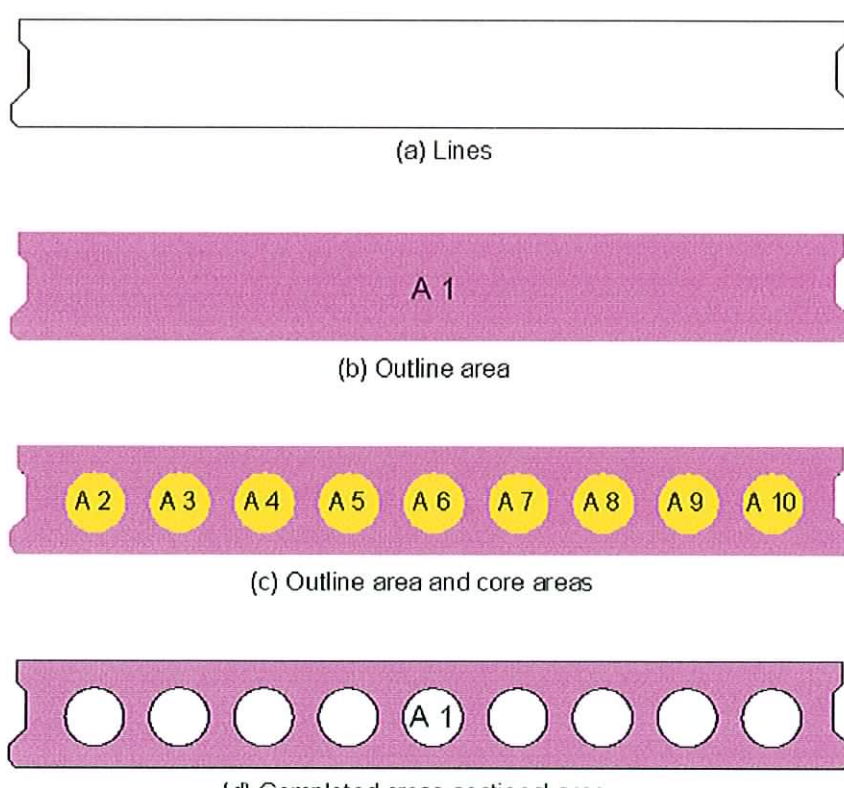

(a) Lines

(b) Outline area

(c) Outline area and core areas

(d) Completed cross sectional area

Figure 5.6 using Boolean commands to create an area

Due to the method in which the mesh was produced for this particular analysis the area itself was not extruded into a volume but the elements produced for this area were. Further details on this are covered in the next section.

5.3.2.3. Creating the Mesh

During the attempt to employ Ansys Workbench to carry out the analysis (see Section 5.3.1.2.) it became clear that great control would have to be exercised over the number of elements in the mesh. To achieve this mapped meshes were used. A mapped mesh has a more clearly defined structure to it than a free mesh.

Meshing the concrete

To minimise the work involved in creating a mesh areas may be divided in such a way as to allow mesh patterns to be copied to other areas with a similar shape. Upon examination of the slab cross sections used in this project, it became clear that the process of producing a complete mesh may be speeded up by considering a small portion of the overall area which may then be replicated across the overall area. Figure 5.7 shows a red hatched which is possibly the most logical sub-area for which a mesh pattern can be developed.

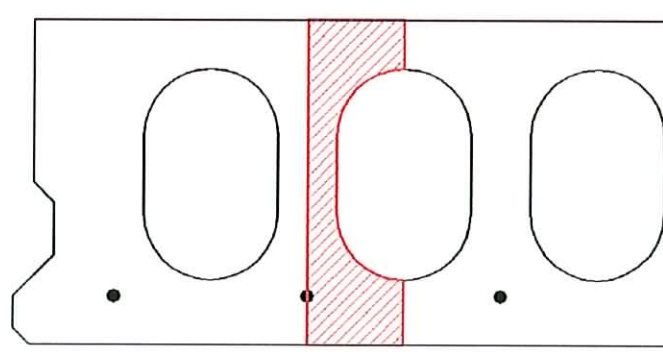

Figure 5.7 repeatable mesh pattern

Once a suitable mesh has been developed for this area, the pattern may be reflected to the other side of the core and then copied along the cross section. This leaves only the left and right side of the cross section to be meshed but

again upon developing a suitable mesh for one side the user may reflect it to the other.

The process of developing a mesh for the area shown above involves some thought. The element type used for meshing this area (SOLID186) allows curvilinear edges to be formed which would help to ensure that good results are achieved close to the cores. The area to be meshed must itself be sub-divided to allow approximately square elements to be used to produce a mapped mesh. Figure 5.8(a) shows the sub area discussed above divided up in such a manner as to give all four sided areas. Also shown in figure 5.8(b) is the same area with a suitable mesh applied to it.

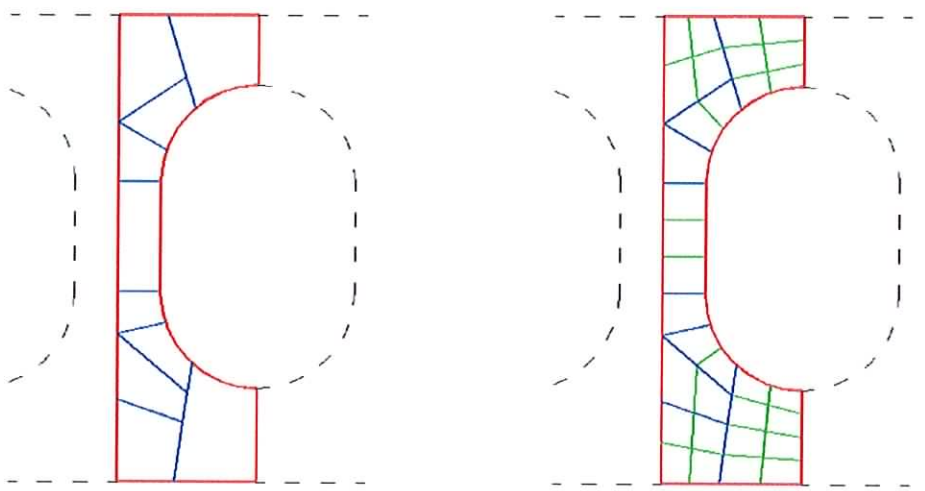

(a) area divided (b) sub areas with mesh applied

Figure 5.8 mesh sub-areas and elements

There are a number of considerations that must be borne in mind whilst creating the mesh. The Ansys help menu suggests that an aspect ratio of less than 20 should be aspired to for the 3D elements produced in the mesh. Therefore, the user must take care and try not to produce any elements that have a particularly small dimension in any direction. Also, by specifying the number of elements along the sides of the sub areas, the shapes of the resulting elements may be controlled. It can generally be said that internal angles of 135° or greater are undesirable and therefore the user must visually inspect the mesh pattern produced in order to avoid this.

The procedure employed to create the mesh shown above involves creating lines that divide the area as shown. Once all four bounding lines have been

created, an area may be defined. Each of the lines defining the area may then have the number of divisions associated with it set. Three divisions along a line leads to the creation of three elements along this edge all with equal edge length along the collinear edge. The user must also ensure that corner nodes meet as nodes on adjacent elements may not lie along the edge of an element. Figure 5.9 shows diagrammatically this error with the problem nodes highlighted by the red circle.

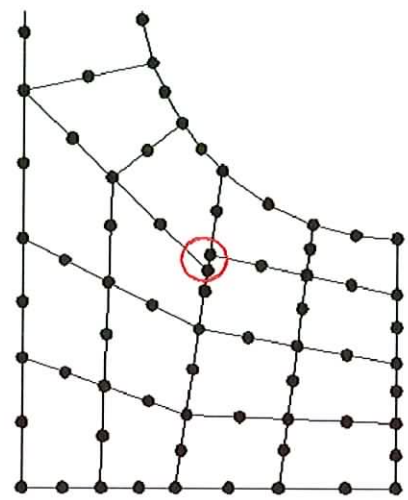

Figure 5.9 a meshing error

The final characteristic that should be avoided are degenerate elements. The first element shown in Figure 5.10 is one of the faces of a 20 node element whose shape is approximately square. The second element shown is a triangular-faced element. However it is formed from a 20 node element, three nodes of which occupy the same coordinate. Allowing degenerating elements may lead to element 'locking' where elements appear to have greater stiffness than is the case in reality. It is generally accepted that to avoid the possibility of this occurrence, the user should use triangles or tetrahedral elements that were formulated as such (Cook *et al.* 2002).

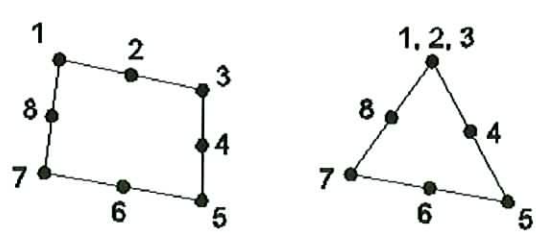

Figure 5.10 a degenerate element

Referring back to Figure 5.8(a) which shows the areas generated upon subdividing the repeatable shapes, the corners of two of these areas were positioned so as to coincide with the location of the end point of a strand. This allows the mesh applied to the line representing the strand to interact fully with the mesh that will be extruded for the concrete elements.

After a suitable area mesh has been formed on the end surface of the slab this must be extruded back through the volume of the slab. The user selects the 'element extrusion option' found under Modelling – Operate – Extrude to set a number of options. Before carrying out the extrusion the user must specify the material from which the extruded volume would consist. At this point the user also specifies that the area mesh is to be changed to the SOLID186 when it is transformed into a volume. Finally, the number of divisions along the length of the extrusion at which elements are to be formed is chosen. This choice, as discussed earlier is made based on the required aspect ratio of the elements and the solution time. The actual extrusion is carried out by specifying the area elements to be extruded and then specifying the axis and distance along the axis which the mesh is to be generated along. Figure 5.11 shows the mesh produced as shown in Ansys.

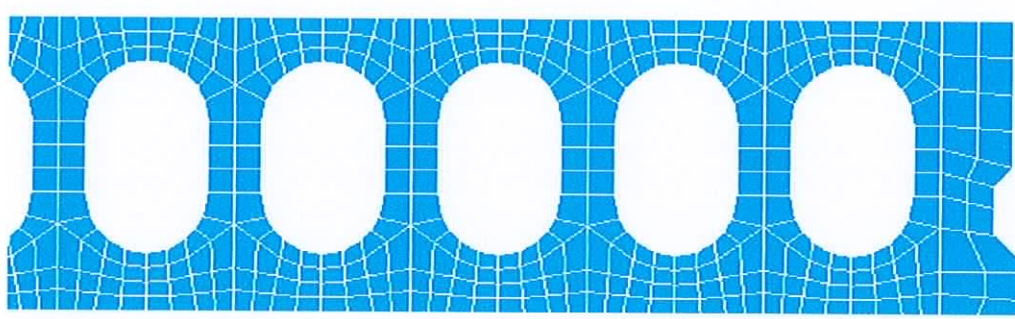

Figure 5.11 an Ansys mapped mesh

Meshing the strands

Before the mesh along the lines representing the strands is created, the '*Real Constant*' relating to the BEAM4 element type must be set. Many of these properties of the strands are most easily calculated manually and typed in.

However, the user may use the '*Parameters*' feature found in the utilities menu to declare variables and then enter the appropriate formula in the real constants form. Typical values used for a 9.5mm diameter strand include an area of 51.61mm^2, an I_{xx} and I_{yy} value of 211.3mm^4 and a thickness of 8.1mm. The prestrain value would typically be of the order of 0.0048 to 0.0055 depending on the losses that are assumed to have occurred.

Meshing the lines that represent the strands is straightforward once they have been identified. This is somewhat complicated by the number of lines running perpendicular to the direction of the span. The normal procedure for selecting any object on screen is to click on it close to its centre of gravity. However, due to the jumble of lines presented onscreen the method chosen to identify the lines involved identifying the ten keypoints at the ends of the strands and from the file containing the list of lines and their associated keypoints, the line numbers were identified. The lines were then displayed using the '*Plot – Specific Entities – Lines*' command to display the lines representing the strands one at a time and thereby allowing them to be meshed individually. Meshing the lines is carried out by setting the attributes of lines such as material type, real constants and the element type with which the line will be meshed. The next step involves specifying the element size that is to be used along the line. From within the meshing sub option in the Ansys Main menu the user selects '*Size Controls – Manual Size – Lines – Picked lines*' and selects the line to be meshed. The user must specify the same number of divisions for the mesh for the line as was used when extruding the area mesh on the concrete into the volume. This ensures that the nodes along the strands coincide with the nodes within the concrete so as to ensure that the prestressing force is applied to the concrete at these nodes as opposed to just at the ends of the slab. Finally the mesh is actually applied to the line through the mesh tool option.

With all the geometry and associated meshes defined the user may move on to loading the slab. However, as a precaution, the user is advised to select the '*Delete Volumes and Below*' option within the Modelling option and select everything on screen. This will lead to all volumes, areas, lines and keypoints that have no mesh associated with them to be deleted therefore removing the

possibility that a load could be applied to a phantom area instead of the areas or volumes holding a mesh and truly representing the structure. This process has no effect on the volumes, areas, lines or keypoints on which the mesh itself is created.

5.3.2.4. Applying loads

The loading options may also be found within Loads menu in the Ansys Main Menu. The three load types that must be defined are structural displacement (supports), gravity loads and pressure loads (imposed loads).

Under the loads option the user selects '*Define loads – Apply – Structural – Displacement – On lines*'. The user then selects the lines on the slab which represent the supported edges. In the case of the slabs under examination, the supported edges are typically those found at the bottom of the slab at opposite ends of the span. The user would see that in the case of the slabs examined in this project, the edge to be supported actually consisted of many short lines each of which forms the lower boundary of the sub areas at the bottom of the slab cross section shown in Figure 5.8(a). The user must then specify the lines upon which the displacements are to be applied. Ordinary supports are defined by setting the displacement value to zero. The displacement relative to each axis must be set independently as selecting the option to restrain all degrees of freedom will also restrain rotations about all three axes and would lead to an effect similar to that given by a fixed support. At one end of the slab a pinned support is set by stipulating zero displacement in the x, y and z direction whereas at the opposite end the roller support is formed by only suppressing the displacement in the vertical direction (y – direction).

The next load type to be considered is the pressure load. The pressure load option is also found under: '*Define loads – Apply – Structural*'. This load is applied to the areas that make up the top of the slab. These areas are the top surfaces of the extruded elements as shown in Figure 5.12. The process of selecting these areas is made simpler by selecting the option to plot the area numbers. The user may then select the areas whose numbers appear on the

top surface of the slab where any incorrect selections would be blatantly obvious. The user then specifies the load in N/mm^2, inputting 0.001 for 1 kN/m^2.

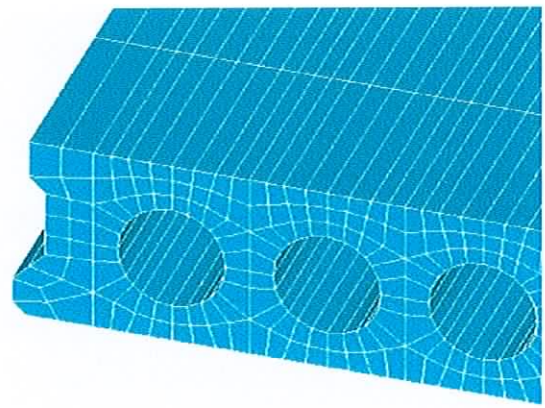

Figure 5.12 a meshed volume

The final load data to be specified is gravity. At the stage where the material properties were specified the user was given the option of including a material density, if the user did so then by selecting: '*Inertia – Gravity – Global*', the value for acceleration due to gravity in any direction may be specified. Therefore, given the orientation of the geometry created earlier, a value of 9.81m/s^2 in the y direction is set for this.

5.3.2.5. The solution stage

The user is now at the stage where the solution may be found. The solution command is found in the Solution option in the Ansys Main menu. The user selects the '*Solve – Current LS*' within the Solution option and the solution begins. If any errors or warnings arise the user may find further details in the Ansys Output Window. The number of elements used for a typical slab would result in a model that would take in the region of 30 – 40 minutes to solve assuming no errors in the model are highlighted. Both before and after the solution is found the work in progress should be saved in case some failure in the Ansys program.

5.3.2.6. Displaying Results

As a first step after the analysis was complete viewing the deflections provides a quick method of verifying that all loads and material properties were input in

the correct manner. For example, if a maximum deflection was expected to be in the 5 – 25mm range but the results suggest a deflection ten or one hundred times greater, then the first item to check would be consistency in the units used. The tools for generating result displays are found in the Postprocessor option in the Ansys main menu. Contour plots produce the most easily read results. To display deflection the user selects '*Plot results – Contour plot – Nodal Solution*'. The menu that appears allows the user to specify the directional component of the displacement which is calculated to have occurred to the slab. The deflection in the y-direction is selected and the user may also specify if the contour plot is to be overlaid on the original shape of the slab or the deflected shape.

Displaying stresses involves slightly more thought. The user selects the Element plot option and is presented with a slightly different set of options. The stresses of greatest interest to precast concrete slab designers are the longitudinal stresses in the slab. The user may choose to examine other stresses such as the principal stresses however the stress in the z direction would prove a good first indicator as to whether the slab design is viable. The options presented to the user are presented in Figure 5.13.

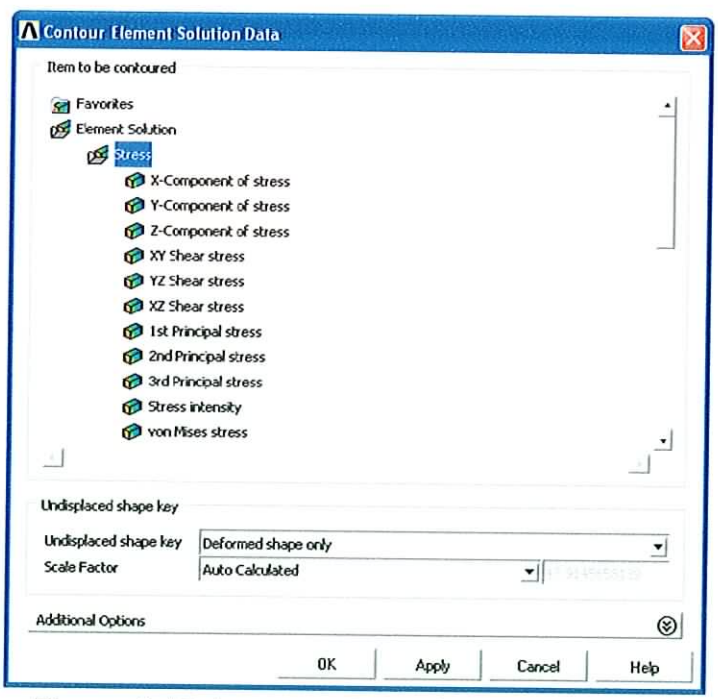

Figure 5.13 Ansys contour plot stress options

The stresses are then plotted on the displaced shape of the slab. Once again the plot appears and the user may rotate it and zoom in or out to examine features of interest.

A problem arises from the stress range produced by the analysis. Stresses found locally around the strands are much higher than the top and bottom fibre stresses in the concrete leading to an anomaly in the legend. The legend is calculated by taking the maximum and minimum stress values and using steps of one tenth of this as the contour values. If it is assumed that the stress range found in the top and bottom fibres of the slab is between 4N/mm^2 in tension and 25N/mm^2 in compression then this range could normally be displayed using contours with steps at every 3N/mm^2. However, close to the strands a local stress is found in the order of 150N/mm^2 in tension. The contour steps are therefore in the order of 18 – 20 N/mm^2 masking the stress variation in the top and bottom fibres in the concrete.

To overcome this difficulty the user must customise the range of stresses shown in the legend so as to focus on the stress range actually encountered in top and bottom fibres. This is achieved by specifying Non-uniform Contours in the sub option found in the '*Style – Contours – Non-uniform Contours*' option in the Ansys Utility menu. This is shown in figure 5.14.

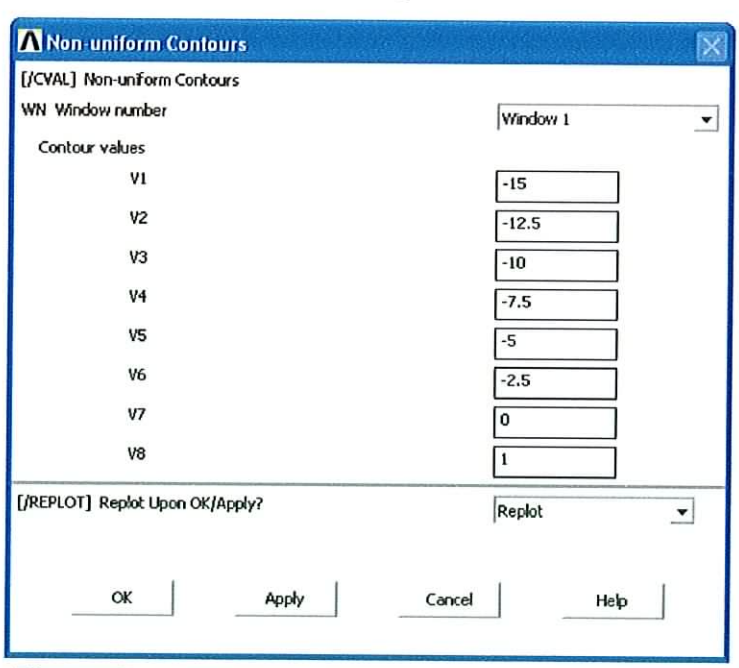

Figure 5.14 Non-uniform contour options in Ansys

An iterative process of reducing the step values between contours and reviewing the resulting displays until the full range of stresses acting on the faces of the slab can clearly be seen. The stresses found around the strands that lead to the distortion of the legend is a falsely high value calculated based on the meshed produced in the last section. This is related to the manner in which the prestressing force is transmitted from the steel into the concrete. In this model the strand is modelled as a line and only a very limited number of elements in the concrete may link to the two nodes present in the beam elements used to model the strands. In an ideal situation where the capacity to solve a model with a far greater number of elements exists, the strand would also be meshed with 3D solid elements and a much greater number of nodes would be present on the surface of the strands to link to the elements in the concrete. The greater number of elements linking the concrete and strand parts allows a more accurate distribution of the stresses at these locations to occur, in turn giving better analysis results.

5.4. Summary

This chapter detailed the methods used in an attempt to ensure the accuracy of the software at many of the stages during development process and then to test the final product. During the construction of the software debugging tools within the Delphi compiler were utilised and then after a logical division of work was completed, a Excel spreadsheet would be used to verify the accuracy of the results produced by the unit. After the software was finished Ansys was chosen to produce results to compare with those produced by the software. Initially Ansys workbench was examined however ultimately the full version, Ansys Classic, was used due to its greater flexibility. The remainder of this chapter then details the components within Ansys that were studied in order to successfully model prestressed slabs. These techniques will be used to produce the results used for comparisons between Ansys and the software shown in the next chapter.

6. COMPARISON OF RESULTS

6.1. Introduction

The procedures outlined in the last chapter allowed sets of results to be generated whereby the analysis software produced for this research was compared to Ansys. The relative accuracy of the software was then be gauged and from this improvements were made. Later in this chapter Ansys analysis results for six design situations will be shown and compared with the results generated using the same design parameters in the software produced for this research.

6.2. Overview of the Ansys models

The Ansys models produced were based on two of the four slab cross-sections. The 150mm deep and 200mm deep slabs were chosen to enable two different slabs with cores in them to be modelled. The limitation on the maximum number of elements used also meant that the 250mm deep slab had to be ignored as the number of elements used in creating a mapped mesh on the end face would, when extruded, produce a larger numbers of elements than allowed by the university version of Ansys in most design cases. This is most clearly pronounced for deeper slabs as they are most commonly used for longer spans and therefore require more elements to satisfy the aspect ratio rules in Ansys.

6.2.1. Assumptions

The Ansys models constructed involved certain simplifications in order to streamline the research. The loads applied to the slab were all uniformly distributed loads. Stresses due to patch loads, point loads and line loads are not investigated in this research. Once again the limits placed on the number of elements used affected the spans used. Therefore, spans that could be considered short for a particular depth of slab were used. However, in order to balance this out, heavier loads were applied to ensure that the stresses produced were high enough to justify the selection of slab depth. For all the

designs carried out a Young's modulus of 30,000 N/mm^2 and a Poisson's ratio of 0.2 were assumed for the concrete. The concrete used for prestressed slabs is almost universally 50 N/mm^2 and therefore the maximum compressive stress for the designs is 16.5 N/mm^2 and a maximum tensile stress is 3.2 N/mm^2 - assuming the slabs are designed as class 2 members as discussed in Section 2.2.1.

The openings and notches on the slab are positioned to accommodate the limitations of the software produced for the research and also keep the meshing process in Ansys as simple as possible.

6.2.2. Details of the slabs to be analysed

As mentioned earlier the slabs analysed were either 150mm or 200mm deep cross sections. The six designs considered were:

1. 150mm deep slab, solid in plan
2. 150mm deep slab, one large notch
3. 150mm deep slab, two notches along the same edge
4. 150mm deep slab, one opening
5. 200mm deep slab, solid in plan
6. 200mm deep slab, one opening

The specific dimensions of the individuals slabs are given in appendix 4. The examples for analysis represent reasonable design parameters that the software could encounter during real world design situations. If the user wished to examine a number of different loading patterns, the geometry and associated meshes could be re-used to further increase the number of design situations examined.

6.2.3. Mesh patterns utilised in Ansys

The mesh patterns used for the two slab depths examined have a number of similarities in the form of the repetition of the sub-patterns used around the

voids. Figure 6.1(a) shows the mesh pattern used for the 150mm deep cross section and Figure 6.1(b) shows the mesh used for the 200mm deep slab.

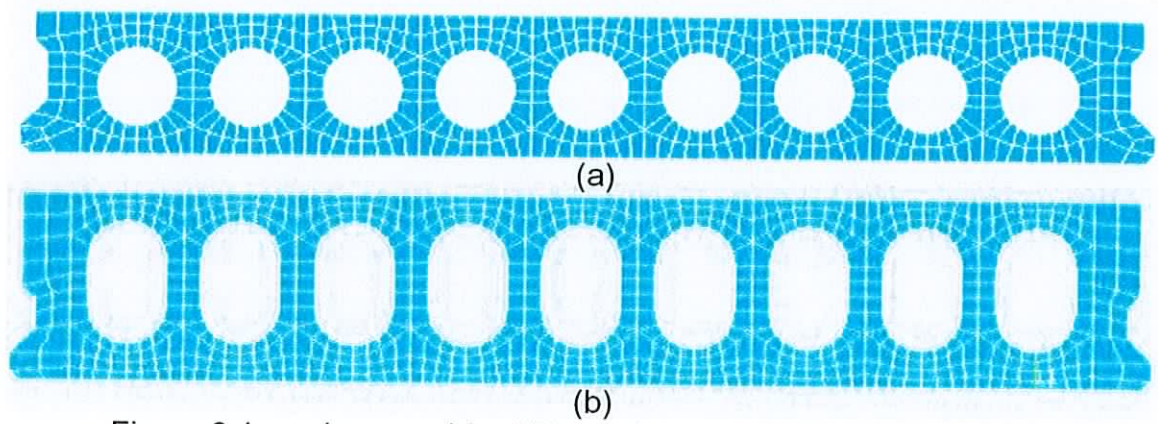

(a)

(b)

Figure 6.1 meshes used for 150mm deep and 200mm deep slabs

From inspection it can be seen that the 200mm deep slab has approximately 50% more elements. The key consideration was to produce the largest element dimensions to avoid problems with the aspect ratio of the elements when extruded.

The mapped mesh produced was altered slightly for the slabs with notches or openings. One of the limitations of the software produced is the requirement that the position of the openings, or notches, coincides with the quarter point between strands so as to suit the element shapes chosen transversely. The openings are formed by excluding portions of the mapped mesh when extruding the areas into volumes. Effectively, the mesh is extruded along the length of the span with a gap left to create the notch or opening. The altered portion of the mesh is shown below in Figure 6.2. The arrows show the location of the quarter point, between the strand centres, where the edge of the openings must be located. In the case of forming an opening modelled with the mesh shown below, the portion of the mesh area to the left of the arrows is extruded onwards along the length of the slab. However the portion of the mesh area to the right, and extending across to the other limit of the opening, is not extruded through this distance. Instead it is copied to the point further along the span corresponding to the end of the opening, and then extruded onwards from there. The resulting volume mesh is shown in Figure 6.3.

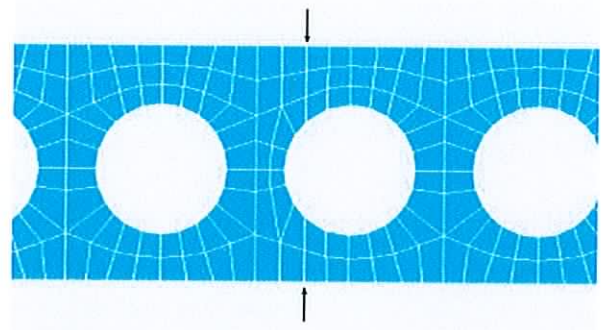

Figure 6.2 alteration to mesh to allow openings and notches

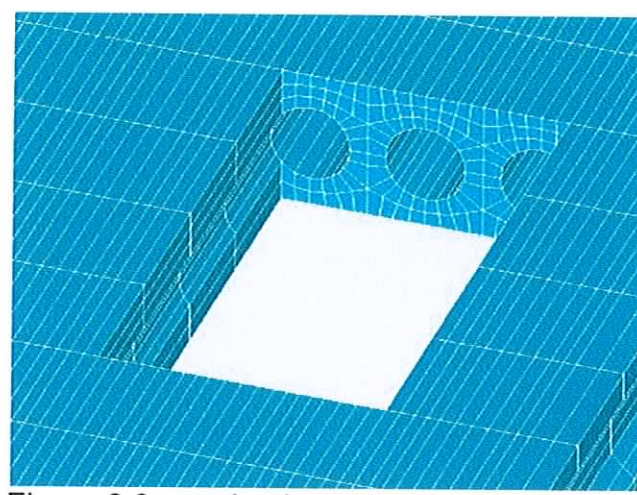

Figure 6.3 opening in an Ansys volume mesh

6.2.4. Loading

The loadings applied to the slabs analysed were generally larger than would be encountered but were chosen to increase the stress values close to the maximum allowable values and therefore justify the selection of slab depth. The uniformly distributed load applied to the slabs varied from 7 kN/m^2 to 10 kN/m^2.

As stated in Section 5.3.2.3., the prestressing force is applied by specifying the prestrain and the area of the strand. The calculation of the losses in prestress for both cross sections is shown in Appendix 5. Two sets of calculations were carried out, one for each cross section considered. It should be noted that since all the analyses carried out for the 150mm deep slab related to one span length, 4900mm, only one set of loss calculations was required, Similarly for the 200mm deep slab, both analyses related to a 6.0m slab and therefore, once again, only one set of calculations was required.

6.3. Ansys Results

The six sets of analyses were carried out and saved in the usual manner. However, the contour plots were also saved in the 'Metafile' image format with a white background. This format may then be opened in almost any of the image viewing packages available. The results of interest were the deflection values and the stresses in the z-direction since most prestressed slab designers will only check this particular stress. Within Ansys, the slab was examined, with points of interest such as stress concentrations near openings, the stresses found near the strands, and points where possible errors may have occurred. The contour plots that were saved included images such as plan views, edge views and isometric views of particular details.

A typical isometric view of a slab is shown below in Figure 6.4. The maximum and minimum stresses (DMX and DMN) shown in the body of text in the top left hand corner are the absolute maximum and minimum values found throughout the depth of the section and include those locally high values. The legend, as mentioned in Section 5.3.2.6., shows contour values as specified by the user. The divisions were devised based on typical requirements that a slab designer would set out.

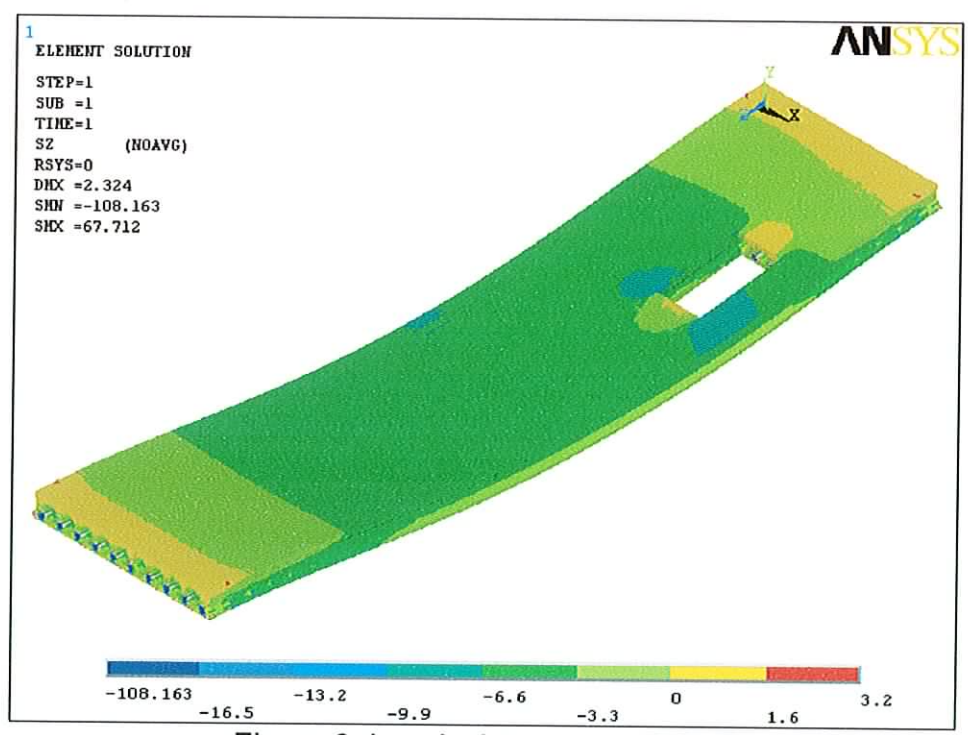

Figure 6.4. typical Ansys result plot

As stated earlier, the maximum allowable compressive stress in the slabs analysed was 16.5 N/mm^2 and 3.2 N/mm^2 in tension. In Figure 6.4, the eight stress step values in the legend are visible. The highest compressive stress is shown by default in blue however the other seven stress values were user defined. The five compressive stress steps were in equal steps from zero up to the maximum allowable compressive stress. The two tensile stress values were similarly found. The legend created above allows the user to determine quickly whether the design is viable, as the critical compressive stresses (greater than 16.5 N/mm^2) shown in blue and critical tensile stresses (greater than 3.2 N/mm^2) are shown in grey.

In the case of each of the six slabs the comparison carried out in the next section has the following format. The Ansys results are shown on the top half of each page with the software results shown below to allow direct comparison.

1. Stresses found in the top fibres of the slab as calculated by Ansys and the results given by the software as seen from a plan view.
2. Stresses found in the bottom fibres of the slab as calculated by Ansys and the results given by the software as seen from below the slab.
3. Deflections as found by Ansys and those found by the software
4. Discussion of similarities or differences.

The comparison of results is somewhat complicated by the differences in the methods in which the contour plots are presented. An Ansys stress plot uses six colours ranging from a dark blue to red. However the software uses twenty one colours in the plot ranging from red to green in smaller steps. The advantages and disadvantages of both methods can be seen by studying both types of stress plot.

6.3.1. A 150mm Deep slab with no opening or notches

This slab was the first analysed as it is the simplest model to create and the simplest to verify by hand calculations. The span was 6.0m and a uniformly distributed applied load of 6 kN/m^2 was assumed.

6.3.1.1. Results

Top fibre stresses

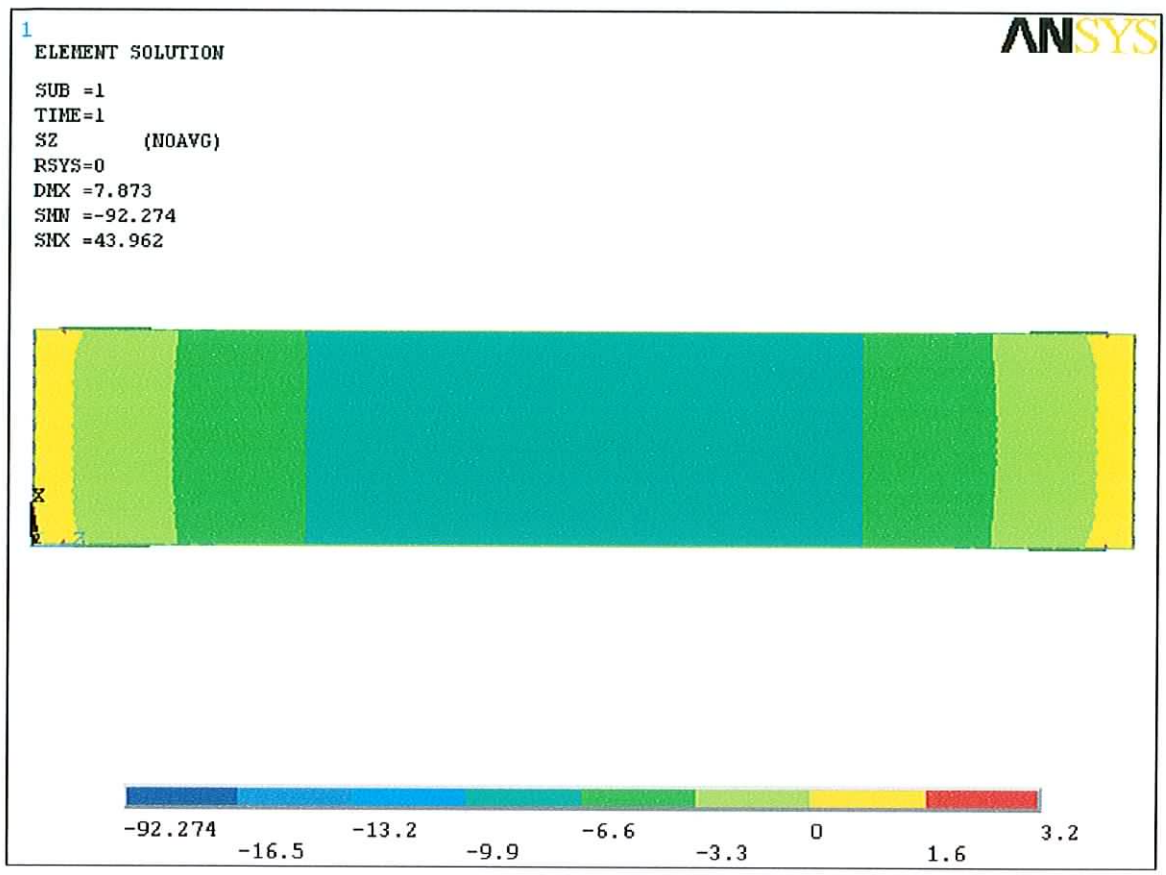

Figure 6.5 Ansys top stress – slab 1

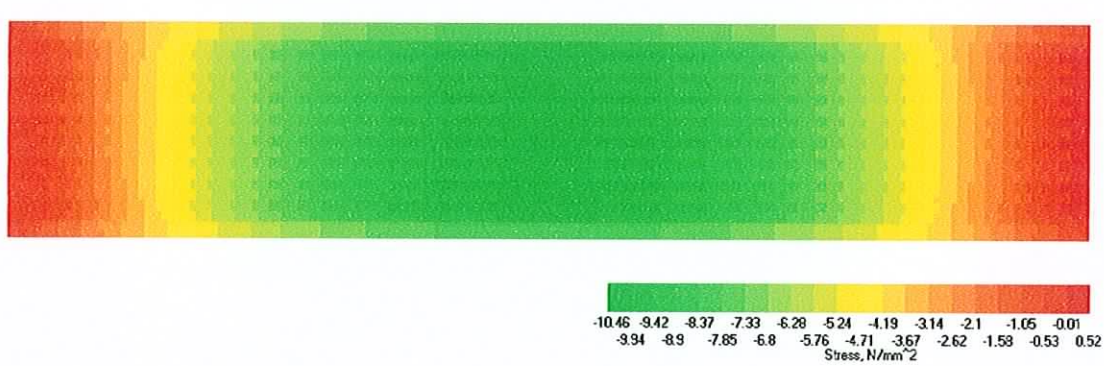

Figure 6.6. Software top stress – slab 1

Bottom fibre stresses

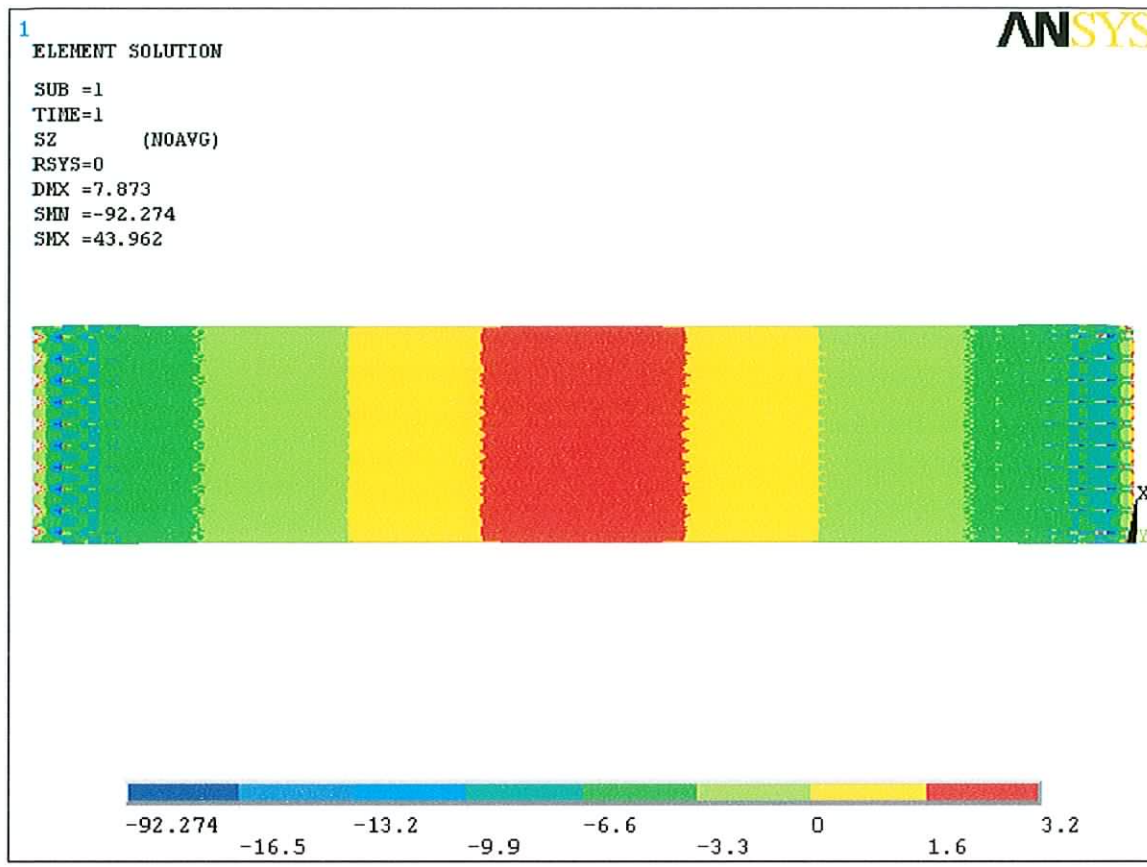

Figure 6.7 Ansys bottom stress – slab 1

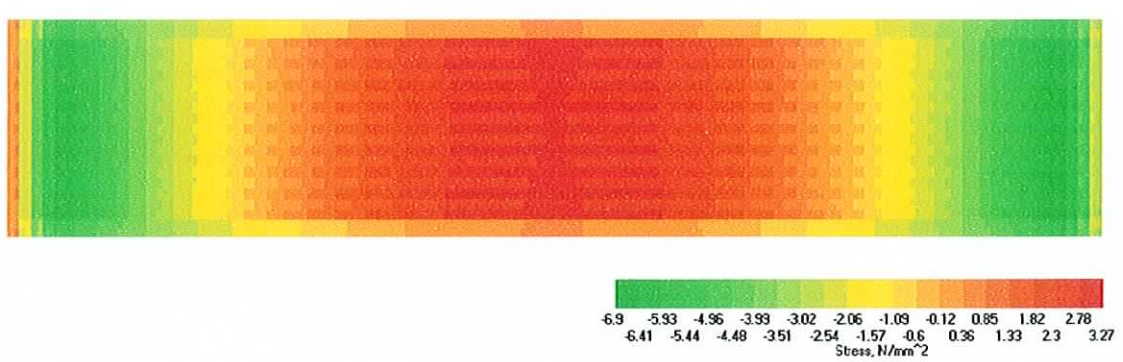

Figure 6.8 Software bottom stress – slab 1

Deflection

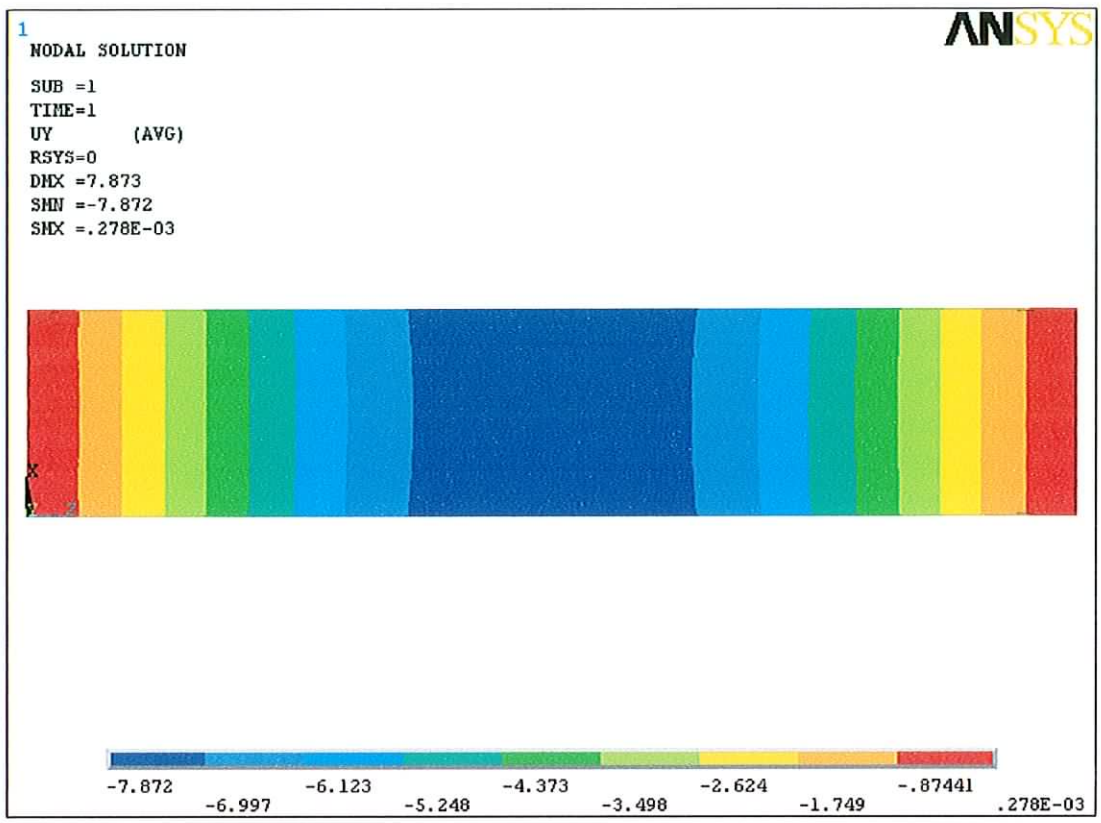

Figure 6.9 Ansys deflection plot – slab 1

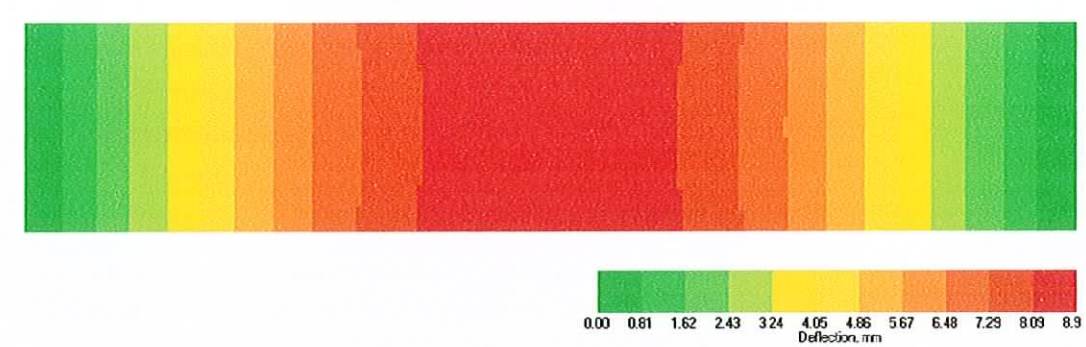

Figure 6.10 Software deflection plot – slab 1

6.3.1.2. Comparison of results

The slab analysed as shown above presents the simplest design case and can be carried out relatively accurately by representing the slab as a prestressed beam using traditional elastic analysis. However, this simple analysis provides a good starting point in the process of verifying the results given by the software.

The first comment that can be made about the slab detailed above is that the design itself appears to pass the design checks in terms of top and bottom fibre stresses. Referring back to Figures 6.5 and 6.6 in which the top stresses given by Ansys and the software produced are shown, despite the different colour coding systems used in the stress diagrams, the similarities in the stress values can be seen. The largest compressive stress found by Ansys is seen to be no greater than 9.9 N/mm^2 whilst the peak value found by the software was 10.46 N/mm^2. Similarly the tensile stresses found in the top fibres at both ends of the slab were generally no greater than 1.6 N/mm^2 as found by Ansys, and a peak of 0.52 N/mm^2 as calculated by the software. This difference is due predominantly to the prestressing forces used in Ansys being constant along the length of the slab whereas the software produced takes into account the fall off in force at the ends of the strands due to anchorage. It can therefore be said that the software more accurately models the prestressing force in these regions and therefore the true stress value for the regions close to the ends of the slabs must be closer to that given by the software. The central 40% of the slab is shown by Ansys to have stresses in the region of 6.6 to 9.9 N/mm^2 in compression, whilst the software finds stresses in the same region to be between 6.8 and 10.46 N/mm^2.

The bottom fibre stresses are shown in Figures 6.7 and 6.8. The maximum tensile stress in the mid-span region as given by Ansys is no greater than 3.2 N/mm^2. However, the values as given by the software are slightly larger at 3.27 N/mm^2. The highest compressive stresses found by the software near to the ends of the slab are once again in line with those found by Ansys. Once again the Ansys values can be seen to be slightly larger due to the constant prestressing force used in the Ansys model.

The deflection values given by Ansys in Figure 6.9 are somewhat lower than those calculated by the software, shown in Figure 6.10, with the difference found to be 11.6% Once again the difference in prestressing force values applied along the length of the slab would play a part in accounting for this difference.

An examination of the results produced by Ansys show a number of areas on the slab where very large stresses differences are found within single elements. A typical example of this is found in Figure 6.11 towards the end of the span.

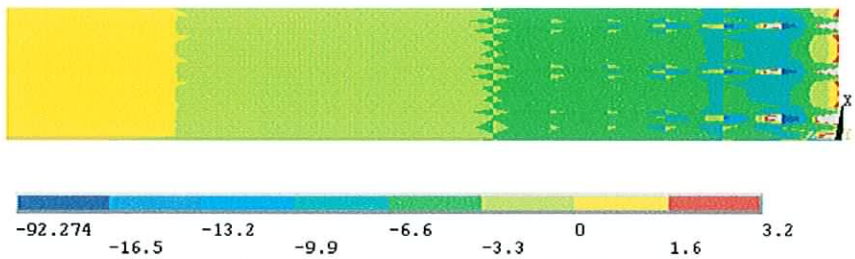

Figure 6.11 locally high stresses

As was discussed in Section 2.4.5, the prestressing force in the ends of the strands falls off due to the lack of a sufficient anchorage distance. Therefore, the extremely high tensile and compressive stresses found by Ansys at the ends of the slab are most likely due to prestressing force values that are not possible in these locations but were modelled as such in Ansys. The stresses in these locations could, in theory, be attained if the slabs were post tensioned, having end blocks to distribute the prestressing force uniformly throughout the length of the slab. A possible second source for this phenomenon are the element shapes used in this region and the aspect ratio of these elements. It could prove beneficial to use a number of shorter columns of elements in such regions where high stress variations occur. The bottom fibre stresses given by the software in Figure 6.8 show a slight anomaly that would require further examination as part of any measures to continue the research or further develop the software. Along the first column of elements in the left hand support a tensile stress appears to be acting which is not present at the other end of the slab or in the Ansys model. This is thought to be due to an anomaly in the code which calculates the forces to be applied at each node along the line of the strands. This is seen in Section 4.9.2.2. where the method used for applying the loads is detailed.

6.3.2. A 150mm deep slab with one opening

The next slab analysed was shorter than the last at 4.9m and has a uniformly distributed load of 7.0 kN/m^2. This layout also has an opening in plan that results in a break in two of the strands.

6.3.2.1. Results

Top fibre stresses

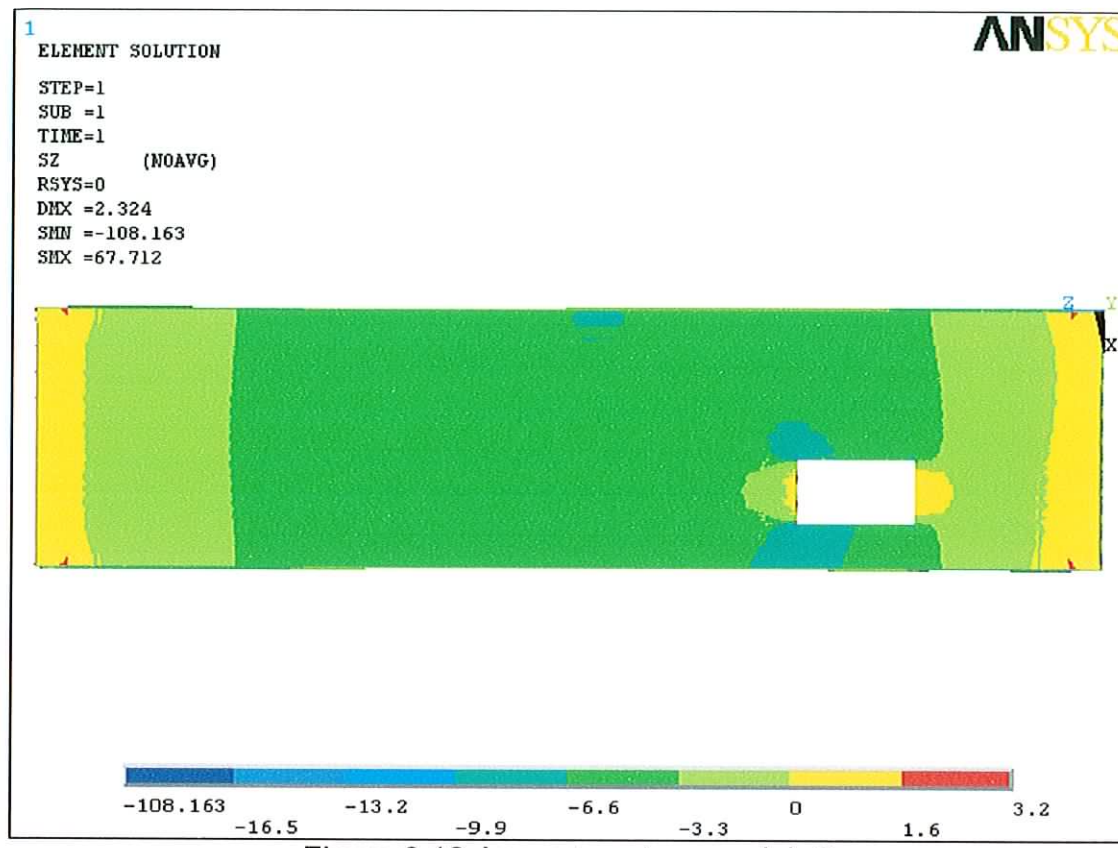

Figure 6.12 Ansys top stress – slab 2

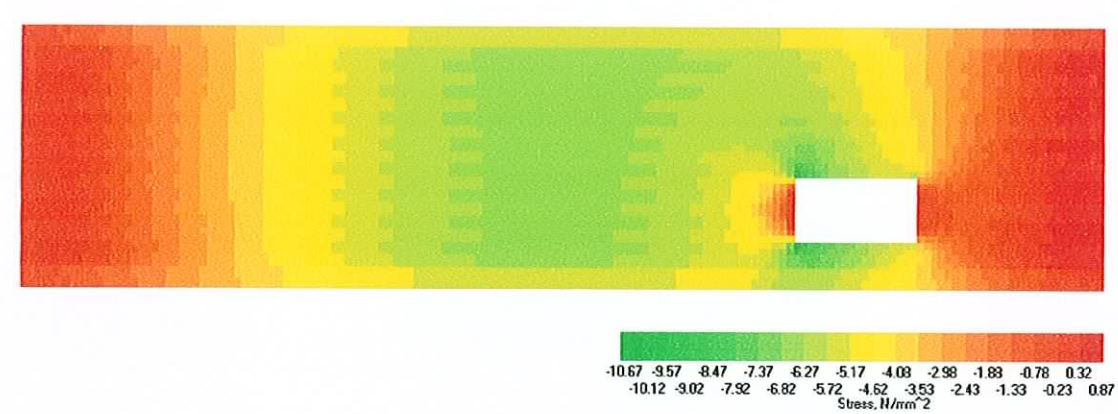

Figure 6.13 Software top stress – slab 2

Bottom fibre stresses

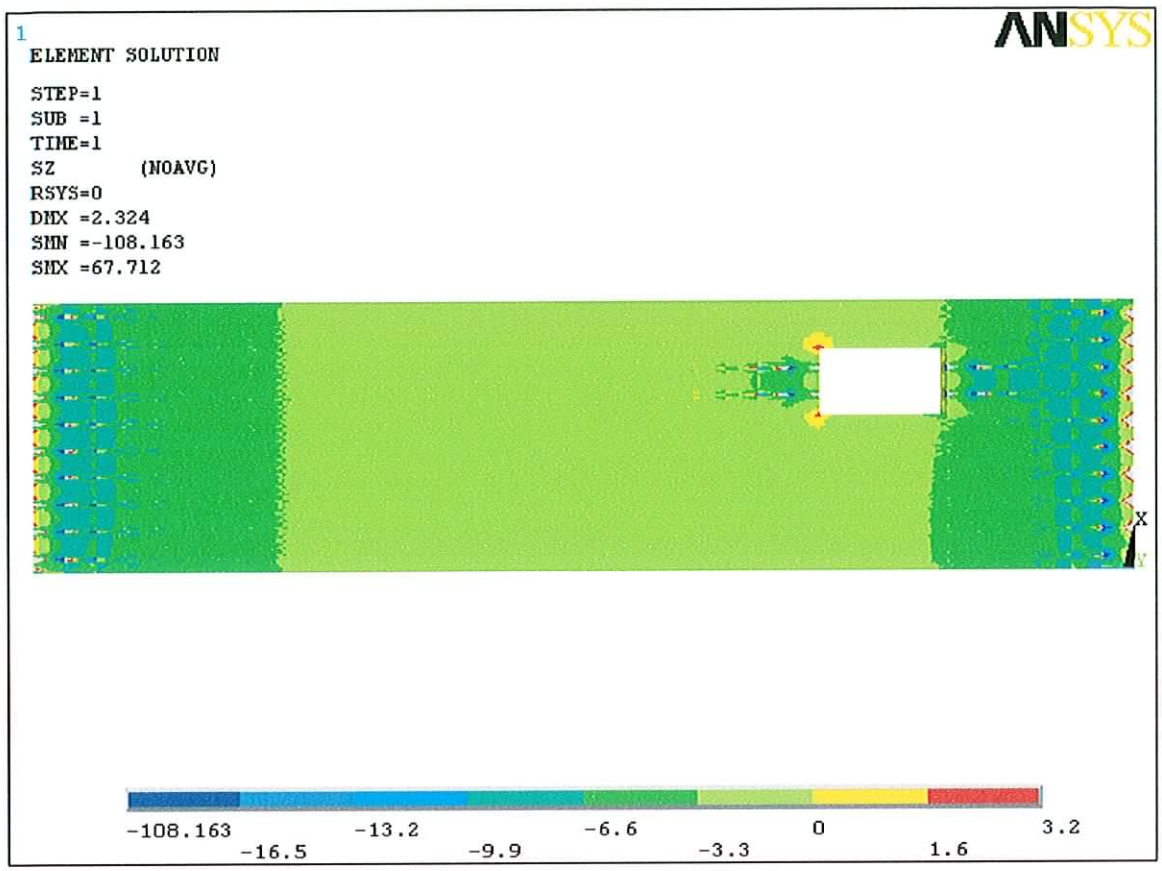

Figure 6.14 Ansys bottom stress – slab 2

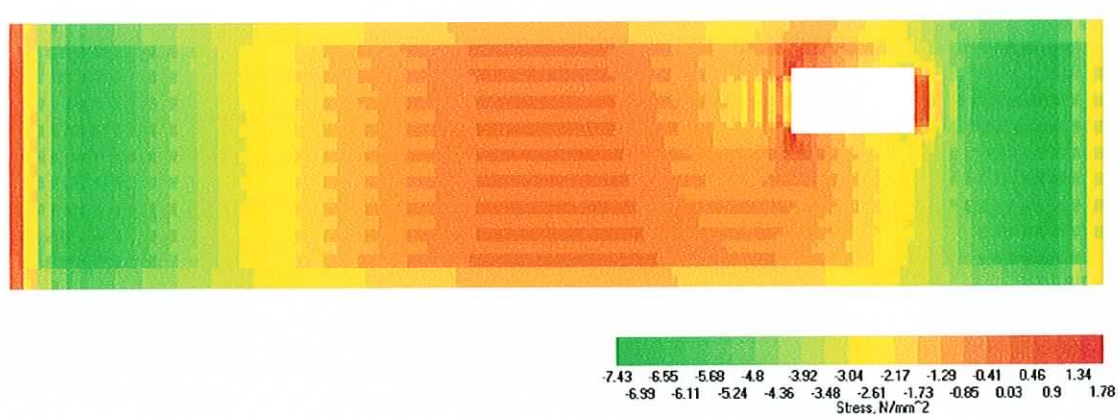

Figure 6.15 Software bottom stress – slab 2

Deflection

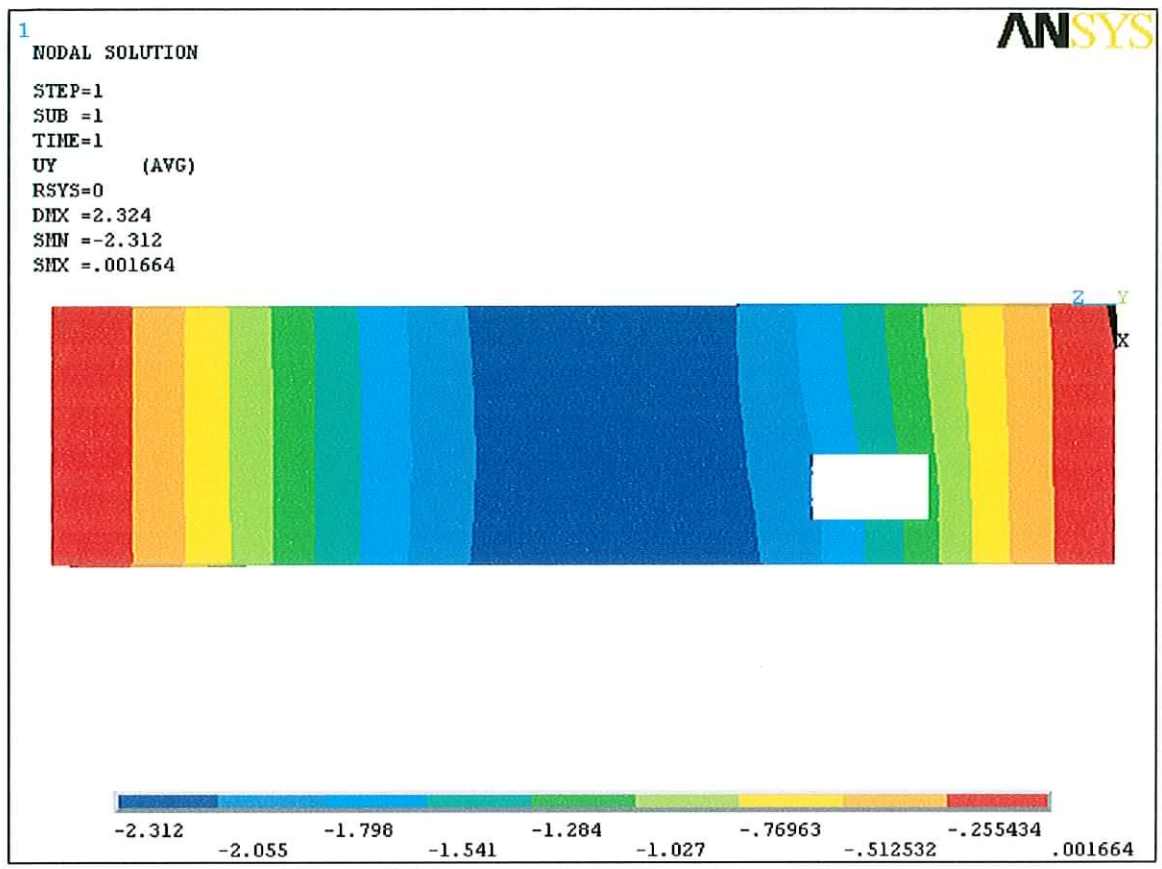

Figure 6.16 Ansys deflection plot – slab 2

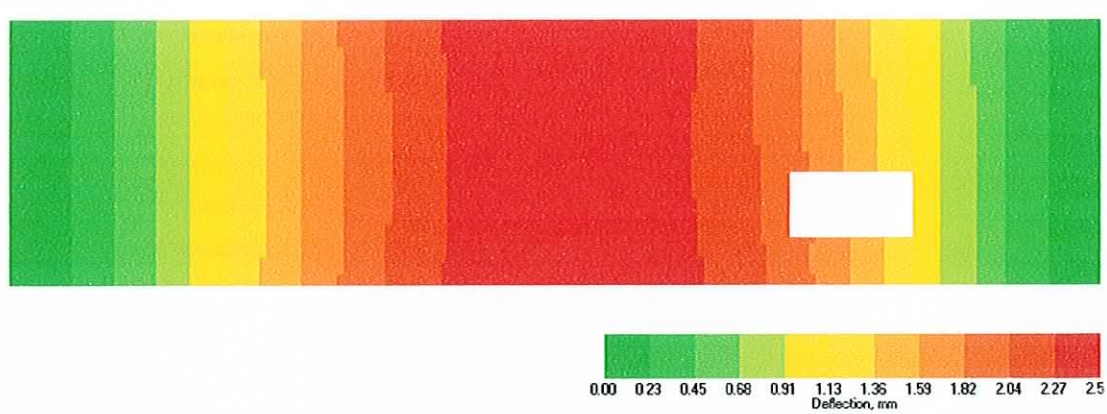

Figure 6.17 software deflection plot – slab 2

6.3.2.2. Comparison of results

This slab represents a slightly more complicated analysis than that shown in the last section. The break in two of the stands should be seen to reduce the

capacity of the slab substantially, as this amounts to a 20% reduction in the prestressing force at any cross section taken at the opening.

Figures 6.12 and 6.13 show the results as given by Ansys and the software respectively. The main features of the first slab analysed follow through to this analysis, such as the discrepancies in the tensile stress at the ends of the slab. The compressive stresses given by Ansys for the mid-span region are generally no greater than 6.6 N/mm^2 with a very small region along an edge where the local stress surpasses 6.6 N/mm^2. The software produced values that peak in at the mid-span point at 6.82 N/mm^2. In a number of the test analyses carried out, the software appeared to show the edge elements as particularly stiff and therefore able to resist the stresses more effectively. This possibly explains why the stress concentration shown at the top of the Ansys model in Figure 6.12 is not present in the plot produced by the software shown in Figure 6.13. It is thought that this is due to an error in the software code however examination of this section of code failed to reveal the cause. The other areas of interest are around the opening on the slab. Once again, by examining the stresses to the left and right of the opening in both Figures 6.12 and 6.13, tensile stresses are visible in both cases, typical of the those found at the ends of the strands with values of 0.87N/mm^2 given by the software and values in the 0 to 1.6 N/mm^2 range given by Ansys. Above and below the openings reasonably large areas of compressive stresses ranging between 6.5 to 10.5 N/mm^2 can be seen to act.

The bottom fibre stresses shown in Figures 6.14 and 6.15 are once again broadly in line with each other in terms of mid-span stresses and stresses near the supports, with the exception of the results found by the software for the first column of elements on the left side of the slab as discussed at the end of Section 6.3.1.2. An examination of the stresses around the opening shows similar stress concentrations around the corners to the left of the opening with peak values of 1.78 N/mm^2 given by the software. The anomaly that was seen to affect the first column of elements at the left side of the slab also effects the column of elements immediately to the right of the opening. However, other than this particular group of elements the software can be seen to give similar stresses at the other locations around the opening.

The deflection values found were again similar at 7.6% and showed generally the same pattern with the maximum deflection as given by Ansys to be 2.21 mm and by the software to be 2.5 mm.

The pattern seen in both the top and bottom stress plots produced by the software includes a teeth like step effect as shown in Figure 6.18. This reflects the difference in stiffness between the lines of elements that include the strands and those with the hollow core running through them.

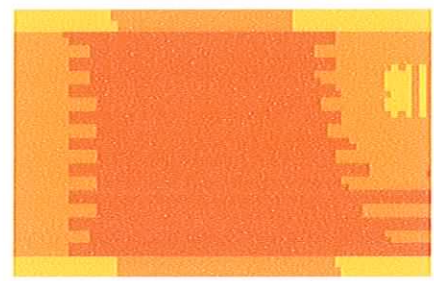

Figure 6.18 stresses over hollow cores

In Ansys, the benefit of the 3-dimensional elements can be seen as the curved element shapes used model the stresses within the individual elements more accuracy. The relates to the ability of the Ansys model to accurately predict the transfer of stresses from the thinnest point over the void to the stiffest point over the strands.

6.3.3. A 150mm deep slab with one notch

This slab is identical to the last in terms of span and loading however the opening is replaced by a notch along one of the edges which intersects two of the strands.

6.3.3.1. Results

Top fibre stresses

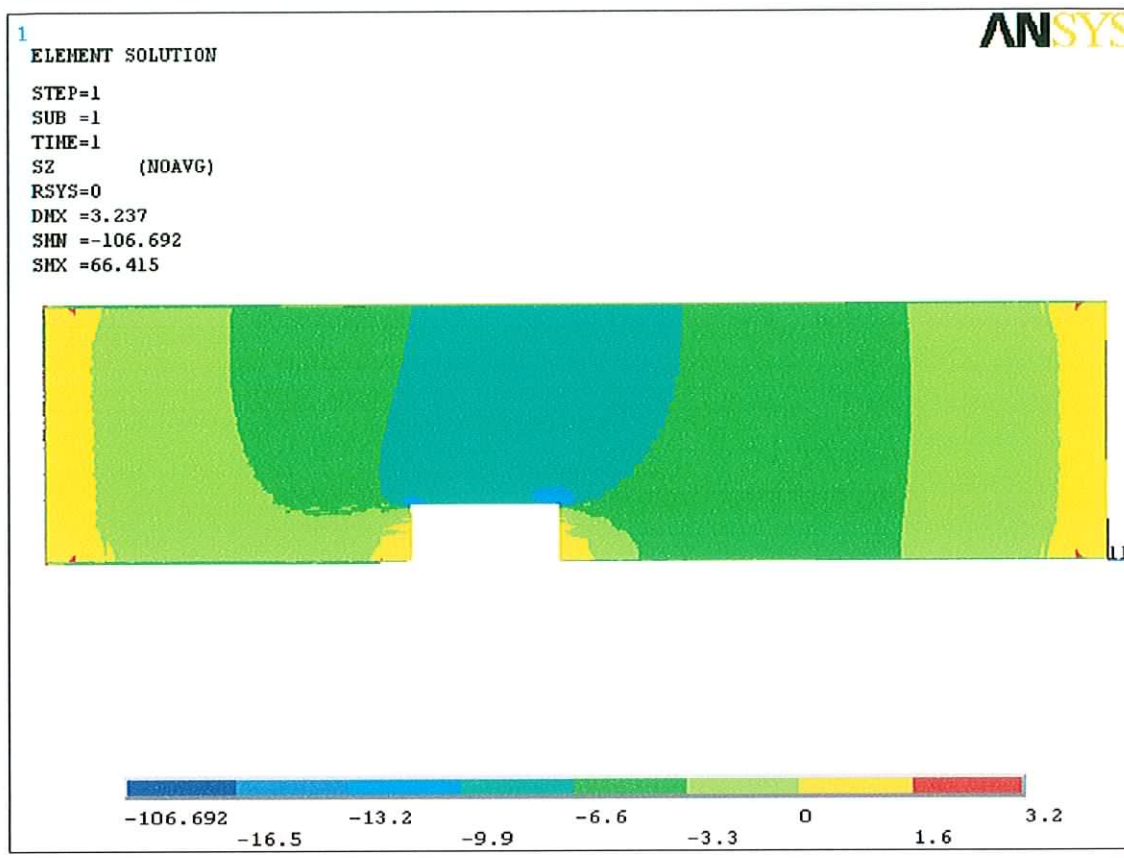

Figure 6.19 Ansys top stress – slab 3

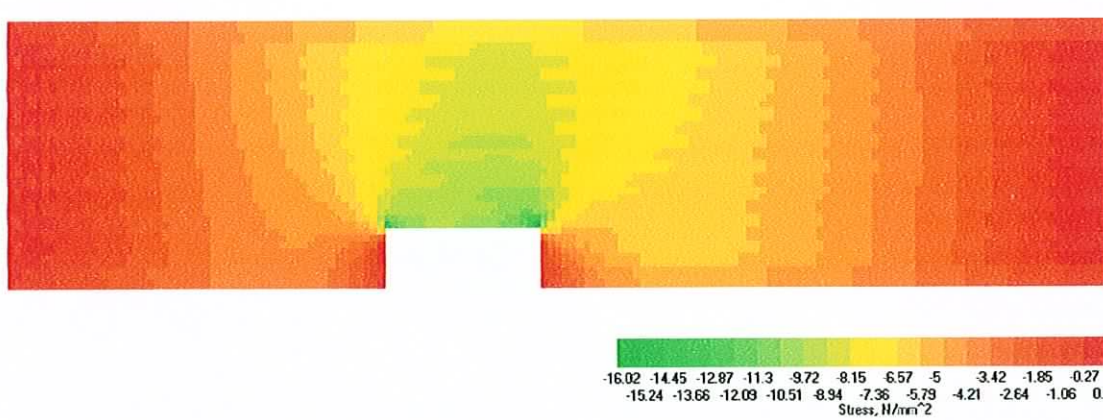

Figure 6. 20 software top stress – slab 3

Bottom fibre stresses

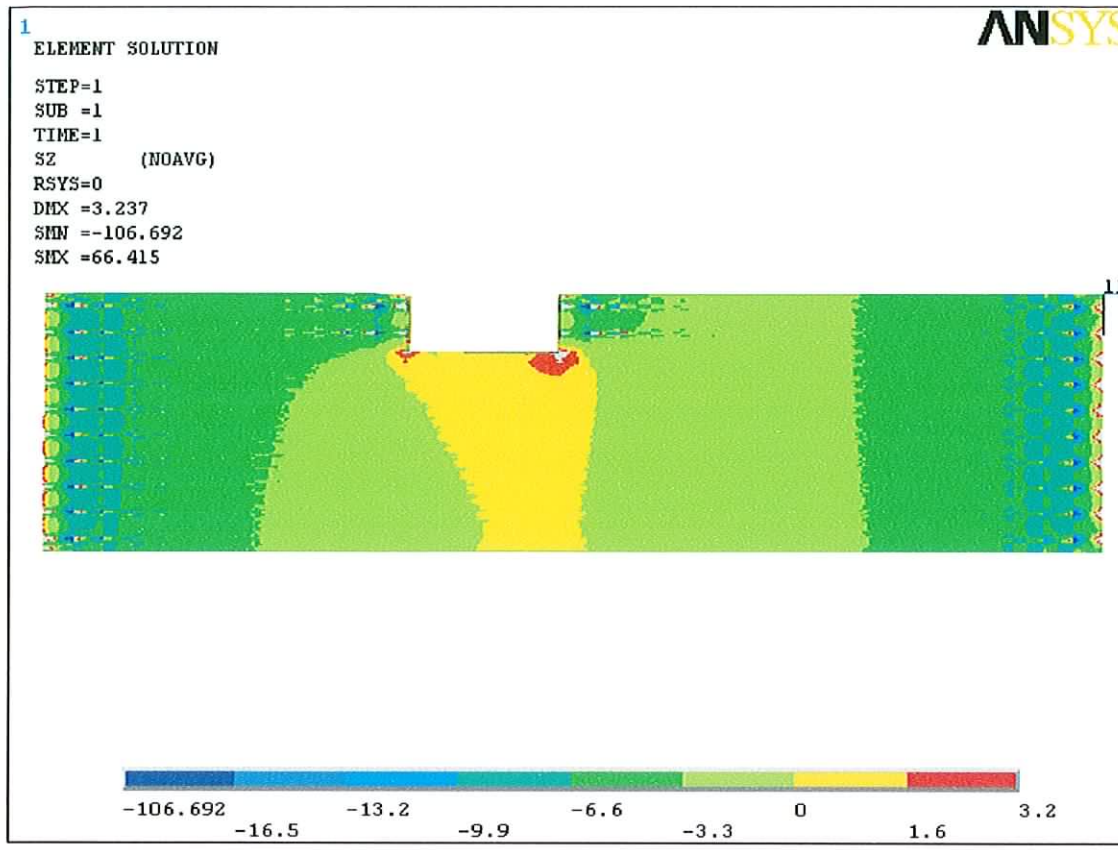

Figure 6.21 Ansys bottom stress – slab 3

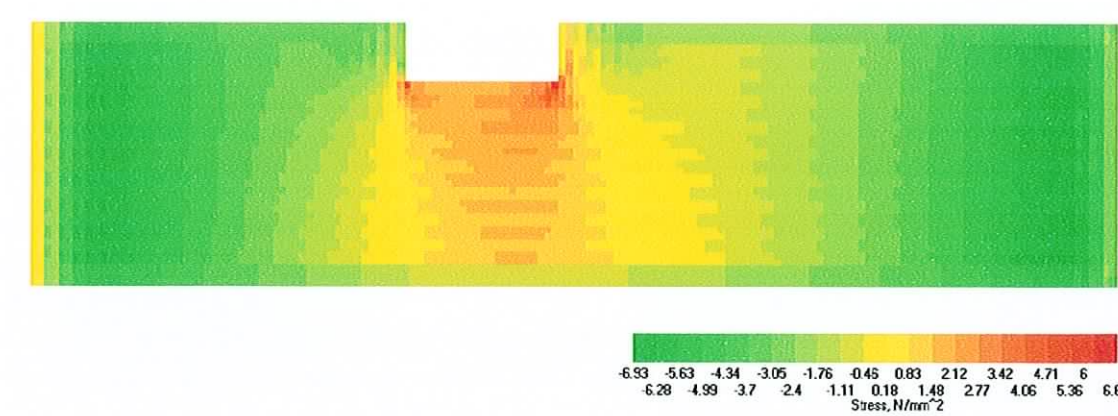

Figure 6.22 Software bottom stress – slab 3

Deflection

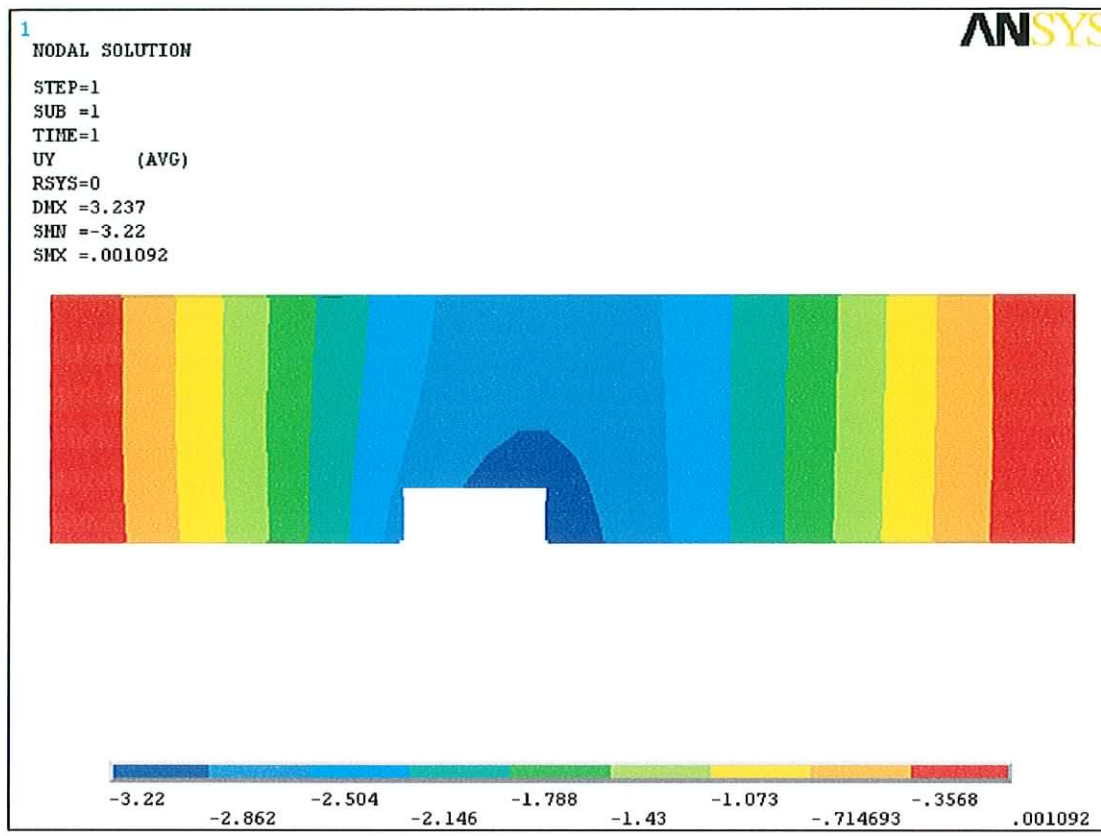

Figure 6.23 Ansys deflection plot – slab 3

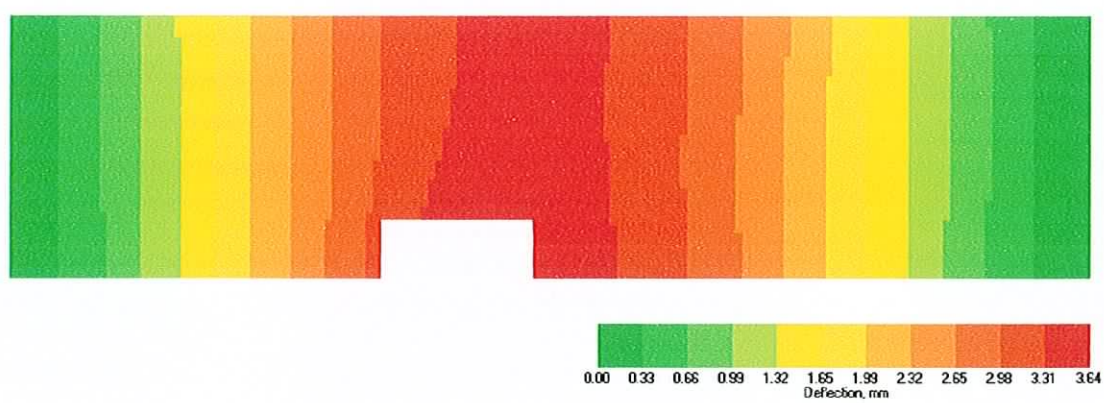

Figure 6.24 Software deflection plot – slab 3

6.3.3.2. Comparison of results

This slab, in common with the previous example has its capacity reduced by the presence of a break in two of the strands. However, with this slab the break in the strands is due to a notch along one of the edges.

Examining the top fibre stresses shown in Figure 6.19 and 6.20, the pattern of stresses seen in the first two analyses at the ends of the span is present. Mid-span and peak stress values show good agreement. It can be seen that the Ansys plot shows a region of compressive stress in the 6.6 to 9.9 N/mm^2 with a corresponding region of stresses plotted by the software with values ranging from 7.36 to 9.72 N/mm^2. Peak stresses given by Ansys are in the 13.2 to 16.5 N/mm^2 region compared with software values of 15.24 to 16.02 N/mm^2 very close to the corners of the notch.

The bottom fibre compressive stresses at the support were found to range between 6.6 and 9.9 N/mm^2 in Ansys and peak somewhere in the region of 6.28 to 6.93 N/mm^2 as calculated by the software. The mid-span Ansys stresses fall in the 0 to 1.6 N/mm^2 tensile range as compared with 0.83 to 1.48 N/mm^2 given by the software. The peak stresses found by Ansys are shown to be greater than 3.2 N/mm^2, as shown by the grey area on the stress plot. The software however, shows these stresses as having a value in the 6.0 to 6.65 N/mm^2 range.

Once again the deflection values produced by both the software and Ansys compare reasonably well with software giving a peak deflection value of 3.64mm and Ansys giving a peak value of 3.22mm, a difference of 11.5%. An examination of the deflection plots also shows a good correlation in terms of the deflection values at various points on the slabs.

6.3.4. A 150mm deep slab with two notches

This slab follows the same span and loading pattern outlined in the last two analyses. There are two notches along the same edge each intersecting the line of two of the strands.

6.3.4.1. Results

Top fibre stresses

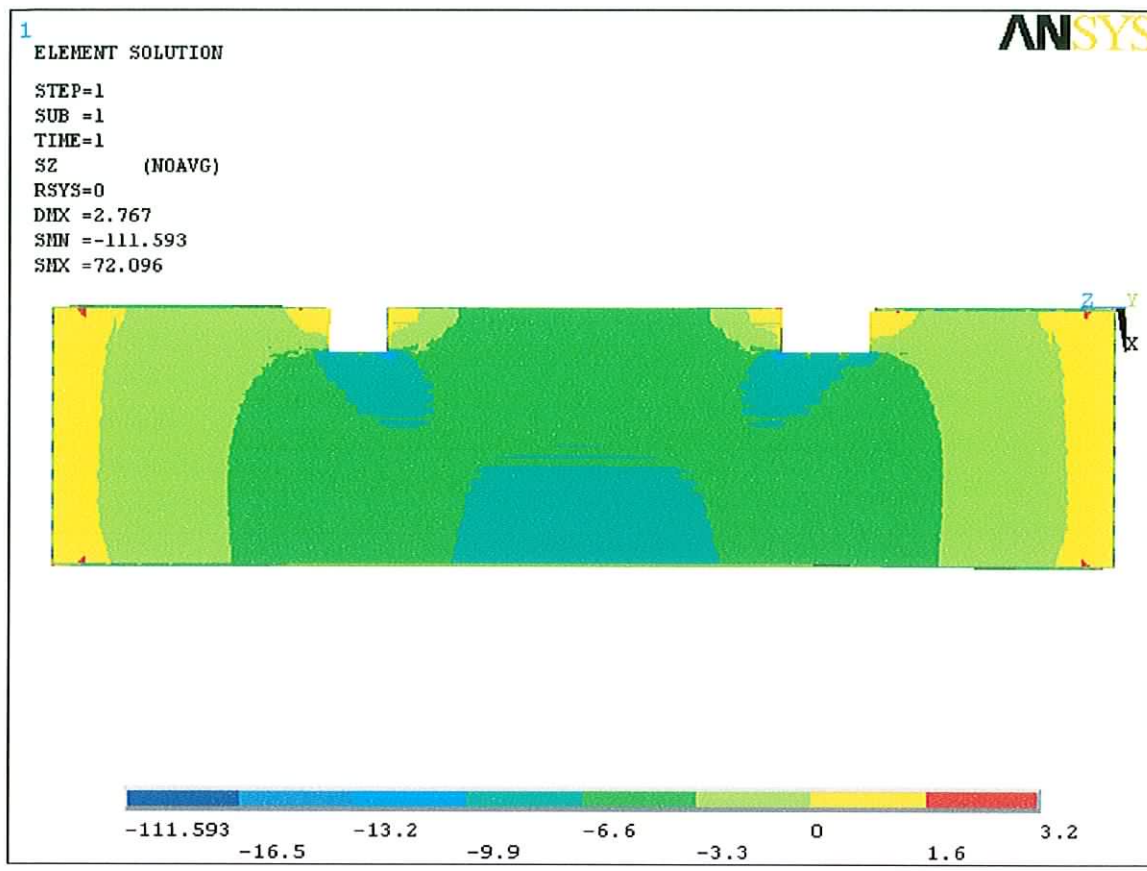

Figure 6.25 Ansys top stress – slab 4

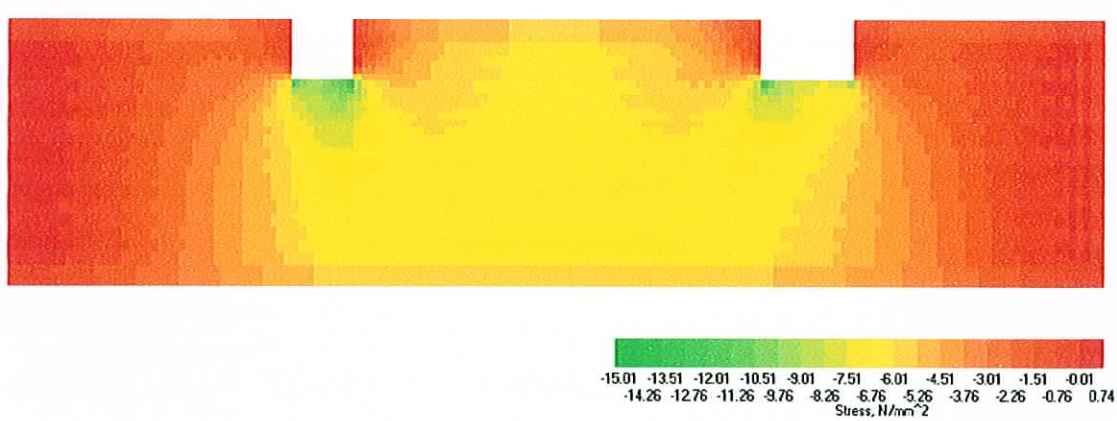

Figure 6.26 Software top stress – slab 4

Bottom fibre stresses

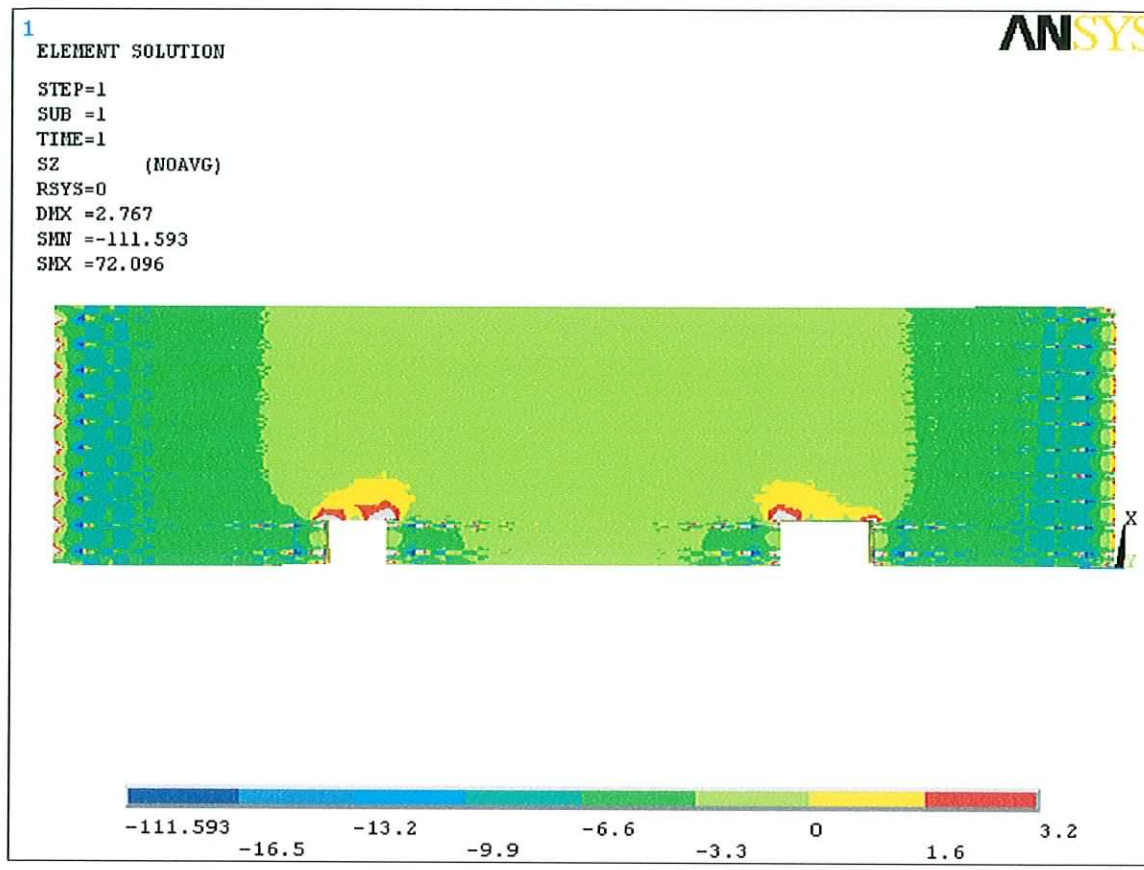

Figure 6.27 Ansys bottom stress – slab 4

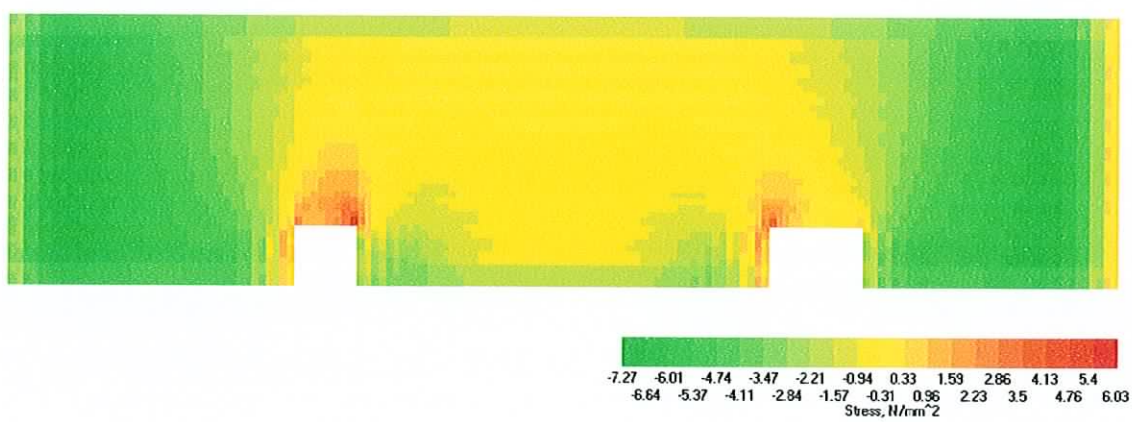

Figure 6.28 Software bottom stress – slab 4

Deflection

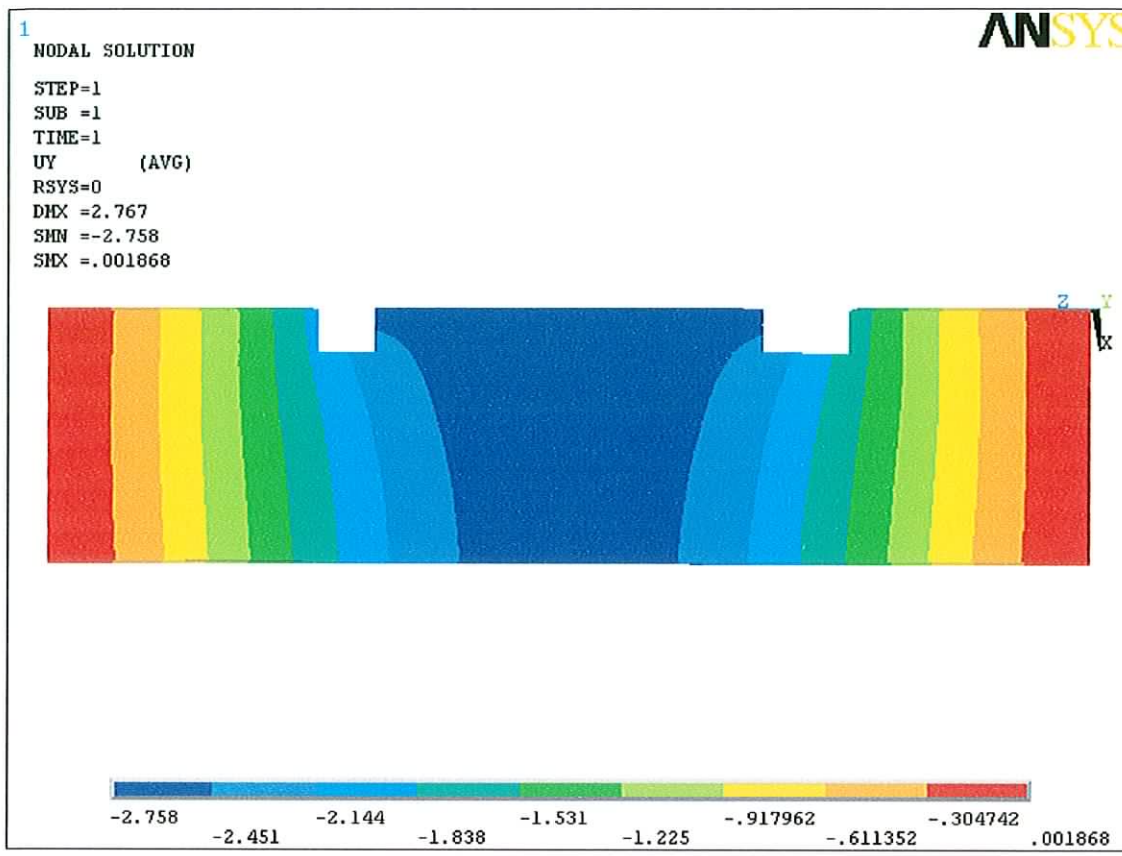

Figure 6.29 Ansys deflection plot – slab 4

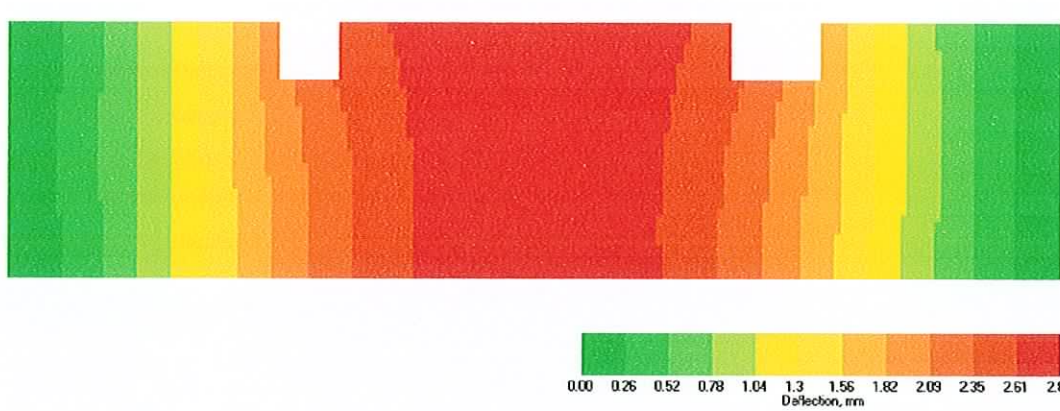

Figure 6.30 Software deflection plot – slab 4

6.3.4.2. Comparison of results

This analysis was set up so as to model a slightly more complicated slab than that seen in the last example. The top fibre stresses are compared in Figure 6.25 and 6.26. As was noticed with the first two analyses the end stresses

produced by Ansys and the software are in good agreement. The maximum stresses found mid-span in Ansys lie in between 6.6 and 9.9 N/mm^2 whilst the peak value given by the software was 7.51 N/mm^2. It should be noted that these stresses were found in the same location on the slab. Examination of the stresses closer to the notches shows a similar picture. Again, the Ansys stress plot shows an area in which the stresses are between 6.6 and 9.9 N/mm^2 close to both of the notches. The stresses shown in the software plot for the same region vary from 6.76 to 9.76 N/mm^2 giving a very close correlation with the Ansys results. The peak stresses found at the corners of the notches were found to be 16.5 and 15.01 N/mm^2 in Ansys and the software respectively.

Bottom fibre stress values generated in Ansys are shown in Figure 6.27 with the equivalent stress diagram generated by the software shown in Figure 6.28. The general pattern of stresses across the slab once again holds true. The stresses found towards the end of the strands compare well with compressive stresses in the 6.6 to 9.9 N/mm^2 range reported by Ansys and a value of 7.27 N/mm^2 produced by the software. The Ansys stress plot shows a large area of the slab with a compressive stress in the 0 to 3.3 N/mm^2 range which compares well with the stress plot produced by the software where stresses in the same area lie between 3.47 N/mm^2 in compression and 0.33 N/mm^2 in tension. It can also be seen that close to the notches Ansys shows stress concentrations at the corners in excess of 3.2 N/mm^2 - the upper limit for tension whilst the software shows values up to 6.03 N/mm^2 in tension.

Finally, deflection values are compared with the results from Ansys and the software shown in Figures 6.29 and 6.30. A brief study of the two deflection plots shows that values are reasonably well matched. The peak mid-span value as given by Ansys is 2.758 mm compared with 2.87 mm as calculated by the software.

6.3.5. A 200mm deep slab with no openings or notches

This deeper slab required a slightly longer span to be economical and therefore a 6m span was once again used. The uniformly distributed load was once again

increased to 8 kN/m^2 in an attempt to model a situation where this choice of slab depth would prove logical.

6.3.5.1. Results

Top fibre stresses

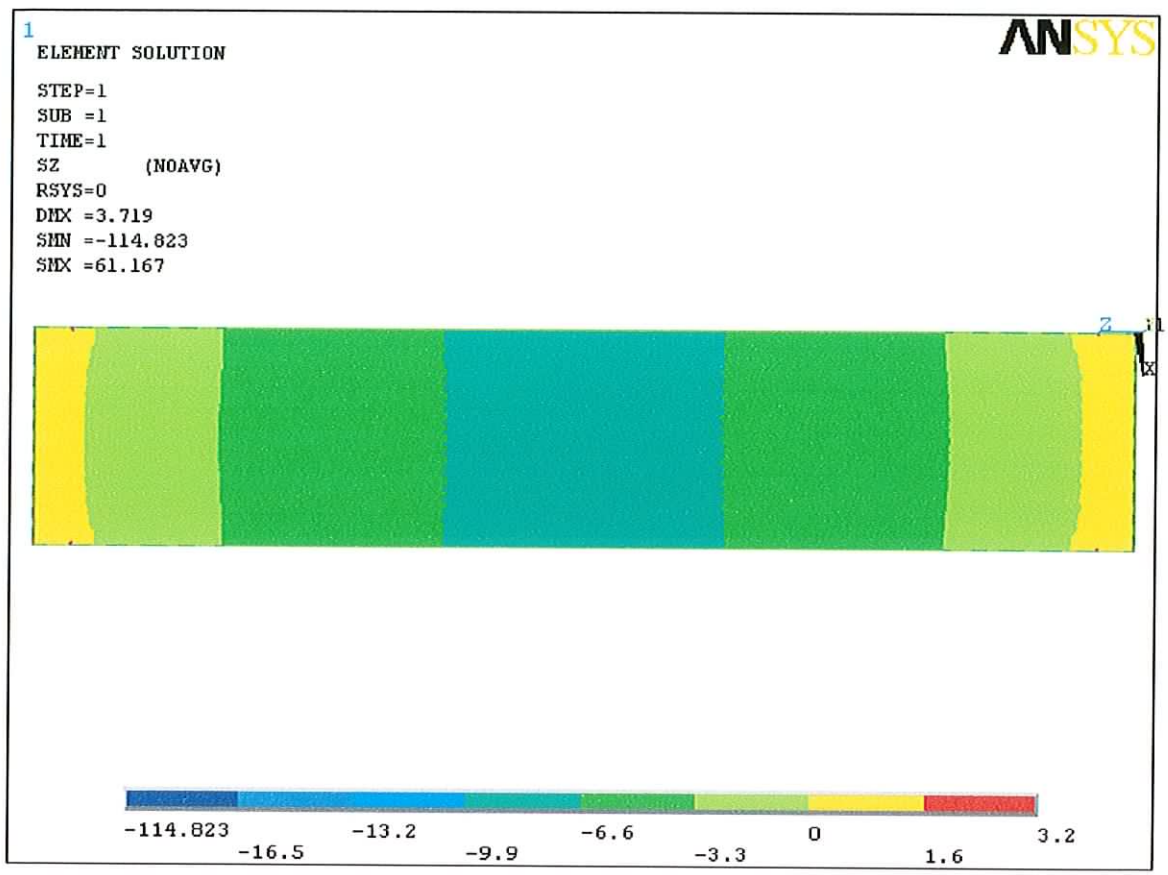

Figure 6.31 Ansys top stress – slab 5

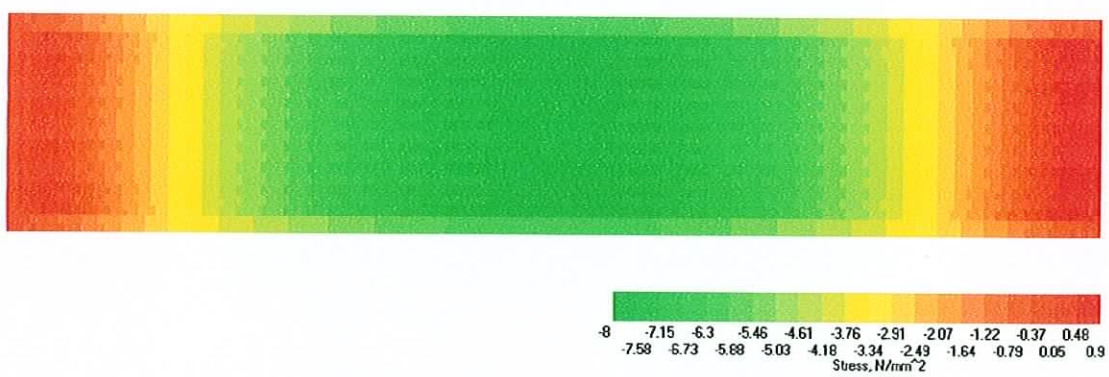

Figure 6.32 Ansys top stress – slab 5

Bottom fibre stresses

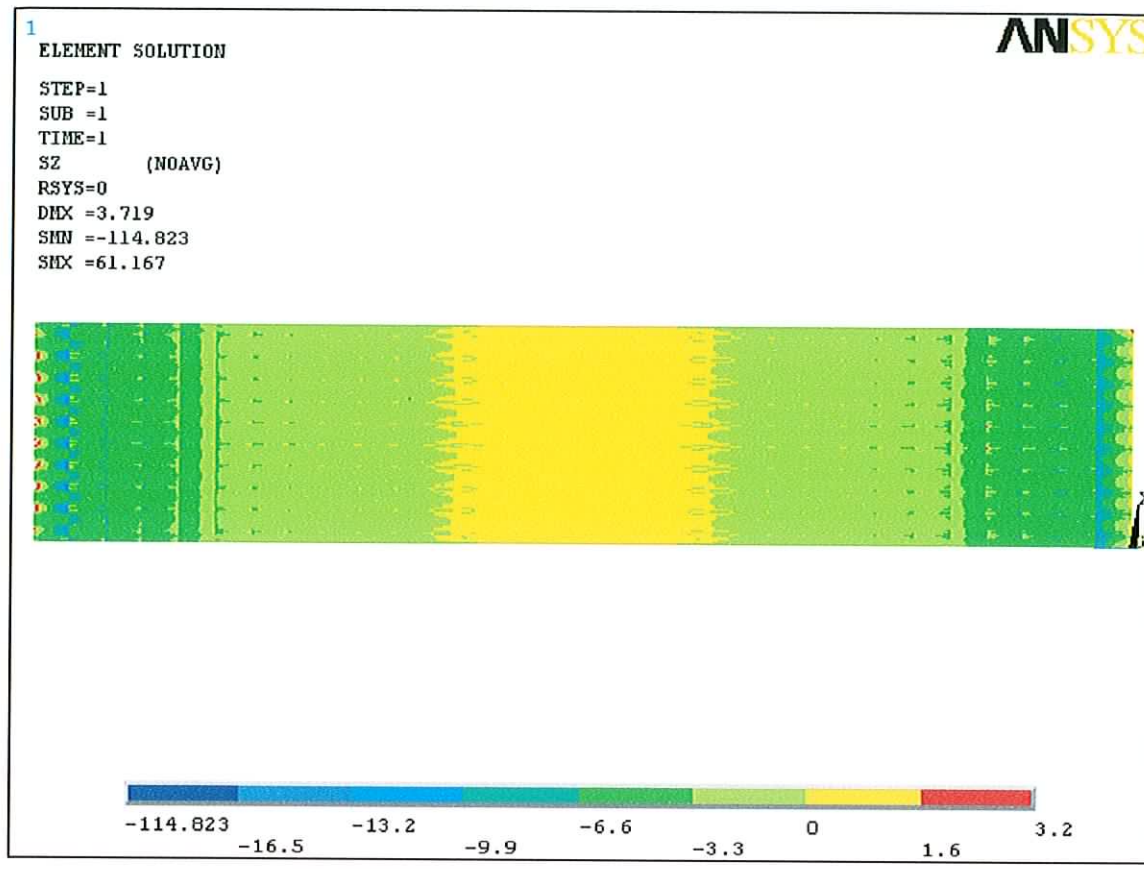

Figure 6.33 Ansys top stress – slab 5

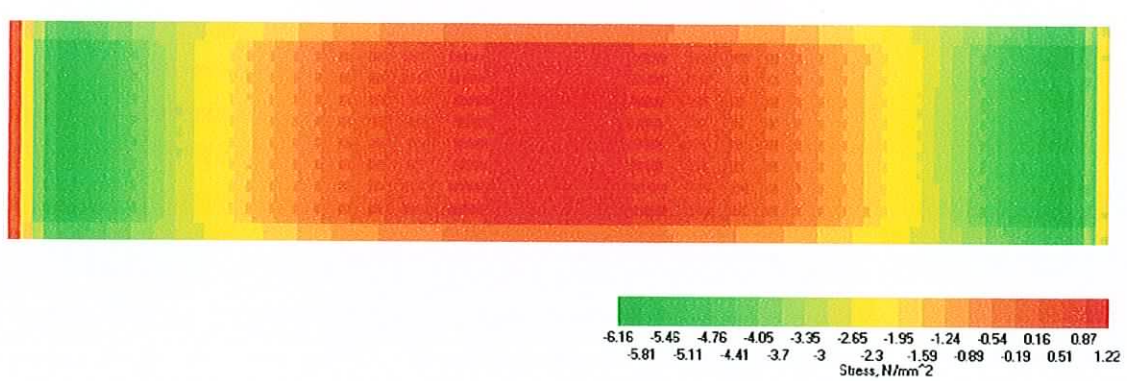

Figure 6.34 Ansys top stress – slab 5

Deflection

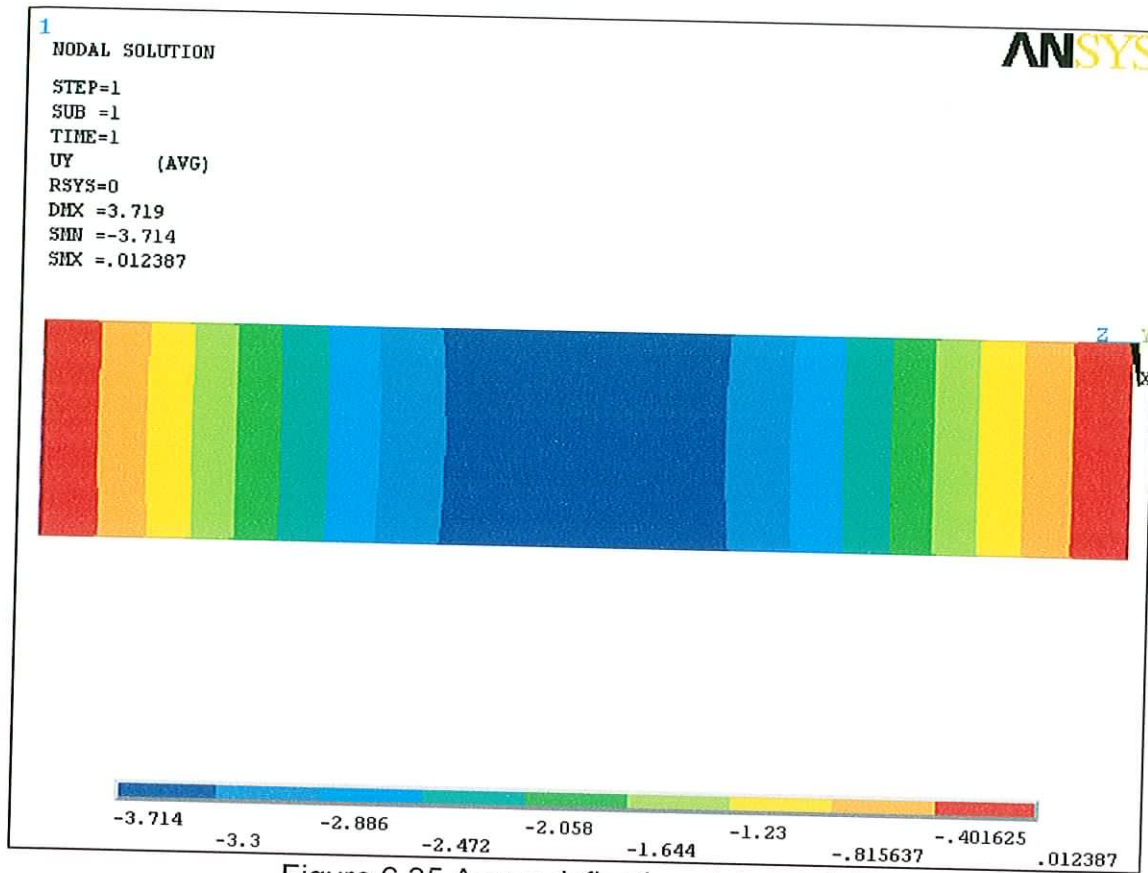

Figure 6.35 Ansys deflection plot – slab 5

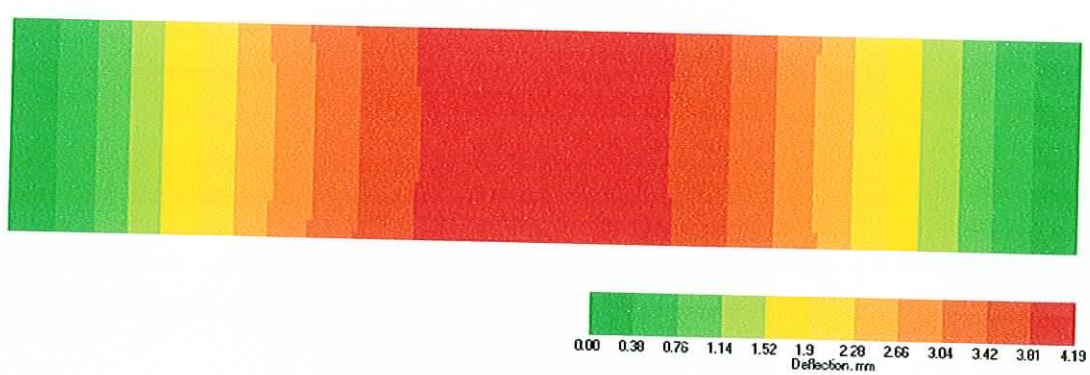

Figure 6.36 Software deflection plot – slab 5

6.3.5.2. Comparison of results

This analysis, along with the next slab were carried out in order to help gain confidence in the software's ability to handle slabs of different depths. This

particular exercise would allow confidence to be built up in that section of code within the software that calculates section properties.

Top fibre stresses are shown in Figure 6.31 and 6.32. The main points of interest, the tensile stresses at the ends of the slab and the maximum compressive stresses found at the mid-span location, are once again in good agreement. The Ansys values produced for the tensile stresses at the end of the slab are in the 0 to 1.6 N/mm^2 range whilst the software gives a peak value of 0.9 N/mm^2. The mid-span stresses are calculated by Ansys to be in the region of 6.6 to 9.9 N/mm^2 in compression whilst the software values for the same region peak at 8.0 N/mm^2. The difficulty in comparing results noted earlier is also evident here however further inspection shows that certain features such as points of contraflexure are at almost identical locations in both stress plots.

Bottom fibre stresses also show the same traits seen in the 150mm deep slab analysed in Section 6.3.1. Ansys gives compressive stresses at the ends of the slab in the 3.3 to 6.6 N/mm^2 range with software values peaking at 6.16 N/mm^2. At the mid-span point the Ansys stress plot gives tensile stresses from 0 N/mm^2 to 1.6 N/mm^2 compared to a peak stress value given by the software of 1.22 N/mm^2. Again the locations at which contraflexure occurs appear to coincide reasonably well.

A quick examination of deflection values show reasonable agreement with Ansys giving a mid-span deflection value of 3.714 mm deflection and the software giving a peak value of 4.19 mm, a difference of 11.5%

6.3.6. A 200mm deep slab with one opening

The final slab analysis was carried out also on a 6m slab but with a narrow opening in the slab in plan which intersects two of the strands. The applied load is 8 kN/m^2.

6.3.6.1. Results

Top fibre stresses

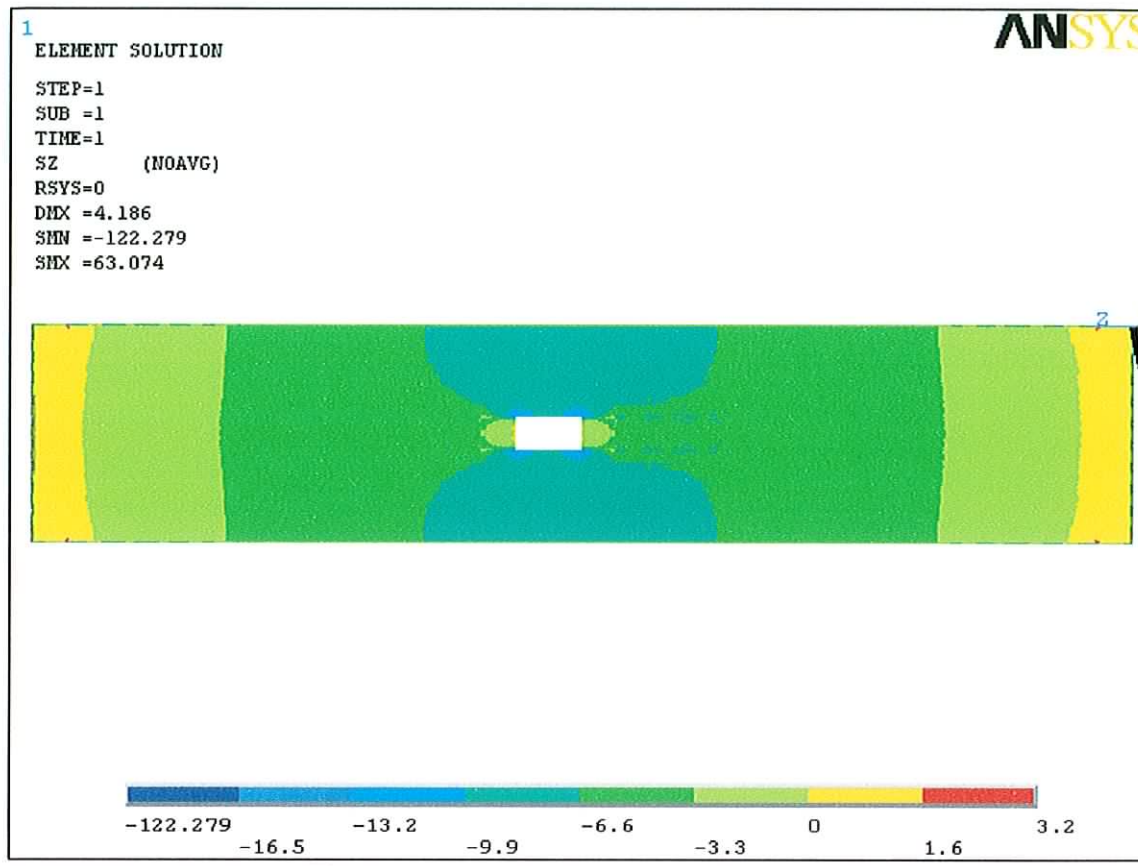

Figure 6.37 Ansys top stress – slab 6

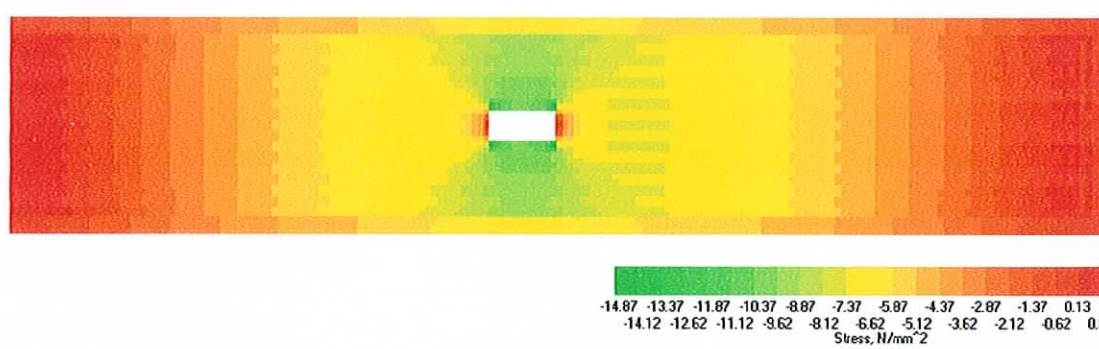

Figure 6.38 Software top stress – slab 6

Bottom fibre stresses

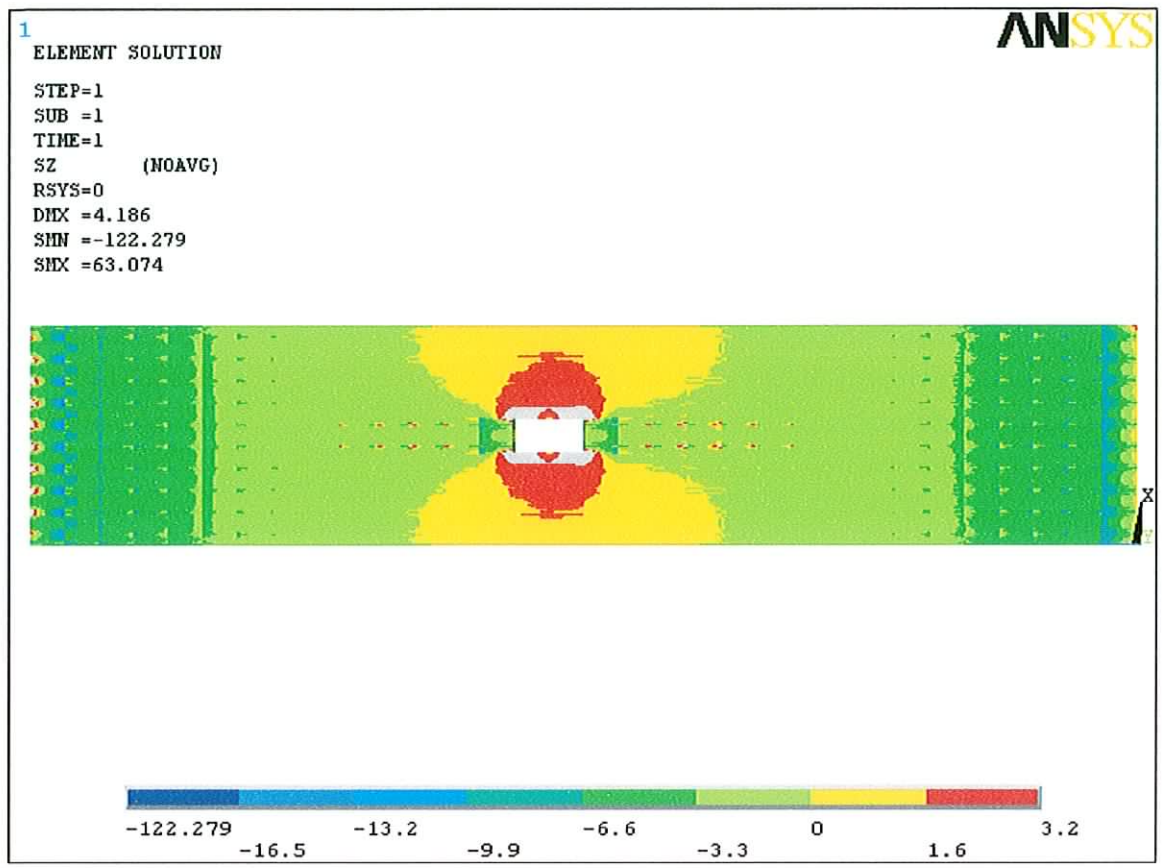

Figure 6.39 Ansys bottom stress – slab 6

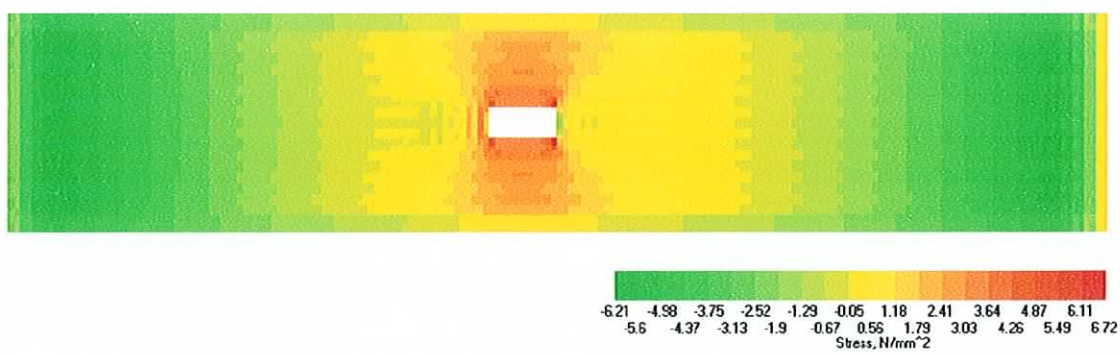

Figure 6.40 Software bottom stress – slab 6

Deflection

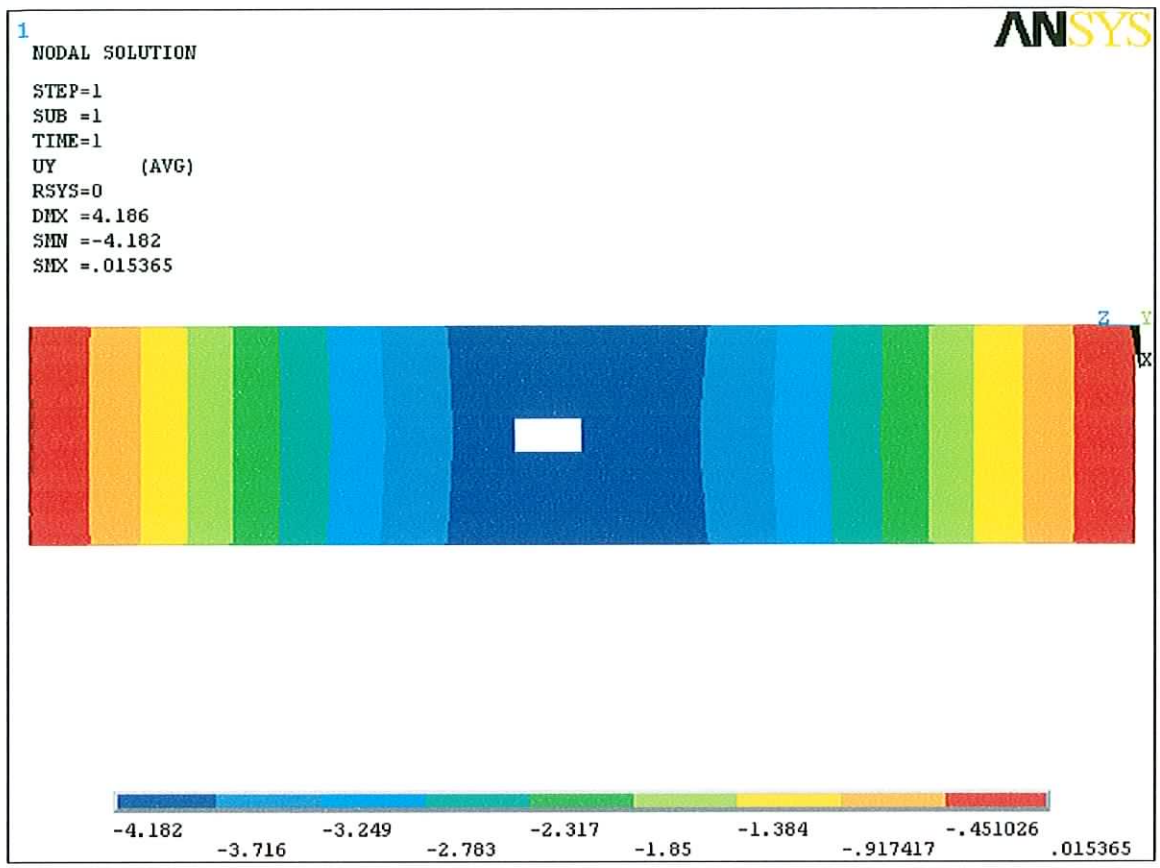

Figure 6.41 Ansys deflection plot – slab 6

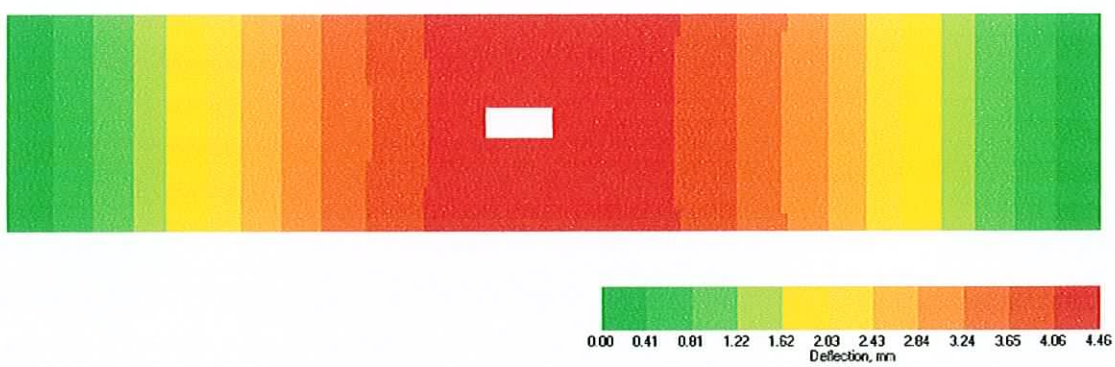

Figure 6.42 Software deflection plot – slab 6

6.3.6.2. Comparison of results

This analysis allows a further examination of the software's performance with the 200 mm deep section. A single opening was chosen so as to start, once

again with the simplest possible situation for analysis and then develop onwards to increasingly complicated situations.

The Ansys results found for top fibre stresses are shown in Figure 6.37 and the software result are shown in Figure 6.38. Once again the end stresses agree well with Ansys values between 0 to 1.6 N/mm^2 in tension and software values of 0.88 N/mm^2. Close to the mid-span point the Ansys stress plot shows compressive stress values between 6.6 to 9.9 N/mm^2 range above and below the opening. The stresses shown in the same region on the stress plot appear slightly different and tend to have values marginally higher. There are a number of stress contours in the software plot within this region ranging from 7.37 N/mm^2 to 10.37 N/mm^2, generally just over 0.5 N/mm^2 higher. The main difference in the stress pattern are shown by the appearance of slight stress concentrations over the hollow cores running through the slab at a location approximately one meter to the right of the opening. This particular pattern was noticed on a number of the other analyses that were performed. The corners of the openings once again show stress concentrations in both stress plots with the Ansys values found to be in the region of 13.2 to 16.5 N/mm^2 and the software giving a peak stress value of 14.87 N/mm^2. To the left and right of the openings the rapid fall off in compressive stress can be seen with small patches of tensile stress visible in both sets of results.

Bottom fibre stresses for Ansys and the software are shown in Figures 6.39 and 6.40 respectively. As expected the Ansys values for the stresses at the end of the slabs compare well with those given by software values with values between 3.3 and 6.6 N/mm^2 in by Ansys compared to a peak value of 6.21 N/mm^2 given by the software. The most interesting stress patterns however are seen close to the opening however and compare quite favourably. The Ansys plot shows a region of tensile stresses above and below the opening in the 0 to 1.6 N/mm^2 range. Comparing this to the same region on the software plot the results shows stresses ranging from 0.56 to 1.79 N/mm^2. Similarly, in the area where the next stress contour is found in Ansys (1.6 to 3.2 N/mm^2), the stress range given by the software is 1.79 to 3.03 N/mm^2. Finally, Ansys shows critical stress (greater than 3.2 N/mm^2) which would cause the slab to fail above and

below the opening whist the software show values ranging from 3.03 to 6.72 N/mm^2.

The deflections shown in Figure 6.41 and 6.42 also appear to match reasonably well. Ansys gives a peak value of 4.182 mm and the software gives a peak value of 4.46 mm.

6.4. Overview of results

The six comparisons carried out above generally show good comparisons between the results found by the software and those found by Ansys. In Section 6.3. the stress patterns plotted by Ansys and the software were shown and discussed. This was complicated by the differences in the format of the display systems used. As stated earlier, Ansys uses eight colours in the contour plot as compared with twenty colours in the plot produced by the software. This allowed the stresses at any point on the software stress plot to be determined more accurately than would be the case with the plots produced by Ansys. Therefore, whilst the contour plots provide an excellent tool for comparison of the stress patterns, a direct comparison on the stress values produced by the two packages proved very difficult. To overcome this difficulty, the stresses at a number of notable points in the contour plot produced by the software were recorded and compared to the numerical stress values found in a list of values produced by Ansys. In order to achieve this, the user must select the option to display the node numbers on the Ansys mesh and through inspection find the nodes nearest the points of interest on the slab for which values are known from the software stress plot. A file listing the stresses was generated using the following command: '*Main Menu – General Postproc – List Results – Nodal Solution*'

This file was then imported into Microsoft Excel to allow the numbers to be most easily sorted and viewed. The appropriate nodal stresses may then be found simply by finding the node number in the spreadsheet and reading the 'sz' value in the corresponding cell. The next two sections show the comparisons between the stresses found at three locations on the slabs to which designers would

typically pay attention. The first of these sections compares top fibre stresses and the second compares bottom fibre stresses. Finally, the deflection values produced by both are compared.

6.4.1. Top fibre stresses

Table 6.1 shows the top fibre stresses from both Ansys and the software. In each case the stress at a generally representative point near the support is examined. The stresses at or close to the mid-span point are also compared. The point at which this stress value is taken depends on the general stress profile of the top of the slab. The stress value taken for comparison was generally taken from the centre of reasonably large areas of high stress close to the mid-span point. The peak stress values were taken as the highest overall value found on the top face of the slab and were found at the corners of the openings or notches. The percentage difference in each case was calculated using the following formula:

$$\% \text{ difference} = \frac{\text{Software} - \text{Ansys}}{\text{Software}} * 100$$

A comparison of the mid-span stresses show reasonably good agreement for the six slabs with differences of between 4.3 to 14.8 %. The stresses at the supports appear to show a greater deviation with differences ranging from 4.6 to 54.9 %. However, if the largest discrepancy is examined, 54.9 %, the stress values, which are both very small, can be seen to differ by only 0.28 N/mm^2. This difference when examined in the context of the stress range found in the analysis is actually very small. The peak stresses found again compared reasonably well with differences ranging from 1.9 to 7.2 %.

Analysis Type		Top Fibre Stresses (N/mm^2)		Difference
		Ansys	Software	
150 dp - solid	Mid-span	9.41	10.46	10.0 %
	support	0.67	0.52	28.8 %
	peak	n/a	n/a	n/a
150 dp - 1 opening	Mid-span	6.54	6.27	4.3 %
	support	0.83	0.87	4.6 %
	peak	9.90	10.67	7.2 %
150 dp - 1 notch	Mid-span	7.62	8.94	14.8 %
	support	0.79	0.51	54.9 %
	peak	16.39	16.02	2.2 %
150 dp - 2 notches	Mid-span	6.92	7.51	7.9 %
	support	0.83	0.74	12.2 %
	peak	15.33	15.01	2.1 %
200 dp - solid	Mid-span	7.19	8.00	10.1 %
	support	0.65	0.90	27.8 %
	peak	n/a	n/a	n/a
200 dp - 1 opening	Mid-span	9.13	9.62	5.1 %
	support	0.62	0.88	29.5 %
	peak	15.10	14.82	1.9 %

Table 6.1

6.4.2. Bottom fibre stresses

The bottom fibre stresses are presented in the same fashion as the top stresses with mid-span, support and peak stress values from Ansys and the software compared. The results of this comparison are given in table 6.2.

Analysis Type		Bottom Fibre Stresses (N/mm^2)		Difference
		Ansys	Software	
150 dp – solid	Mid-span	1.97	3.27	39.8 %
	support	7.47	6.90	8.3 %
	peak	n/a	n/a	n/a
150 dp – 1 opening	Mid-span	0.92	0.63	46.0 %
	support	7.15	7.43	3.8 %
	peak	2.51	1.78	41.0 %
150 dp – 1 notches	Mid-span	1.21	2.12	42.9 %
	support	7.52	6.93	8.5 %
	peak	6.53	6.65	1.8 %
150 dp – 2 notches	Mid-span	0.67	0.33	103.0 %
	support	7.07	7.27	2.8 %
	peak	6.58	6.03	9.1 %
200 dp – solid	Mid-span	0.45	1.22	63.1 %
	support	6.41	6.16	4.1 %
	peak	n/a	n/a	n/a
200 dp – 1 opening	Mid-span	2.94	3.03	3.0 %
	support	6.33	6.21	1.9 %
	peak	6.68	6.72	0.6 %

Table 6.2

The most notable feature of the comparison between the Ansys and the software results for the mid-span stresses are the large percentage differences compared to table 6.1. As with the top fibre support stresses, the fact that most of these stress values are small, contributes to the percentage difference shown. However, in comparison to the top fibre support stresses, these stresses are slightly larger and the differences greater. In the case of the 150mm deep slab with no openings or notches the software gives a mid-span stress of 3.27 N/mm^2, whereas the Ansys value was 1.97 N/mm^2, 1.3 N/mm^2 smaller. This is most probably related to an error, either in the software code or the application of the underlying theory relating to the application of the moment due to the prestressing force. The support stresses compare favourably to each other with differences of between 1.9 and 8.5 %, with most of the differences in

the region of 4 %. Many of the peak stresses were seen to have small values giving relatively large percentage differences, where the numerical differences were small, the largest actual difference was 0.73 N/mm^2.

6.4.3. Deflection

The deflection values are the final set of results that were used to measure the accuracy of the software. Only the peak deflection values were compared, as the deflection patterns are best examined though the direct study of the deflection plots. Table 6.3 gives the maximum values for comparison and the percentage differences.

Analysis type	Maximum Deflection values (mm)		Difference
	Ansys	Software	
150 dp - Solid	7.87	8.90	11.6 %
150 dp - 1 opening	2.31	2.50	7.6 %
150 dp - 1 notch	3.22	3.64	11.5 %
150 dp - 2 notches	2.76	2.87	3.8 %
200 dp - Solid	3.71	4.19	11.5 %
200 dp - 1 opening	4.18	4.46	6.3 %

Table 6.3

Once again the values compare reasonably well with the difference in deflection varying by between 3.8 and 11.6 %. In each case the deflection given by the software was larger which is not consistent with the pattern of percentage differences seen in the discussion relating to the stresses.

6.5. Summary

The results shown in the last three sections indicate that whilst further verification of the results would most certainly be required, and possibly also some alteration of the software, the results show that the software is potentially viable.

7. CONCLUSIONS

7.1. Introduction

The purpose of this research was to develop a software package to analyse the stresses in prestressed concrete slabs using finite element theory. This chapter presents a summary of the research, the conclusions reached from the research and possible research which could build upon this study. The first of these three sections addresses the steps involved in gathering the theory, implementing it within the program and finally testing the resulting software by comparing its results with those produced by Ansys. The second section details the conclusions made from the comparison of results and the processes themselves. The final section gives a number of suggestions for further research that became evident during the research itself.

7.2. Summary

The aim of this research was to construct a software package to assist in the analysis and design of prestressed concrete slabs. In order to achieve this goal the theory upon which the prestressing is based was studied and some aspects of theory of particular relevance were highlighted. The particular aspects of theory examined were the calculation of transfer and service stresses, the ultimate moment capacity, ultimate shear capacity, deflection and the losses in prestress encountered during the life of the structure. The manufacturing technique and its effects on the theory were considered as were the material properties of the steel and concrete.

Plate bending and plane stress theory were also examined with the aim of implementing them as the analysis engine for the package. A method was found to allow the stiffness of hollow-core cross-section of the slabs to be modelled successfully. The effect of prestressing the slab was modelled by applying an axial force to the corner nodes of the elements in the plane stress model and then applying the moment due to the eccentricity of the force at the corners of the elements in the plate bending model. After supports were applied

to the model and suitable loads were defined the global stiffness matrix and the load vector were defined and the displacement vector was calculated. The displacement vector, and stress-displacement matrix, for each element then allowed both plane stresses and plate stresses to be found and combined in a suitable manner to give the final stresses in the slab.

The next chapter detailed the process of constructing the software. The links between the software and Auto-CAD were shown and the process of ascertaining the stiffness of the individual elements in the mesh outlined. The methods employed for calculating the prestressing force after losses at the horizontal nodal intervals along the span direction was shown. The process of applying the supports and loads, in particular, the patch loads was programmed so as to allow the user to select these items onscreen using mouse clicks only. The construction of the global stiffness matrix was an important aspect to the software design as optimising memory storage space was seen to become critically important as the matrices got larger. The Cholesky method was used to solve these matrices, this was relatively easily programmed and seen to work very efficiently. A section of code was written to displace a wireframe displaced shape diagram of the slab and in a new form display the stresses using contour plots. A final feature was added to allow the user to export the numerical values calculated by the software to Excel for the user to examine further.

The Ansys suite was studied and then ultimately employed to test the validity of the results produced by the software. Initially, it was hoped that Ansys workbench could be used due to its user friendly interface, with the geometry itself being created in Solid Edge. However, the requirement for stricter control over the mesh density and shape resulted in Ansys classic being used for the testing. 20 node brick elements were used to model the concrete with the prestressed strands being modelled by beam elements with a prestrain applied. Six potential slab design situations were identified and analyses were carried out in both Ansys and the software produced for this research. Identical spans, slab cross-sections, material properties and loading values were used in each pair of comparative analyses. Finally, the results were compared and possible reasons for some of the discrepancies discussed.

7.3. Conclusions

The conclusions that the author arrived at upon completing this research stem from two areas, the performance of the software written and the processes involved in constructing and testing the software.

The performance of the software was discussed in some detail at the end of Chapter 6 with Tables 6.1, 6.2 and 6.3 showing the comparative values and percentage differences. The software was seen to generally compare well with the Ansys results for all of the analyses carried out. It was found to be most useful to compare the contour plots produced by both Ansys and the software rather than comparing numbers directly. The stress patterns produced by both appeared to agree reasonably well. Critically, both sets of results tended to agree in terms of the critical stresses that would result in the slab failing.

The top and bottom fibre stresses towards the ends of the slab are obviously greatly effected by the prestressing force at the particular cross-section under consideration. However, in the Ansys model the prestressing force value was seen to be constant along the span not taking account of anchorage at the ends of the sections of the strand or the variation in force though out the remaining length of the span due to the relieving effect that self weight has on losses. Therefore, it can be said that the end stresses given by the software are more accurate. Peak stresses in the slab near openings also compared well although the percentage differences occasionally gave a distorted comparison. In these cases the stresses were seen to have low numerical values in the order of 0.5 N/mm^2 which when compared to an insignificantly larger stress of 0.7 N/mm^2 appeared as a large percentage difference.

Clearly further testing would be required to validate the results and possibly further comparisons with spreadsheets to verify prestressing force loss calculations. However, as the aim of this research was to produce a prototype, the accuracy was deemed to be adequate

The other area in which the author feels that comment is due relates to the process of testing. Each model that was setup in Ansys took a considerable amount of time to generate the geometry, mesh it, prestress the slab and run the analysis itself. Indeed, running the analysis itself normally took up to three quarters of an hour. Whilst a mesh pattern itself could be reused, the presence of openings or notches lead to alterations in the mesh that added further to the time spent setting up the model. It was also noted that the process of selecting the lines to mesh with the prestrainable beam elements took a great amount of time and was open to user errors being made that would not appear obviously incorrect. These factors lead the author to believe that Ansys is not suitable for use in industry as the time and expertise required to carry out these analyses would not be forthcoming. The author notes Ansys obvious strength as a general analysis package but in so far as the prestressed concrete industry would be concerned the complexity resulting from its eminent flexibility render it unwieldy.

This reinforces the author opinion that with further development and testing the software produced would generate interest from industry and provide a powerful tool for checking the more complex design situations that regularly occur.

7.4. Recommendations for further research

As the research progressed the author was required to limit the scope of the study due to time constraints. An example of this could be seen during the study of the ultimate moment capacity of prestressed slabs. The theory was examined with a view to implementing it, however a significant additional unit of code would have been required to add this feature. As discussed in Section 4.13. the theory used in the finite element analysis would have to be altered to allow for the non-linear behaviour of the concrete at the limit state. This additional work required would have proved significant in comparison to the relatively straightforward process of generating a second load vector to allow transfer stresses to be examined in addition to service stresses. The other main area upon which time constraints limited the research was the deflection of the slabs. The deflection calculations carried out by the software are only performed as

an intermediate step towards finding the stresses. These deflection values are not found based on the theory discussed in Section 2.2.5. Instead, the deflections are found as part of the displacement vector based on the finite element theory from chapter 3. A number of stress calculations could be carried out as part of a fuller study into the service live cycle and values such as the range of deflections encountered during service could be found. Shear stress calculations provide yet another field in which further study could be carried out. This part of the analysis would be carried out after the ultimate moment capacity values had been found in order to allow the cracked and uncracked areas on the slab to be identified.

The finite element component of the research also lends itself to further research. The plate bending aspect of the model used in this study was set very early in the research as it had been used successfully in other unfinished research. Building upon the work carried out for this thesis, other more complicated finite element models could possibly be applied to this task and tested. 3-D elements could be used instead of the 2-D plate elements however, the use of curvilinear elements with a large number of nodes would lead to computer processor and memory capacity problems arising. The matrix storage and solution code would have to be made more efficient and the researcher could examine the possibility of writing these two pieces of code in the compiler's assembler suite. Shape function could potentially be used to allow irregularly shaped elements to be mapped to the regular shapes of the elements used in the theory in this research. This would offer immense flexibility when generating the mesh, allowing the user to place more elements near areas where stress concentrations are expected.

The software as it stands would require further testing possibly against other established software packages besides Ansys. If its accuracy was deemed to be adequate the software would have to be expanded to accept the cross-sectional geometry of other slab profiles in use in industry. The unit of code currently employed within the software accepts only the cross-section shown in Figure 4.3. However this could be expanded by examining the possibility of writing code to accept any cross-sectional shape and calculating its properties.

Finally, a study into the possibility of modelling prestressed slabs with structural screeds applied could be carried out. This branch off the research would also most likely study the effects of propping the slabs whilst the screed itself cures and gains strength.